

The motion of a pushed, sliding workpiece

Michael Peshkin and A. C. Sanderson

IEEE Transactions on Robotics and Automation 4:6 (December 1988)

The Motion of a Pushed, Sliding Workpiece

Michael A. Peshkin

Arthur C. Sanderson

Reprinted from
IEEE JOURNAL OF ROBOTICS AND AUTOMATION
Vol. 4, No. 6, December 1988

The Motion of a Pushed, Sliding Workpiece

MICHAEL A. PESHKIN, MEMBER, IEEE, AND ARTHUR C. SANDERSON, SENIOR MEMBER, IEEE

Abstract—It occurs frequently in robotic applications that a robot manipulates a workpiece which is free to slide on a work surface. Because the pressure distribution supporting the workpiece on the work surface cannot in general be known, the motion of the workpiece cannot be calculated uniquely. Yet despite this indeterminacy, several researchers have shown that sliding motions can be employed to accurately align workpieces without visual or other feedback.

Here we find the locus of centers of rotation of a workpiece for all possible pressure distributions. The results allow a quantitative understanding of open-loop robot motions which guarantee the alignment of a workpiece. Several sample problems are solved using the results, including the distance that a flat "fence" or robot finger must push a polygonal workpiece to assure that a facet of the workpiece comes into alignment with the fence.

I. MOTIVATION

SLIDING OPERATIONS are encountered frequently in robotics. It is almost inevitable that when the position of a workpiece that is to be acquired by a robot is not perfectly known, a sliding phase will occur before the robot can acquire the workpiece. Mason [10] was the first to identify sliding operations as *fundamental* to manipulation, and especially to grasping.

The sliding phase need not be considered an undesirable but unavoidable fact of life. In the examples which follow sliding operations are used constructively to manipulate and acquire workpieces, without sensing, and despite uncertainty in the initial orientation and position of the workpiece. Yet in each example quantitative information about the motion of the workpiece, which would be needed to guarantee the success of the operation, is lacking. It is the objective of this paper to solve completely for the motion of a sliding workpiece, thus allowing proof of the success of operations which rely on sliding, and facilitating the design of such operations.

A. Automatic Feeders

Sliding occurs when a workpiece on a moving belt interacts with a fence across the belt. (An equivalent interaction occurs when the workpiece is stationary on a work surface, and a fence or gripper under control of a robot pushes it.) And similar interactions occur in bowl feeders, as parts interact with fences as the parts move along a ramp.

Manuscript received January 14, 1986; revised October 26, 1987. This work was supported by a grant from the Xerox Corporation and by the Robotics Institute, Carnegie-Mellon University, Pittsburgh, PA.

M. A. Peshkin was with the Robotics Institute, Carnegie-Mellon University, Pittsburgh, PA 15213. He is now with the Mechanical Engineering Department, Northwestern University, Evanston, IL 60201.

A. C. Sanderson was with the Robotics Institute, Carnegie-Mellon University, Pittsburgh, PA 15213. He is now with the Electrical, Computer, and Systems Engineering Department, Rensselaer Polytechnic Institute, Troy, NY 12180.

IEEE Log Number 8819997.

One of the many possible behaviors of the workpiece when it hits a fence is to rotate until a flat edge is flush against the fence, and then to slide along the fence (if the fence is sufficiently slanted). Another behavior is to roll along the fence instead of sliding. Or the workpiece may stop rotating and simply stick to the fence.

To design feeders the behavior of the workpiece must be understood. This problem has been considered explicitly by Mani and Wilson [9] and also by Brost [2]. (Related work includes [4], [7], and [14].) Mani and Wilson developed strategies for manipulation which can orient a workpiece on a table by a carefully planned sequence of pushes with a fence. Each push aligns a facet of the workpiece with the fence, until an initially randomly oriented workpiece is reduced to a unique final orientation.

In the case of Mani and Wilson's fence-pushing aligner, the quantitative information needed is the distance a polygonal workpiece must be pushed to align a given facet with the pushing fence. Sometimes a workpiece may have to be pushed a great distance before it will align with the fence pushing it. To make Mani and Wilson's manipulation strategies into guaranteed strategies we need an upper bound on the distance a workpiece must be pushed to align.

B. Grasping Strategies

In a typical grasping operation, the robot opens a two-jaw gripper wide enough to accommodate both the workpiece to be grasped and any uncertainty in the workpiece's position. Then the gripper begins to close. Generally the workpiece will be closer initially to one jaw than to the other, and the closer jaw will make contact first.

There follows a sliding phase until the second jaw makes contact. During the sliding phase, the workpiece is likely to rotate, especially if the face of the jaw is in contact with a corner of the workpiece rather than a flat facet. The behavior of the workpiece during grasping is discussed by Brost [2], who finds grasp strategies which bring the workpiece into a unique orientation in the gripper, despite substantial uncertainty in its initial orientation and position.

To fully characterize the configuration of the workpiece in the gripper when a grasping operation is complete, we need more complete information about the motion of the workpiece than was available to Brost. Bounds can be obtained for the translation of the workpiece (perpendicular to the direction it is pushed by the gripper) as well as for its rotation as it is pushed.

Paul invented [16], and Mason later analyzed [10], a clever grasping sequence on a hinge plate (Fig. 1). The strategy makes use of sliding to simultaneously reduce the uncertainty of a hinge plate's configuration to zero, and then to grasp it.

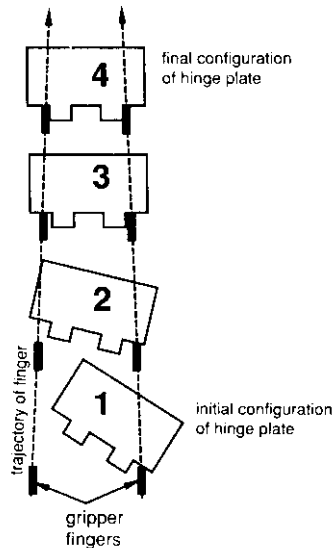


Fig. 1. Hinge grasp strategy (Paul [16] and Mason [10]). The robot fingers follow the trajectory indicated by the dotted lines, closing as they translate. On contact with the hinge plate the trajectory causes the plate to rotate into alignment with the gripper and then to self-center. This open-loop strategy requires no sensing and succeeds despite some uncertainty in the initial configuration of the plate.

The hinge grasp works only for a certain range of initial hinge orientations. For orientations outside of this range, the jaws will be closing too fast for the hinge plate to complete its rotation into alignment, before the jaws close. To find the range of orientations for which this grasp will work, for a given convergence angle of the jaws, we need to know the slowest possible rotation rate of the hinge plate as it is pushed.

C. Grasp Strength

Barber *et al.* [1] have analyzed the resistance of a two-fingered robot grasp of a workpiece to applied torques and forces. A grasped workpiece slides relative to the gripper fingers as the grasp fails, and the resistance of a grasp to this failure can be used as a measure of the quality of the grasp in automated grasp selection algorithms.

In order to determine the force or torque which is needed to cause a grasp to slip, Barber *et al.* assumed a linear variation of pressure over the grasped surface of the workpiece. The utility of this measure of grasp quality could be extended if the assumption of linear pressure variation could be removed, since in general the pressure distribution is unknown.

D. Statement of "The Sliding Problem"

The prototypical sliding problem is to solve for the motion of a workpiece on a planar surface with friction, when a force is applied to it at a known point. This is a problem in classical mechanics, indeed in quasi-static mechanics. It was recognized but never solved in the heyday of classical mechanics [6], [8], [17], although the answers turn out to be simple and of analytical form. The sliding problem is difficult because the pressure distribution beneath the workpiece is in general unknown. The 19th and early 20th century classical mechanicians (cited above) assumed a particular form of the pressure distribution, either uniform or with linear variation over the

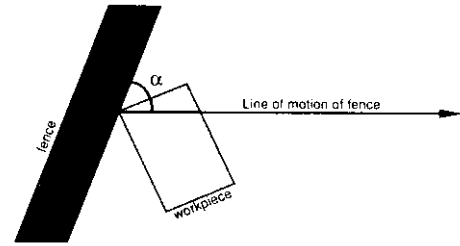


Fig. 2. The edge of an advancing fence pushing a corner of a sliding workpiece. The motion of the workpiece depends on the angle (α) of the front edge of the fence, measured relative to its line of motion, which in this case is horizontal.

bottom surface of the workpiece, and solved the difficult mechanics problem which resulted.

Mason realized the only useful result would be one which applied for all pressure distributions, as the pressure distribution is unknown. Mason was able to find the direction (clockwise or counterclockwise) of rotation of a pushed, sliding workpiece, when the pressure distribution is unknown [10]. His result is remarkable in that the direction turns out to be independent of the pressure distribution. Mason's results are used extensively in Mani and Wilson's work [9], Brost's work [2], and also here.

Our work solves the "other half" of the sliding problem. We determine the motion of the sliding workpiece completely. The motion is most conveniently expressed as a center of rotation (COR) of the sliding workpiece. (The COR lies somewhere in the plane of sliding.) Unlike Mason's sense of rotation result, the COR does depend on the pressure distribution supporting the workpiece, and that pressure distribution is in general unknown. But we are able to find the locus of centers of rotation (that is, the set of all possible motions) for all pressure distributions.

Using our results, manipulation and grasping strategies can be designed which are guaranteed to succeed [14], because all the possible motions of the pushed workpiece are predictable.

II. RANGE OF APPLICABILITY

A. Workpiece Shape

In this paper we will treat the workpiece as a two-dimensional rigid body, since we are only concerned with the interaction of the workpiece with the table on which it is sliding. All pushing forces will be restricted to lie in the plane of the table. The results may be applied to three-dimensional workpieces, so long as the vertical component of the pushing force is negligible, and so long as the point of contact is near the table.

B. Point of Contact Between Workpiece and Pusher

In the general case, when a workpiece is being pushed, there is only one point of contact between the workpiece and the pusher. The contact may be where the flat edge of a pushing fence or robot finger touches a corner of the workpiece (Fig. 2), or it may be where a pushing point touches an edge of the workpiece (Fig. 3). In most of this paper we will assume that the pusher is a point in contact with a flat facet of the workpiece, but the analysis applies equally well if the

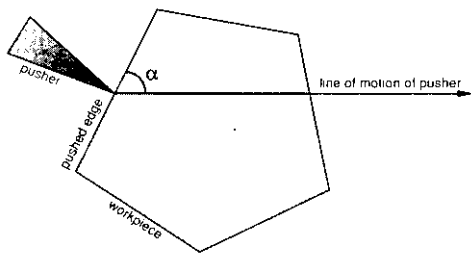


Fig. 3. A corner of an advancing pusher pushing an edge of a sliding workpiece. The motion of the workpiece depends on the angle (α) of the edge being pushed, measured relative to the line of motion of the pusher, which in this case is horizontal. Compare to the meaning of α in Fig. 2. The analysis done in this paper applies equally well to either figure.

pusher is a flat surface in contact with a corner of the workpiece.

Motion of a workpiece when there are two or more points of contact between pusher and workpiece has been considered by Brost [2] and by Mani and Wilson [9].

C. Position Controlled Pusher

It is assumed the pusher will move along a predetermined path in the plane, i.e., it is under position control. Equivalently, the surface on which the workpiece slides may move, carrying the workpiece relative to a fixed pusher; for example, on a conveyor belt. The workpiece has two degrees of freedom, with the third degree of freedom of its motion fixed by the contact maintained between the pusher and the workpiece. Our results may be easily converted to the case where the pusher exerts a known force on the workpiece rather than following a known path.

D. Center of Rotation (COR)

The two degrees of freedom of the workpiece are most conveniently expressed as the coordinates of a point in the plane called the *center of rotation* (COR). Any infinitesimal motion of the workpiece can be expressed as a rotation $\delta\theta$ about some COR, chosen so that the infinitesimal motion of each point \vec{w} of the workpiece is perpendicular to the vector from the COR to the point \vec{w} . If the workpiece is a disc, and the motion it performs is pure rotation in place, the COR is at the center of the disc. Motions we might describe as “mostly translation” correspond to COR’s far from the point of contact. In the extreme case, pure translation occurs when the COR is at infinity.

All kinematic results can be obtained once the COR is found.

E. Pressure Distribution Between Workpiece and Table

The weight of a workpiece is supported by a collection of contact points between the workpiece and the table. The pressure distribution may change as the workpiece moves relative to the table. Finding the COR is complicated by the fact that changes in the pressure distribution under the workpiece substantially affect the motion, i.e., such changes affect the location of the COR. Intuitively, if pressure is concentrated near the center of mass (CM), the workpiece will tend to rotate more and translate less than if the pressure is

uniformly distributed over the entire bottom surface of the workpiece.

The pressure distribution may be changed dramatically by tiny deviations from flatness in the workpiece’s bottom surface (or of the surface it is sliding on). Indeed, if the workpiece and the table are sufficiently rigid and not perfectly flat, they may be expected to make contact at only three points. The three points may be located anywhere on the workpiece’s bottom surface, but like the legs of a three-legged stool, the triangle formed by the points of support always encloses the projection of the CM onto the surface.

Since any assumption we could make about the form of the pressure distribution (for instance, that it is uniform under the workpiece as in [17]) would not be justified in practice, our goal is to find the locus of COR’s under *all* possible pressure distributions.

Let the CM be at the origin, and \vec{w} be a point in the plane. All that is known about the pressure distribution $P(\vec{w})$ is that

- $P(\vec{w})$ is zero outside the workpiece. The workpiece can be entirely contained within a circle of radius a centered at the CM;
- $P(\vec{w}) \geq 0$ everywhere;
- the total pressure

$$\int P(\vec{w}) d\vec{w} = Mg$$

the weight of the workpiece, and

- the first moment of the distribution,

$$\int P(\vec{w}) \vec{w} d\vec{w} = 0.$$

This means that the centroid of the distribution is at the CM of the workpiece, which is at the origin.

F. Coulomb Friction

It turns out that the coefficient of friction of the workpiece with the supporting surface (called μ_s for “sliding friction”) does not affect the motion of the workpiece if we use a simple model of friction. We assume that μ_s is constant over the work surface, that it is independent of normal force magnitude and tangential force magnitude and direction (isotropic), and that it is velocity-independent. In short, we assume Coulomb friction.

There is another coefficient of friction in the problem, μ_c (for “contact friction”), at the point of contact between the edge of the workpiece and pusher. This is distinct from the coefficient μ_s between workpiece and table, discussed above. Initially we consider only $\mu_c = 0$. This assumption is relaxed in Section VI.

G. Quasi-Static Motion

It is assumed that all motions are slow. This *quasi-static approximation* requires that frictional forces on the workpiece (due to the coefficient of friction with the surface μ_s) quickly dissipate any kinetic energy of the workpiece

$$v^2 \ll Xg\mu_s \tag{1}$$

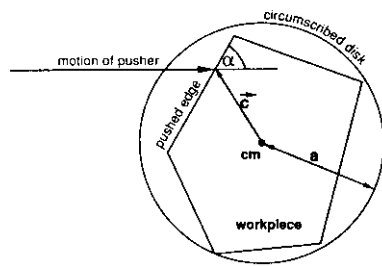


Fig. 4. Parameters of the pushing problem. Important geometric parameters are the angle α of the edge being pushed relative to the line of motion of the pusher, the vector \vec{c} from the center of mass (CM) to the point of contact between pusher and workpiece, and the radius a of the disc which circumscribes the workpiece. When these parameters are given the locus of centers of rotation for all possible pressure distributions can be found.

where v is the velocity of the workpiece, g is the acceleration due to gravity, and X is the precision with which it is desired to calculate distances. The high-speed limit is discussed in Section XII-C. Characteristic speeds for quasi-static motion are discussed in [15] and [11].

H. Bounding the Workpiece by a Disc

We will take the workpiece being pushed to be a disc with its CM at the center. Given another workpiece of interest we can consider a disc centered at the CM of the workpiece, big enough to enclose it. The radius a of the disc is the maximum distance (from the CM) of the workpiece to any point of the workpiece. Since any pressure distribution on the workpiece could also be a pressure distribution on the disc, the COR locus of the disc must enclose the COR locus of the workpiece. The locus for the disc provides useful bounds on the locus for the real workpiece.

I. Geometric Parameters

Geometric parameters of the problem are the point of contact \vec{c} between the pusher and the workpiece, and the angle α between the edge being pushed and the line of pushing, as shown in Fig. 4. The values of α and \vec{c} shown are useful in considering the motion of the five-sided workpiece shown inscribed in the disc. We do not require the point of contact to be on the perimeter of the disc, as this would eliminate applicability of the results to workpieces inscribed in the disc. Indeed, for generality we do not even require the point of contact to be within the disc. Similarly, we will not require α to be such that the edge being pushed is perpendicular to vector \vec{c} , as it would be if the workpiece were truly a disc. The disc (with radius a), α , \vec{c} , and the CM, are shown in Fig. 4.

III. OVERVIEW

In this paper we wish to find not the *sense* of rotation (CW or CCW) as Mason did, but the motion itself, expressed as a COR somewhere in the plane.

First we approach the problem numerically. A formulation of Newton's laws of motion which we call "minimum power mechanics" [21] suggests that for a given pressure distribution $P(\vec{w})$ and advance of the pusher dx , the COR is at that point

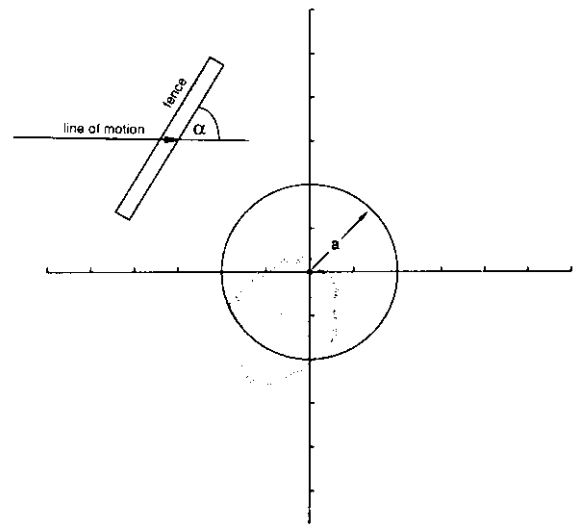


Fig. 5. COR locus for a disc found by iterative minimization (dots). The disc shown encloses the workpiece of interest. The pusher moves horizontally along the line indicated, and contacts the edge of the workpiece at the arrowhead. (In reality this point of contact would always fall within the disc bounding the workpiece, but numerical convergence is simplified for this unrealistic case.) The angle α of the edge which the pusher contacts is indicated. Dots indicate the locations of the center of rotation for 500 000 randomly chosen pressure distributions supporting the workpiece.

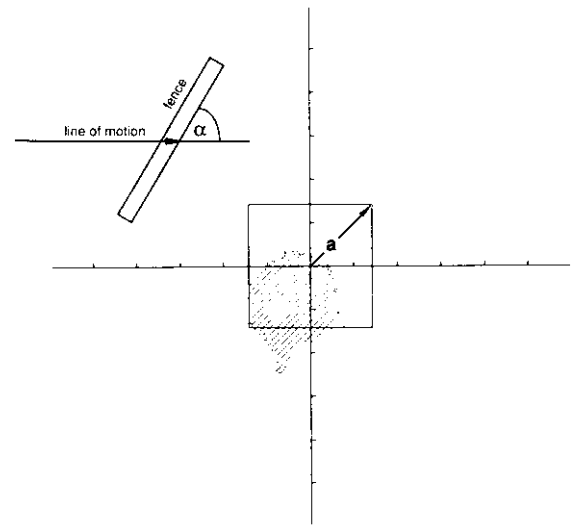


Fig. 6. COR locus for a square found by iterative minimization. Now the workpiece is taken to be a square rather than a disc. (Again we unrealistically choose a point of contact not on the perimeter of the workpiece.) Note that the locus of possible COR's (dots) can be entirely contained within the locus calculated for a disc (Fig. 5).

which minimizes the energy lost to sliding friction. Figs. 5 and 6 show the COR's so found for hundreds of thousands of randomly selected pressure distributions, for a pushed disc and a pushed square, respectively. In these figures the point of contact between pusher and workpiece is unphysically chosen to be *outside* the perimeter of the workpiece to ease problems of numerical convergence.

Note that if the centers of mass of the disc and the square are superimposed, the COR locus for the disc will entirely cover the COR locus for the square. As discussed in Section II-H, this is because the disc entirely covers the square, so any

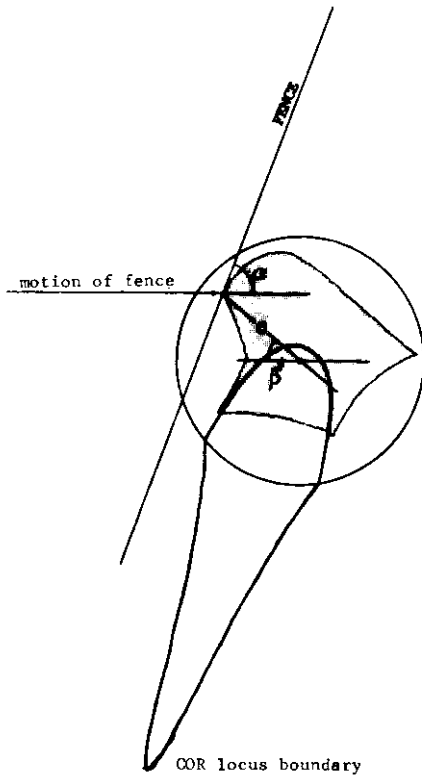


Fig. 7. A typical pushing problem and the boundary of the COR locus found. A point pusher is advancing horizontally, and is pushing the edge of a workpiece. The circle represents the circumscribing disc for which the center of rotation locus can be found. The bold outline is the boundary of the COR locus for this pushing operation; regardless of the actual pressure distribution supporting the workpiece the center of rotation will lie somewhere in this boundary. Any kinematic result can be obtained once the COR locus has been found.

pressure distribution on the square could be a pressure distribution on the disc. The COR which results from any pressure distribution on the square therefore must also be a possible COR for the disc. To bound the COR locus for any workpiece it is therefore only necessary to find the COR locus for a disc which circumscribes the workpiece of interest.

Next we approach the problem analytically. We express the energy lost to sliding friction for a fixed advance of the pusher dx as an integral of the pressure distribution $P(\vec{w})$. The disc will seek that COR which minimizes the energy lost to sliding friction. Minimizing this energy with respect to the location of the COR, we find an intrinsic solution for the COR in terms of two moments of the unknown pressure distribution $P(\vec{w})$. The COR is related to the ratio of these moments. When the pushed workpiece is a disc, we are able to identify two classes of pressure distributions which are responsible for extremal values of the moment ratio, and therefore also are responsible for extremal values of the COR. These special pressure distributions are simply dipods: pressure distributions consisting of just two points of support. In one class of dipods, one point of support is anywhere on the perimeter of the disc and the other diametrically opposite it. The second class is only slightly more complicated. By solving for the COR analytically for these special classes of pressure distributions, the boundary of the COR locus is found.

In Fig. 7 we show a typical pushing problem and the

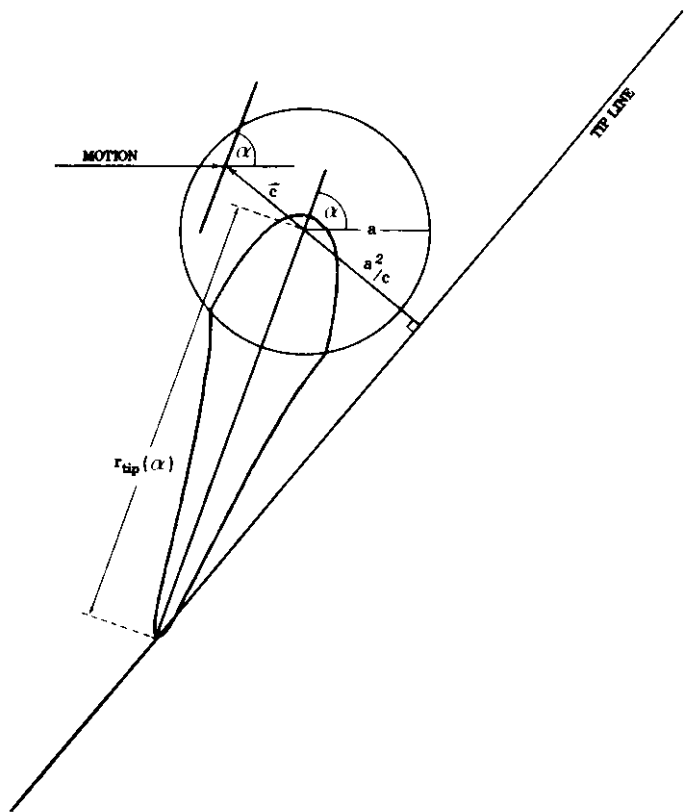


Fig. 8. $r_{tip}(\alpha)$ versus α , and construction of the tip line. The most useful point on the COR locus boundary seems to be the tip, as this is the COR for which rotation of the workpiece is slowest. The distance to the tip (from the CM) is given by the simple formula $r_{tip} = a^2/\alpha \cdot \vec{c}$. As the angle of the pushed edge α is varied, the tip of the COR locus sweeps out a straight line called the tip line.

boundary of the locus of all possible centers of rotation of the pushed workpiece.

Note that the COR locus is symmetric about the angle of the pushed edge α , which is shown as a line α in Fig. 8. The farthest point of the COR locus from the CM falls on α . For most applications this "tip" of the COR locus is of particular importance, as it specifies the slowest possible rotation of the workpiece as it is pushed, regardless of the pressure distribution. The distance r_{tip} from the center of the disc to the tip of the COR locus has a simple relation to the parameters of the problem

$$r_{tip} = \frac{a^2}{\alpha \cdot \vec{c}} \quad (2)$$

This formula has an interesting geometric interpretation. As the edge angle α is varied, the tip of the COR locus traces out a straight line called the "tip line," and shown in Fig. 8. The tip line is perpendicular to \vec{c} and a distance a^2/c from the CM. Simple formulas exist for the curvature of the boundary of the COR locus at the tip (and at the interior end as well), and for the points of intersection of the boundary of the COR locus with the perimeter of the disc. For most purposes, the formulas for these points of the COR locus suffice, and it is unnecessary to find the entire locus.

As an application of the results so far, we can calculate the maximum distance it is necessary to push a polygonal

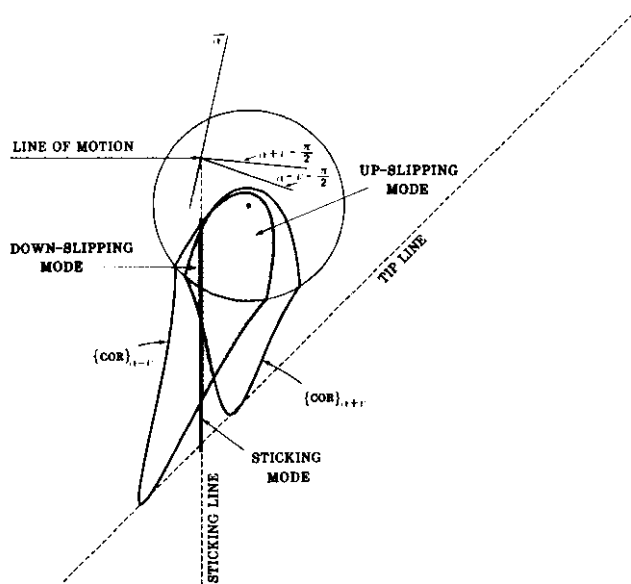


Fig. 9 Construction of the COR sketch. When the coefficient of friction between pusher and edge of workpiece $\mu_c > 0$, the locus of possible COR's can be constructed from two of the simpler COR loci which we calculated for $\mu_c = 0$. The two $\mu_c = 0$ loci are shown in outline, while the COR "sketch" for a nonzero μ_c is shown shaded. Depending on where the COR falls in the COR sketch, slipping of the workpiece (either up or down) relative to the pusher, or sticking, may be predicted.

workpiece with a frictionless fence, in order to guarantee alignment of an edge of the workpiece with the fence, regardless of the pressure distribution beneath the workpiece [see equation (42)].

As noted, the COR loci discussed above apply only when μ_c , the coefficient of "contact friction" between the pusher and the pushed workpiece, is zero. In Section VI we generalize to $\mu_c > 0$. The COR locus for $\mu_c > 0$ turns out to be a combination of two of the COR loci calculated for $\mu_c = 0$. The two COR loci used are those with "effective" edge angles $\alpha \pm \tan^{-1} \mu_c$. Part of each of these two loci, plus a linear segment just above the tip line, constitute all the possible centers of rotation for $\mu_c > 0$. In Fig. 9, the shaded and bold sections are the resulting COR locus for $\mu_c > 0$. (Similar "effective angles" were shown in Mason and Brost's figure 5 [12].)

As examples of the $\mu_c > 0$ results we find the distance a polygonal workpiece must be pushed by a fence to assure alignment of an edge of the workpiece with the fence, now with $\mu_c > 0$. We also analyze the motion of a sliding disc as it is pushed aside by the corner of a workpiece in linear motion. Finally, we study the effectiveness of an open-loop manipulation strategy based on "herding" a disc toward a central goal by moving a pusher in a decreasing spiral about the goal.

A. Minimum Power Mechanics

Suppose that the geometry of a pushing operation is specified; that is, the radius a of the disc enclosing the workpiece, the point \vec{c} at which the workpiece is being pushed, and the angle α of the flat surface involved in the push. If we suppose further that a single pressure distribution is specified, then a unique COR at a single point must be the result.

Our system is *constrained* because the pusher and the workpiece are in contact, the pusher is advancing a distance δx in a given instant, and the workpiece must slide enough to accommodate the advance of the pusher. The COR could be at almost any point in the plane, and still allow the workpiece to accommodate the advance of the pusher. However, some of these locations will require a greater rotation of the workpiece (about the COR) to accommodate the advance of the pusher than do others.

To solve for the COR we use a formulation of Newton's laws for constrained motions which we call minimum power mechanics [21]. Minimum power mechanics expresses the intuitively appealing idea that the motion a system makes (e.g., the COR about which the workpiece actually *does* choose to rotate) will be the one for which the energy dissipated to sliding friction is minimized.

We have proven that minimum power mechanics is correct under some fairly restrictive conditions [21]: slow (quasi-static) motion is required, and the only dissipative forces which may occur in the system are (slightly generalized) analogues of Coulomb friction. The present system qualifies. (Minimum power mechanics should not be confused with the principle of virtual work, which applies to static systems without dissipation, and sets energy to zero rather than minimizing it.) Recently, Goyal and Ruina have done further work on minimization principles in quasi-static mechanics [5].

B. Notation

- Vectors are indicated by an arrow, e.g., \vec{v} .
- \vec{r} is the vector from the CM to the COR. r is the magnitude of that vector, i.e., the distance from the CM to the COR.
- A Greek letter is used to represent both an *angle* and a *unit vector* which makes that angle with respect to the x -axis (measured CCW). An arrow is used to indicate the unit vector: $\vec{\alpha} = (\cos \alpha, \sin \alpha)$.
- We indicate functional dependence with subscripts. E_r is a function of \vec{r} (the COR).
- All integrals are over the area of the disc.
- Curly brackets indicate a locus of values of a quantity.

IV. SOLUTION FOR THE COR LOCUS

In this section we compute the energy that is dissipated due to friction when the pusher advances a distance δx , as a function of the center of rotation \vec{r} , and for a given pressure distribution $P(\vec{w})$. We will then minimize the energy with respect to \vec{r} to find the COR about which the workpiece actually *does* choose to rotate.

It may help to imagine the disc "pinned" at the COR. This is not difficult to imagine if the COR happens to fall inside the perimeter of the disc, and one's intuition can be extended to include the case where the COR is outside the perimeter. Either way, the disc is free to rotate *only* about the COR, and the COR itself stays stationary.

Given the COR, the motion of the disc is fully determined when we apply our constraint: the edge being pushed (at \vec{c}) must move out of the way of the advancing pusher, but stay in contact.

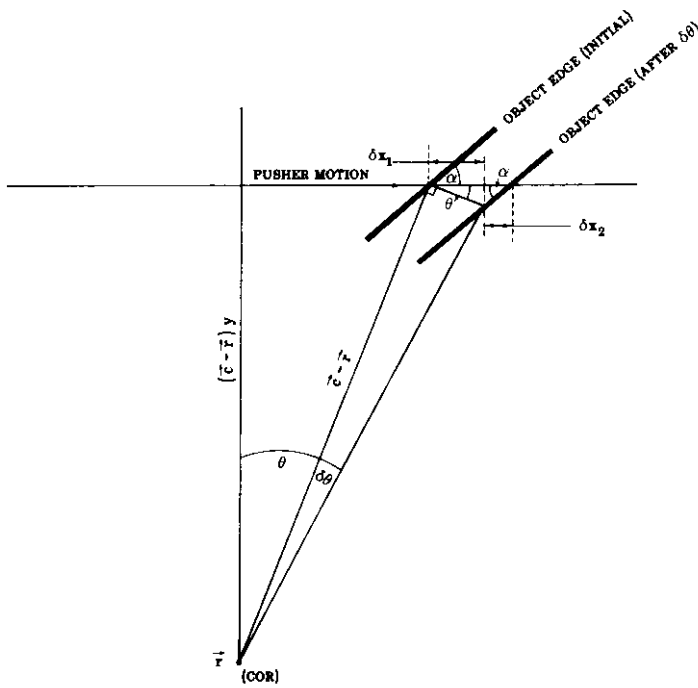


Fig. 10. Relation between advance of pusher (δx) and rotation about the COR ($\delta\theta$). For fixed COR the pusher may advance a distance δx while the workpiece rotates an angle $d\theta$ about the COR. δx consists of two parts: movement of the workpiece edge (δx_1), and slipping of the pusher along the edge (δx_2).

A. Relation Between Motion of the Pusher and Rotation of the Workpiece

In order to accommodate the advance δx of the pusher, the disc will rotate an amount $\delta\theta$ about the center of rotation \bar{r} . A rotation of $\delta\theta$ allows an advance of the pusher δx consisting of two parts, as shown in Fig. 10.

$$\delta x_1 = \delta\theta |\bar{c} - \bar{r}| \cos \theta = \delta\theta (c_y - r_y)$$

$$\delta x_2 = \delta x_1 \frac{\tan \theta}{\tan \alpha} = \delta\theta \frac{c_x - r_x}{\tan \alpha} \quad (3)$$

Note that δx_2 corresponds to slipping of the point of contact along the workpiece edge.

Defining the unit vector $\bar{\alpha} = (\cos \alpha, \sin \alpha)$ we can write

$$\delta x = \delta x_1 + \delta x_2 = \frac{\delta\theta}{\sin \alpha} \bar{\alpha} \cdot (\bar{c} - \bar{r}) \quad (4)$$

To avoid proliferation of absolute value signs, henceforth $\bar{\alpha} \cdot (\bar{c} - \bar{r})$ will be taken to be positive. Considerations of symmetry will allow application of the results to cases where $\bar{\alpha} \cdot (\bar{c} - \bar{r})$ is negative. Physically, $\bar{\alpha} \cdot (\bar{c} - \bar{r}) > 0$ corresponds to clockwise rotation of the workpiece as it is pushed.

B. Energy Lost to Friction with the Table

An area element of the disc at \bar{w} supports a force $P(\bar{w}) d\bar{w}$ normal to the table. The element will slide a distance

$$\delta\theta |\bar{w} - \bar{r}| \quad (5)$$

due to the rotation $\delta\theta$ about the center of rotation \bar{r} , and in the process will dissipate an amount of energy

$$dE_r = \mu_s P(\bar{w}) d\bar{w} \delta\theta |\bar{w} - \bar{r}| \quad (6)$$

Integrating over the area of the disc, the total energy dissipated due to rotation $\delta\theta$ is

$$E_r = \delta\theta \mu_s \int P(\bar{w}) |\bar{w} - \bar{r}| d\bar{w} \quad (7)$$

where we write E_r to remind ourselves that the energy is a function of the presumed location of the center of rotation \bar{r} . Substituting for $\delta\theta$, we have

$$E_r = \frac{\delta x \mu_s \sin \alpha}{\bar{\alpha} \cdot (\bar{c} - \bar{r})} \int P(\bar{w}) |\bar{w} - \bar{r}| d\bar{w} \quad (8)$$

The system will find a location for \bar{r} which minimizes E_r . At this minimum, the derivatives of E_r with respect to both \bar{r}_x and \bar{r}_y must be zero. Evaluating the derivative of E_r with respect to \bar{r} and setting it equal to zero we find

$$\nabla E_r = \delta x \mu_s \sin \alpha \frac{[d_r \bar{\alpha} - \bar{v}_r \bar{\alpha} \cdot (\bar{c} - \bar{r})]}{[\bar{\alpha} \cdot (\bar{c} - \bar{r})]^2} = 0 \quad (9)$$

where

$$d_r = \int P(\bar{w}) |\bar{w} - \bar{r}| d\bar{w} \quad (10)$$

a scalar, can be physically interpreted as the weighted distance from the COR to the pressure distribution, and

$$\bar{v}_r = \int P(\bar{w}) \frac{\bar{w} - \bar{r}}{|\bar{w} - \bar{r}|} d\bar{w} \quad (11)$$

a vector, can be interpreted as the weighted direction from the COR to the pressure distribution.

C. A Digression: Iterative Numerical Solution

Minimization of E_r can be carried out in an iterative manner to find the COR for a given pressure distribution $P(\bar{w})$. Fig. 5 shows the locus of COR's obtained in this manner. Each point is the COR for a randomly chosen three-point pressure distribution. Only pressure distributions consisting of three points (a tripod) need be considered since according to Mason's theorem 5 [10] three points are sufficient. Weights were computed for the three points in such a way as to satisfy the constraint that the CM be at the center of the disc. (If this required any of the weights to be negative, the tripod was discarded.) An initial guess was made for the location of the center of rotation \bar{r} , and ∇E_r evaluated at that point.

The minimization technique used requires computation of $\nabla(\nabla E_r)$, the second derivative of E_r (a two-by-two matrix), which can be obtained analytically. A new guess for \bar{r} is then made by adding to the old guess

$$\Delta \bar{r} = \frac{-\nabla E_r}{\nabla(\nabla E_r)} \quad (12)$$

This method usually converged quickly if the initial guess was

sufficiently close to the correct answer. By moving only one leg of the tripod at a time, and by only a small amount, the value of \vec{r} found for one tripod could be used as an initial guess for the next. Fig. 5 represents 590 000 tripods, taking 4 CPU hours on a VAX-780. Similar figures done with four points of support instead of tripods are identical, numerically validating Mason's theorem 5 [10].

D. Analytic Solution

Resuming our analytical discussion from Section IV-B, we set $\nabla E_r = 0$ in (9). The constant terms drop out leaving

$$r^2 \vec{\alpha} = \vec{q}_r [\vec{\alpha} \cdot (\vec{c} - \vec{r})] \tag{13}$$

where we define the *quotient moment*, a vector, as

$$\vec{q}_r = r^2 \frac{\vec{v}_r}{d_r} \tag{14}$$

with \vec{v}_r and d_r given in (10) and (11). \vec{q}_r is a function of the COR \vec{r} and the pressure distribution $P(\vec{w})$, and has units of distance. In this section we *hold the center of rotation \vec{r} fixed*, and analyze the quotient moment for all pressure distributions $P(\vec{w})$.

The *quotient locus* $\{\vec{q}_r\}$ is the set of \vec{q}_r for all possible choices of the pressure distribution $P(\vec{w})$ consistent with the requirements listed in Section II-E. It is still a function of \vec{r} , but the dependence on $P(\vec{w})$ has been removed. Unfortunately we have been unable to develop any physical intuition about the meaning of the quotient locus. We regard it merely as an intermediate mathematical construction, more tractable than the COR locus to which it is related.

We will always plot the quotient locus displaced by \vec{r} , i.e., based at the COR. $\{\vec{q}_r\}$ may be plotted as a region of space, if we remember that a given $\vec{q} \in \{\vec{q}_r\}$ is a *vector* with its tail at the COR and its head anywhere in that region.

We will find the boundary of the quotient locus. The results will allow us to find the boundary of the COR locus in Section IV-I.

To simplify discussion, we take the total weight of the workpiece $Mg = 1$, that is

$$Mg = \int P(\vec{w}) d\vec{w} = 1. \tag{15}$$

Since multiplying the pressure distribution P by a constant factor changes both numerator and denominator of \vec{q}_r by that same factor, the assumption is harmless. Physically, the mass of the disc has no effect on the motion, so we can choose it arbitrarily.

E. Extrema of the Quotient Locus

Since \vec{v}_r (11) can be interpreted as a weighted average of *unit vectors* from the COR to the pressure distribution, the greatest magnitude \vec{v}_r can have will be 1, and will be attained when the pressure distribution is concentrated at the CM. In all other cases, the direction to elements of the pressure distribution varies, and so some cancellation is inevitable. When the magnitude of \vec{v}_r is maximal, it must be directed from the COR to the CM.

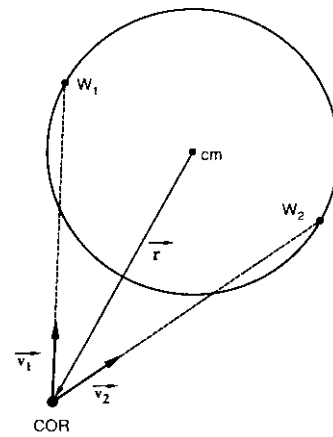


Fig. 11. Dipod responsible for the smallest value of \vec{v}_r , for $r > a$. We study extrema of the moments \vec{v}_r and d_r of the pressure distribution to find extrema of the "quotient moment" $\vec{q}_r = \vec{v}_r/d_r$. We study extrema of the quotient moment \vec{q}_r to obtain bounds on the COR to which it is related. \vec{v}_r is the weighted unit vector from the COR (\vec{r}) to the pressure distribution. It is maximized when the pressure distribution supporting the workpiece is concentrated at the CM. When $r > a$, \vec{v}_r is minimized by the pressure distribution shown here: half the weight of the workpiece is concentrated at each of the two points of support \vec{w}_1 and \vec{w}_2 , which are chosen to provide as little agreement in direction from the COR as possible.

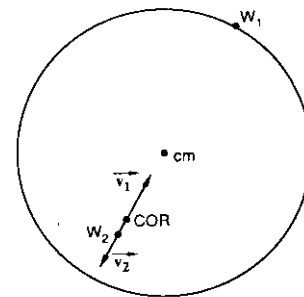


Fig. 12. Dipod responsible for a negative value of \vec{v}_r , for $r < a$. If the COR is within the disc ($r < a$), it is even possible to arrange for \vec{v}_r to point from \vec{r} away from the CM, by choosing the pressure distribution to be a dipod such as this one. As w_2 is closer to the CM than w_1 , it bears more than half the weight of the disc.

The smallest magnitude \vec{v}_r can achieve depends on whether the COR is inside or outside the disc, i.e., on whether $r > a$ or $r < a$, where a is the radius of the disc. In either case we wish to achieve the maximum amount of cancellation of direction possible. If $r > a$, this occurs when the pressure distribution consists of two points at opposite edges of the disc, providing the minimum possible agreement on direction between the two vectors, as shown in Fig. 11.

If $r < a$, we can arrange for \vec{v}_r to be zero. Indeed, we can arrange for \vec{v}_r to point from the COR maximally away from the CM by making a two-point pressure distribution as shown in Fig. 12. (In the figure the distance from w_2 to the COR is infinitesimal.) The two vectors \vec{w}_1 and \vec{w}_2 point in opposite directions. To maintain the centroid of the pressure distribution at the CM, we find the weights of \vec{w}_1 and \vec{w}_2 are

$$P_1 = \frac{r}{r+a} \tag{16}$$

and

$$P_2 = \frac{a}{r+a}$$

Therefore, \vec{w}_2 is more heavily weighted than \vec{w}_1 , and

$$\vec{v}_r = P_1 \vec{v}_1 + P_2 \vec{v}_2 = (P_2 - P_1) \vec{v}_2 = \frac{a-r}{a+r} \vec{v}_2 \tag{17}$$

points from the COR away from CM.

Now consider d_r (10). Clearly, if the pressure distribution is concentrated at the CM, the weighted distance from the COR to the pressure distribution is just r . In fact, r is the smallest value which d_r can attain. In the configuration shown in Fig. 12

$$d_r = P_1 \cdot (a+r) + P_2 \cdot 0 = r. \tag{18}$$

d_r takes on its maximum value when the pressure distribution consists of two points as in Fig. 11. That value is

$$d_r = (r^2 + a^2)^{1/2}. \tag{19}$$

Since \vec{q}_r is the quotient of \vec{v}_r and d_r , extreme values of $|\vec{q}_r|$ occur when \vec{v}_r is maximal and d_r minimal, and when \vec{v}_r is minimal and d_r maximal. Figs. 11 and 12 illustrate the pressure distributions which (simultaneously) minimize \vec{v}_r and maximize d_r , for $r > a$ and $r < a$, respectively.

F. Numerical Exploration of the Quotient Locus

We can find the locus of all possible quotients numerically. It is much easier to find the $\{\vec{q}_r\}$ locus (for a given value of \vec{r}) than it is to find the COR locus. No iteration is required; for a given tripod, the moments \vec{v}_r and d_r can be calculated immediately. Figs. 13 and 14 show typical $\{\vec{q}_r\}$ loci for $r < a$ and $r > a$, respectively. The dots are values of \vec{q}_r found numerically, while the solid curve is the empirical boundary of the locus as described below.

The dots in Figs. 13 and 14 represent over 3 000 000 and 500 000 randomly chosen tripods, respectively. The solid curves which appear to bound the dots are generated by two classes of dipods, discussed below. On the basis of numerical studies such as shown in these figures, we believe that no value of \vec{q}_r generated by a tripod or any other pressure distribution falls outside the dipod curve. Therefore, the dipod curve is the exact boundary of $\{\vec{q}_r\}$. We have not been able to prove analytically that no value of \vec{q}_r falls outside the dipod curve, so the boundaries should be considered empirically justified only.

G. Boundary for $|COR| < a$

We observe that for $r < a$ the boundary of the locus is a circle. This empirical boundary can be generated by two-point pressure distributions (dipods) of the type shown in Fig. 15, where the angle ω can vary. These dipods are a generalization of the one shown in Fig. 12. (The distance from \vec{r} to \vec{w}_2 is infinitesimal.) We can then calculate a parametric form for the boundary in terms of ω

$$\vec{q}_r = \vec{w} \frac{r}{r+a} (a\vec{w} - \vec{r}) \tag{20}$$

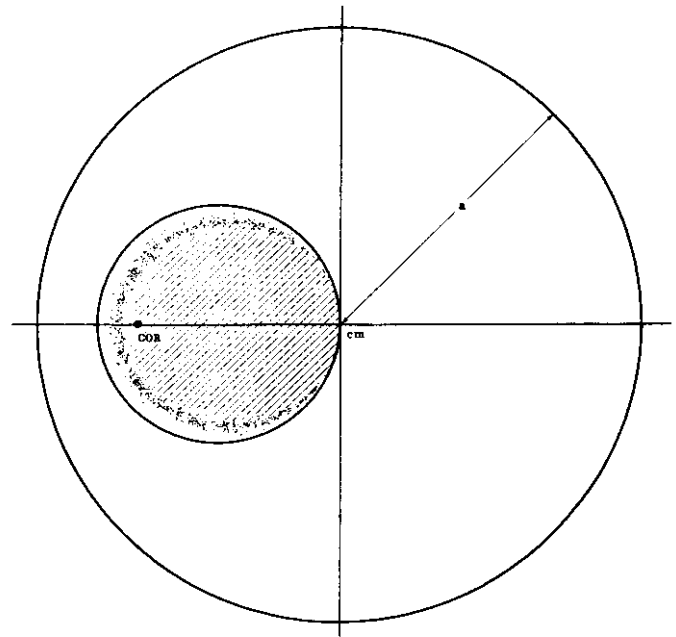


Fig. 13. Quotient locus $\{\vec{q}_r\}$ (dots), and empirical boundary (solid), for $r < a$. Hundreds of thousands of randomly selected pressure distributions were chosen, and for each the quotient moment was evaluated and plotted (dots). All the observed values of the quotient moment fall within the boundary (solid curve) generated by quotient moments of special pressure distributions consisting of just two points of support: dipods. In fact, the boundary turns out to be a circle, the radius of which can be determined analytically.

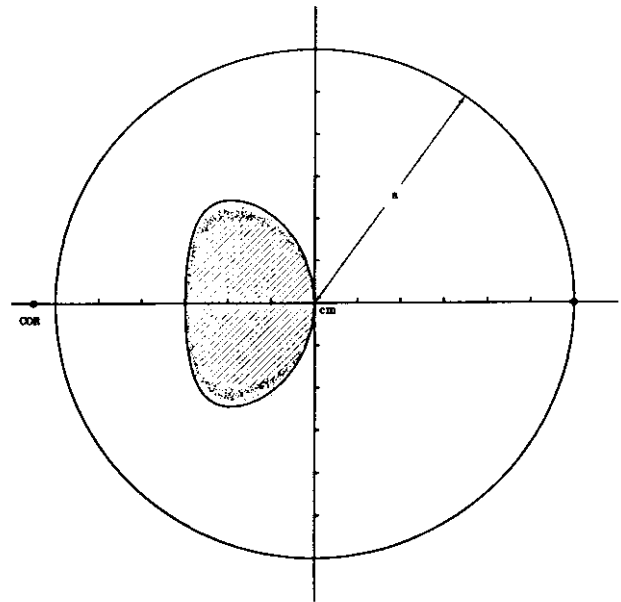


Fig. 14. Quotient locus $\{\vec{q}_r\}$ (dots), and empirical boundary (solid), for $r > a$. As in Fig. 13, the quotient moments for randomly generated pressure distributions all fall within the boundary generated by quotient moments of a special group of dipods. Here $r > a$, and the bean-shaped boundary does not have a simply named shape such as the circle we found for $r < a$. However, it is still described by analytic formulas.

where $\vec{w} = (\cos \omega, \sin \omega)$. This generates a circle of radius

$$b = \frac{ar}{r+a} \tag{21}$$

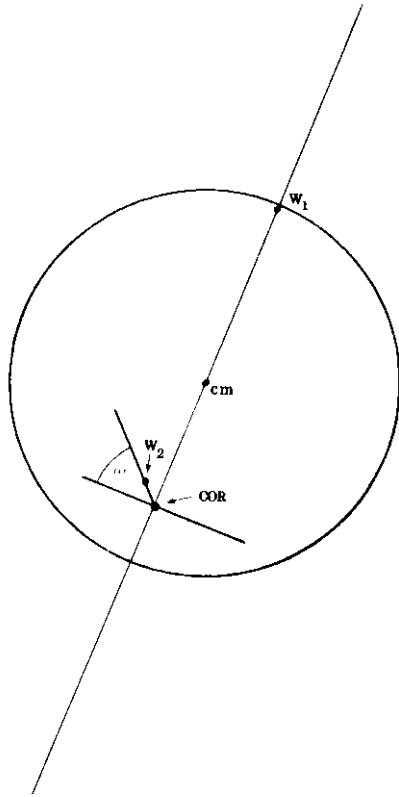


Fig. 15. Dipods contributing to the boundary of $\{\bar{q}_r\}$, for $r < a$. When $r < a$, i.e., when the COR turns out to be within the disc, these are the pressure distributions which are responsible for the boundary of the quotient locus, and thus also are responsible for the boundary of the COR locus. They are simply dipods, in which one point of contact between workpiece and sliding surface is at the periphery of the disc, and the other point is internal to the disc, near what turns out to be the COR. More than half the weight is supported by the internal contact, as it is nearer to the CM. It is not surprising that the workpiece rotates about a COR essentially coincident with a point supporting most of the weight of the workpiece [5]. As the internal point of support is moved in an infinitesimal circle parametrized by angle ω , the corresponding COR traces out the boundary of the COR locus inside the disc.

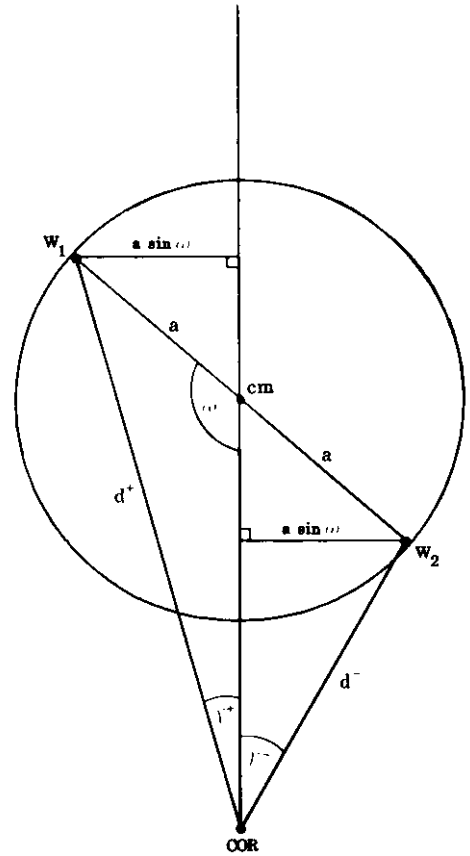


Fig. 16. Dipods contributing to the boundary of $\{\bar{q}_r\}$, for $r > a$. When $r > a$, i.e., when the COR turns out to be outside the disc, these are the pressure distributions which are responsible for the boundary of the quotient locus, and thus also are responsible for the boundary of the COR locus. Again they are simply dipods, but now in each dipod both points of contact with the sliding surface are at the periphery of the disc, and so each supports half the weight of the workpiece. As the dipod system rotates around the CM (parametrized by angle ω), the corresponding COR traces out the boundary of the COR locus outside the disc.

H. Boundary for $|COR| > a$

For $r > a$, the empirical boundary of the locus $\{\bar{q}_r\}$ is generated by dipods of the type shown in Fig. 16, where ω is allowed to vary. These dipods are a generalization of the dipod shown in Fig. 11. Again, the boundary can be calculated parametrically from ω (via intermediate terms d^+ , d^- , γ^+ , and γ^-) as

$$d^\pm = (r^2 + a^2 \pm 2ar \cos \omega)^{1/2}$$

$$\sin \gamma^\pm = \frac{a \sin \omega}{d^\pm}$$

$$\cos \gamma^\pm = (1 - \sin^2 \gamma^\pm)^{1/2}$$

$$\vec{v}_r = \left(\frac{\sin \gamma^+ - \sin \gamma^-}{2}, \frac{\cos \gamma^+ + \cos \gamma^-}{2} \right)$$

$$d_r = \frac{d^+ + d^-}{2}$$

$$\bar{q}_r = r^2 \frac{\vec{v}_r}{d_r} \tag{22}$$

It is the boundaries of $\{\bar{q}_r\}$ that will be used (in Section IV-I) to determine the boundaries of the COR locus. Therefore, the boundaries of the COR locus, too, can be found by considering only dipods. This is a stronger statement than Mason's theorem 5, which requires tripods. Additionally, we have found the two points constituting the dipods. However, it should be noted that the sufficiency of tripods holds for any workpiece, whereas dipods are sufficient only for a disc.

Figs. 13 and 14 demonstrate that the two classes of dipods considered above, and illustrated in Figs. 15 and 16, generate extremal quotient moments. In other words, the locus $\{\bar{q}_r\}$ of values of \bar{q}_r for all pressure distributions $P(\vec{w})$ satisfying the conditions of Section II-E fall inside the empirical boundary generated by the above dipods. The boundaries themselves

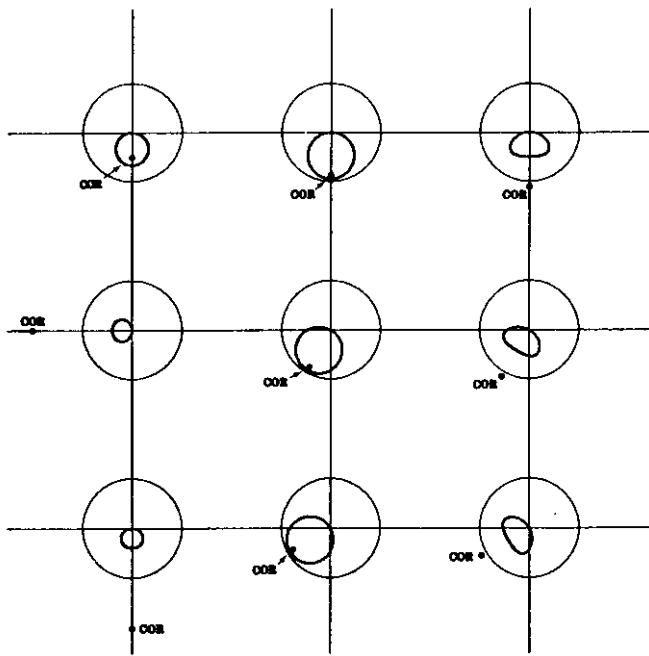


Fig. 17. Boundaries of quotient loci $\{\bar{q}_r\}$ for various \bar{F} . As \bar{F} is changed, the boundary of the quotient locus changes continuously. Sweeping \bar{F} around the CM causes a corresponding rotation of the quotient locus boundary. Changing the distance of \bar{F} from the CM changes the shape and size of the quotient locus boundary.

are, of course, part of $\{\bar{q}_r\}$ since the boundaries are generated by acceptable pressure distributions.

I. Analytic Form of the COR Locus

Having found a parametric representation of the $\{\bar{q}_r\}$ locus, we can find the COR locus. Recall the requirement for minimizing the energy lost to friction (13)

$$r^2 \bar{\alpha} = \bar{q}_r [\bar{\alpha} \cdot (\bar{c} - \bar{F})]. \tag{23}$$

The COR locus is the set of all \bar{F} for which there exists a $\bar{q}_r \in \{\bar{q}_r\}$ satisfying (23).

Equation (23) is a vector equation. The left side obtains its direction from $\bar{\alpha}$. The right side obtains its direction from \bar{q}_r , since $\bar{\alpha} \cdot (\bar{c} - \bar{F})$ is a scalar. To satisfy the vector equation \bar{q}_r must have direction $\bar{\alpha}$. We can rewrite (23) in scalar form, retaining the direction constraint on \bar{q}_r separately

$$r^2 = |\bar{q}_r| [\bar{\alpha} \cdot (\bar{c} - \bar{F})] \tag{24}$$

where $\bar{q}_r \in \{\bar{q}_r\}$ and $\bar{q}_r \parallel \bar{\alpha}$.

We wish to find the locus of \bar{F} for all distributions $P(\bar{w})$. It is best to imagine \bar{F} to be an independent variable. Each value of \bar{F} yields a locus $\{\bar{q}_r\}$, with one element $\bar{q}_r \in \{\bar{q}_r\}$ corresponding to each acceptable pressure distribution $P(\bar{w})$. For some values of \bar{F} the value of \bar{q}_r required to satisfy (24) is in $\{\bar{q}_r\}$; for other values it is not. The former values constitute the COR locus.

It is confusing, but unavoidable, that the locus $\{\bar{q}_r\}$ shifts as we consider different locations of the center of rotation \bar{F} . In Fig. 17 we have plotted several $\{\bar{q}_r\}$ loci for different values of \bar{F} . Note that varying the magnitude of \bar{F} continuously

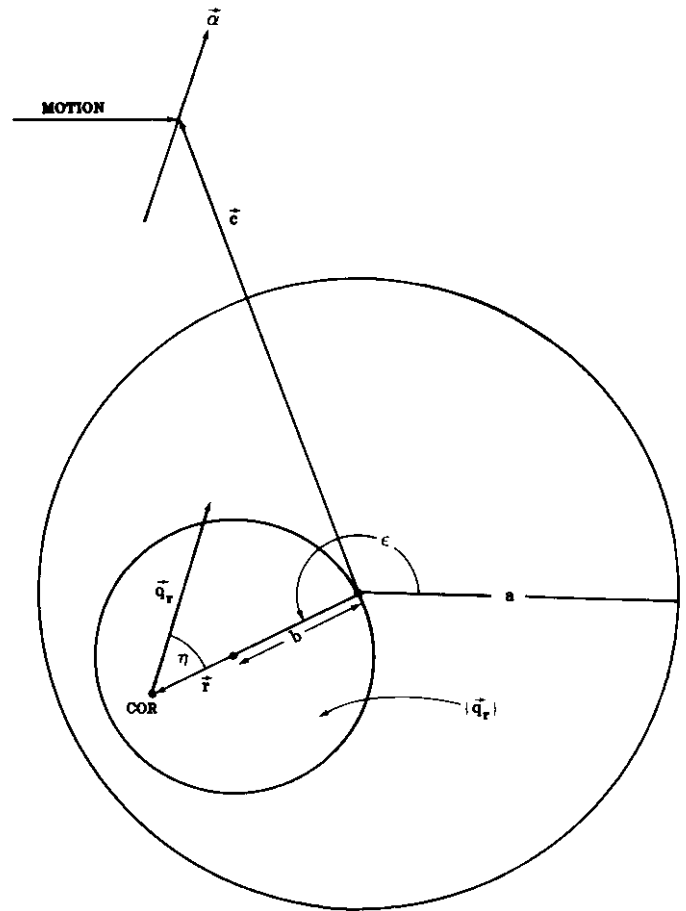


Fig. 18. Variables of (24) for a value of \bar{F} not in the COR locus. Is a proposed value of \bar{F} the COR of the workpiece for some pressure distribution? First generate the quotient locus boundary for the proposed \bar{F} . In this case it is a circle, because \bar{F} falls within the disc. Now compute the value of \bar{q}_r which would be required to satisfy energy minimization (24). Plot it too. If \bar{q}_r falls within the quotient locus boundary (which it does not here), then \bar{F} is the COR of the workpiece for some pressure distribution.

changes the shape or size of the $\{\bar{q}_r\}$ loci. But changing the direction of \bar{F} only causes a corresponding rotation of the $\{\bar{q}_r\}$ locus.

The variables of (24) are shown geometrically in Figs. 18–20. In each figure we have plotted a value of \bar{F} and the locus $\{\bar{q}_r\}$ for that \bar{F} . We then calculate and plot the value of \bar{q}_r required to satisfy (24). In Fig. 18, the value of \bar{q}_r required does not fall in $\{\bar{q}_r\}$, so the value of \bar{F} shown is not in the COR locus. In Fig. 19, the value of \bar{q}_r required does fall in $\{\bar{q}_r\}$, so the value of \bar{F} shown is in the COR locus. In Fig. 20, the value of \bar{q}_r required to satisfy (24) happens to be on the boundary of the $\{\bar{q}_r\}$ locus. The boundary of the COR locus is generated by such cases. Interior points of the COR locus are generated when the \bar{q}_r required is interior to the $\{\bar{q}_r\}$ locus, as in Fig. 19. Since we are interested only in the boundary of the COR locus, we will consider only values of \bar{q}_r which are on the boundary of the $\{\bar{q}_r\}$ locus, as shown in Fig. 20.

J. Solution for the $|COR| < a$ Part of the COR Locus

It will be convenient to represent the COR by its polar coordinates (r, ϵ) , and to define the relative angle η . Both

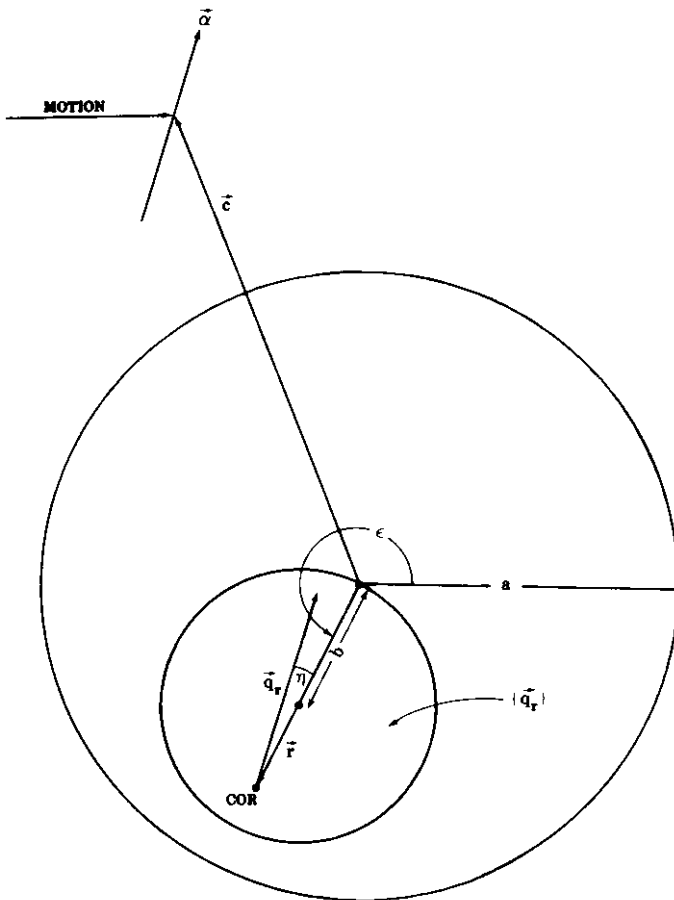


Fig. 19. Variables of (24) for a value of \bar{r} in the COR locus. Here \bar{q}_r does fall within the quotient locus boundary, so the COR is at \bar{r} for some pressure distribution.

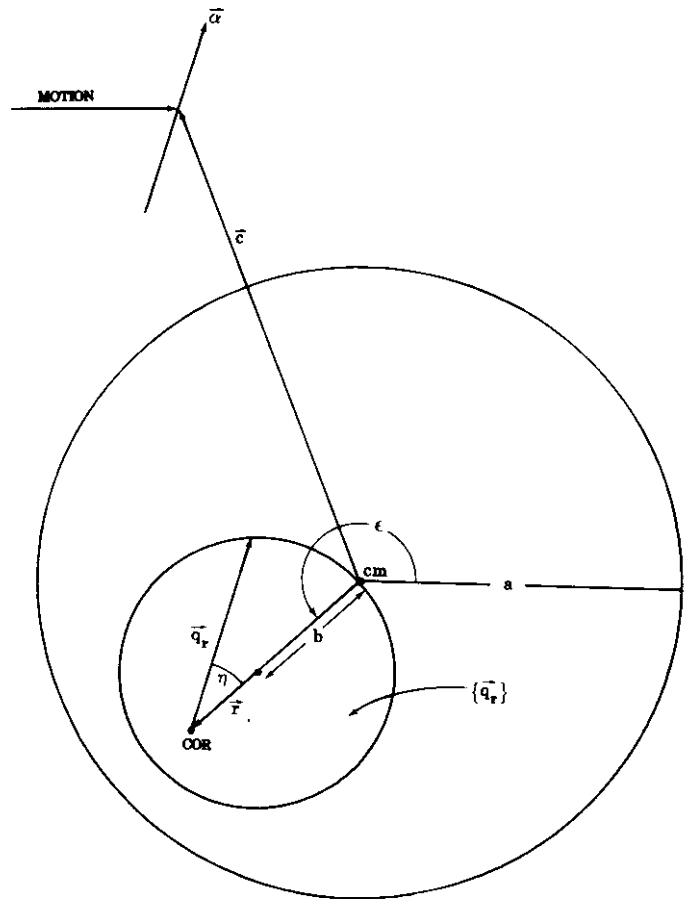


Fig. 20. Variables of (24) for a value of \bar{r} on the boundary of the COR locus. Here \bar{q}_r falls on the boundary of the quotient locus, so \bar{r} is on the boundary of the COR locus. We could test all values of \bar{r} to see if they fall on the boundary in this way. Instead, we generate the boundary of the quotient locus (parametrized by an angle ω in the dipods) and solve for the value of \bar{r} which gives rise to a \bar{q}_r satisfying this figure.

angles are shown in Fig. 20. We have

$$\epsilon = \pi + \alpha - \eta. \tag{25}$$

If $r < a$, the boundary of $\{\bar{q}_r\}$ is a circle. The condition that \bar{q}_r lie on the circle can be expressed as

$$||\bar{q}_r| \bar{a} + (r-b)\bar{c}| = b \tag{26}$$

where b is the radius of the circle, from (21). Equation (26) can be expressed in terms of the angle η as

$$(|\bar{q}_r| - (r-b) \cos \eta)^2 + ((r-b) \sin \eta)^2 = b^2. \tag{27}$$

Solving this quadratic equation for $|\bar{q}_r|$ we find

$$|\bar{q}_r| = (r-b) \cos \eta \pm (b^2 - ((r-b) \sin \eta)^2)^{1/2}. \tag{28}$$

Inserting this value of $|\bar{q}_r|$ into (24) and eliminating the square root we obtain

$$\left(\frac{r^2}{\bar{\alpha} \cdot (\bar{c} - \bar{r})} - (r-b) \cos \eta \right)^2 = b^2 - ((r-b) \sin \eta)^2. \tag{29}$$

Substituting b from (21) and simplifying we find

$$r^2(a+r) + (r-a)[\bar{\alpha} \cdot (\bar{c} - \bar{r})]^2 - 2r^2[\bar{\alpha} \cdot (\bar{c} - \bar{r})] \cos \eta = 0 \tag{30}$$

where $[\bar{\alpha} \cdot (\bar{c} - \bar{r})] = \bar{\alpha} \cdot \bar{c} + r \cos \eta$.

Equation (30) is cubic in r and quadratic in $\cos \eta$. The solution for $\cos \eta$ is

$$\cos \eta = \frac{r((r+a)^2 + (\bar{\alpha} \cdot \bar{c})^2)^{1/2} - a(\bar{\alpha} \cdot \bar{c})}{r(r+a)}. \tag{31}$$

The other quadratic root is invalid. Since η is related by (25) to the polar angle ϵ , (31) describes the boundary of the COR locus in the polar coordinates r, ϵ , for $r < a$. A typical COR locus boundary generated using (31) is shown in Fig. 21.

1) *Extremal Radius of the COR Locus Boundary for $|COR| < a$:* The minimum radius of the COR locus boundary occurs at $\epsilon = \alpha$, which corresponds to $\eta = \pi$. From (30) we find

$$r_{\min} = \frac{a(\vec{\alpha} \cdot \vec{c})}{2a + (\vec{\alpha} \cdot \vec{c})} \tag{32}$$

Note that r_{\min} is not the minimum distance from the CM to an *element* of the COR locus; that distance is zero. r_{\min} is the minimum distance from the CM to the *boundary* of the COR locus. r_{\min} is indicated in Fig. 21.

It will also be useful to have the angles at which the COR locus boundary intersects the disc boundary. From (31) we obtain

$$\cos \eta_{r=a} = \frac{((\vec{\alpha} \cdot \vec{c})^2 + 4a^2)^{1/2} - (\vec{\alpha} \cdot \vec{c})}{2a} \tag{33}$$

From (30) we can find the radius of curvature of the COR locus boundary at r_{\min} to be

$$s = \frac{a(\vec{\alpha} \cdot \vec{c})(\vec{\alpha} \cdot \vec{c} + 2a)^2}{(\vec{\alpha} \cdot \vec{c})^3 + 4a(\vec{\alpha} \cdot \vec{c})^2 + 8a^2(\vec{\alpha} \cdot \vec{c}) + 4a^3} \tag{34}$$

K. Solution for the $|COR| > a$ Part of the COR Locus

If $r > a$, we cannot find a simple equation analogous to (26) constraining \vec{q}_r to the boundary of $\{\vec{q}_r\}$. An effective approach is to parametrize the boundary of the $\{\vec{q}_r\}$ locus by the angle ω of (22), and solve for both ϵ and r by binary search.

For each ω the following procedure is used: We guess a value of r , in the range $a < r < r_{\text{tip}}$, where r_{tip} is an upper bound to be found in Section IV-J1. Equation (22) is then used to calculate a value of \vec{q}_r . Angle η is related to the terms of (22) by

$$\eta = \arctan \frac{-\vec{v}_x}{\vec{v}_y} \tag{35}$$

and so can be computed from ω . Equation (24) can be written in terms of the angle η as

$$r^2 = |\vec{q}_r|(\vec{\alpha} \cdot \vec{c} + r \cos \eta) \tag{36}$$

which is easily tested. If it is satisfied, we have found angle η and magnitude r describing a point on the boundary of the COR locus. ϵ is then obtained from η using (25).

If the left-hand side of (36) is greater (respectively, less) than the right-hand side, we increase (respectively, decrease) the value of r guessed above. In this way we perform a binary search, quickly converging on a solution for r and ϵ .

Fig. 22 shows the boundary of the COR locus for various \vec{c} and α . The part of the boundary inside the disc was computed using (31), while the part outside the disc was found by binary search as outlined here. Calculation of each locus required about 2 CPU seconds on a VAX-780.

1) *Tip Line:* We can calculate the extremum of the COR locus analytically. For many purposes this may be all that is required. Additionally, it gives us a range within which to conduct the binary search discussed in Section IV-K. By

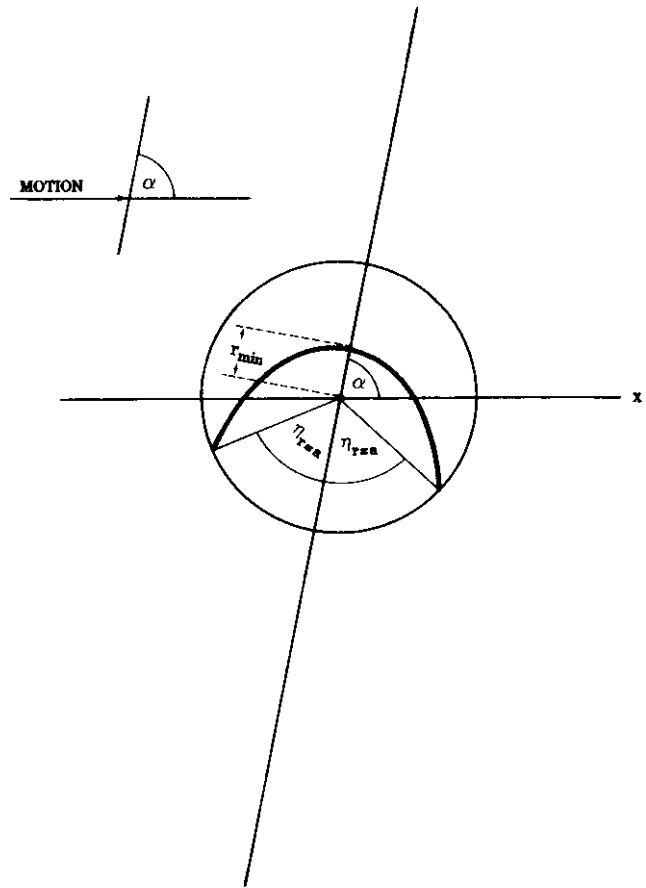


Fig. 21. COR locus boundary for $r < a$. Shown is the part of the COR locus boundary internal to the disc. The pressure distributions which give rise to COR's on the bold boundary are dipods, with one point of support at the COR and the other on the periphery of the disc as far as possible from the COR. r_{\min} is the minimum distance from the CM to the boundary of the COR locus. Note that r_{\min} is not the minimum distance from the CM to an *element* of the COR locus; that distance is zero.

symmetry, r takes on an extremal value when $\eta = 0$. In Fig. 16 this corresponds to $\vec{v}_x = 0$, which in turn occurs only when $\omega = 0$ or $\omega = \pi/2$.

The extremum at $\omega = 0$ has no apparent meaning. At $\omega = \pi/2$ we find from (22)

$$\vec{q}_r = \vec{\alpha} \frac{r^3}{r^2 + a^2} \tag{37}$$

At this value (24) yields

$$r_{\text{tip}} = \frac{a^2}{\vec{\alpha} \cdot \vec{c}} \tag{38}$$

This is the greatest distance \vec{r} may be from the CM, and it occurs at polar angle $\epsilon = \pi + \alpha$. In Fig. 8 we plot r_{tip} versus contact angle α , for a given value of \vec{c} . As α is varied, the tip of the COR locus at distance r_{tip} from the CM traces out a straight line, the *tip line*.

The use of this graphical construction is illustrated in Fig. 8. For a given value of α , as shown, r_{tip} is at the intersection of the tip line described above with a ray from the CM at angle $\pi + \alpha$.

An interesting case occurs when $\vec{\alpha}$ becomes perpendicular to \vec{c} . (Note that this does not require $\alpha = \pi/2$.) As $\vec{\alpha} \cdot \vec{c} \rightarrow 0$,

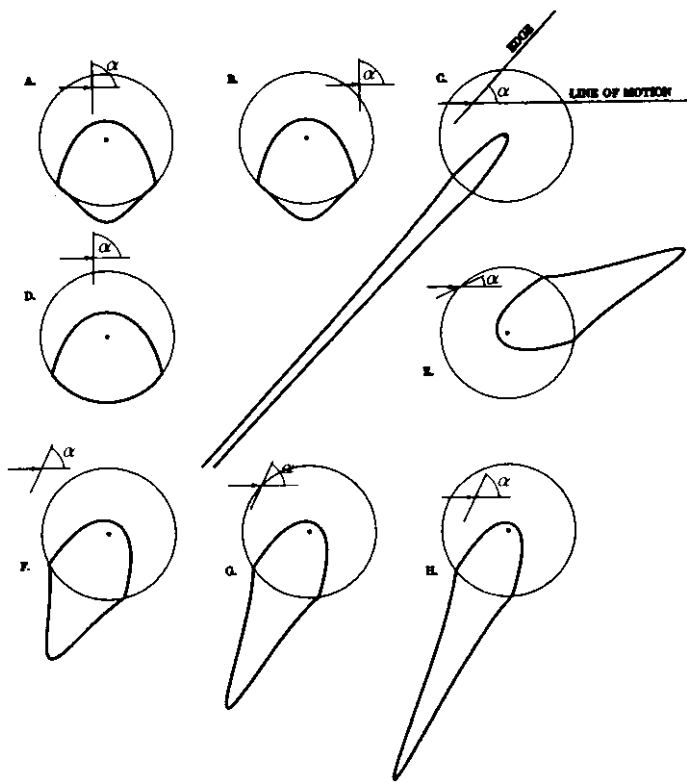


Fig. 22. Boundaries of COR loci for various \bar{c} and α . The pressure distributions which give rise to COR's on the boundary of the COR locus external to the disc are dipoles, with both points of support on the periphery of the disc diametrically opposite each other. The boundary is generated as the angle ω parametrizing the dipoles is varied (Fig. 16). In the figures the point at which the workpiece is being pushed is indicated by an arrowhead, and the angle (α) of the edge being pushed is indicated by the line the arrowhead contacts. (In several cases the arrowhead is outside the disc; this is unrealistic.)

we have $r_{tip} \rightarrow \infty$. The COR at infinity corresponds to pure translation perpendicular to \bar{c} . In Fig. 22, sketch (C) shows a case in which \bar{c} is almost perpendicular to \bar{c} . Note that $r_{tip} \rightarrow \infty$ does not mean that pure translation is assured; only that it is possible. The COR may fall at any distance less than r_{tip} .

The radius of curvature of the COR locus boundary at the tip can be found analytically to be

$$s = \frac{r_{tip}}{\frac{1}{2} + \frac{r_{tip}^4}{a^4}} \quad (39)$$

L. Symmetries of the COR Locus

We now have the ability to quickly compute the COR locus for any \bar{c} and α .

The COR locus is a function of four parameters: the disc radius a , the edge angle α (which may be the angle of the pushing fence or of the workpiece edge pushed, measured with respect to the line of motion of the pusher), and the two components of the point of contact \bar{c} between pusher and pushed workpiece. However, the COR locus is really much simpler in functional dependence than the existence of four parameters would seem to imply.

The most obvious symmetry is one of total size: if both \bar{c} and a are changed by a factor of γ , the COR locus will be scaled by a factor of γ as well.

Note that the COR locus has an axis of symmetry through the CM at angle $\bar{\alpha}$. The "tip" of the locus falls on this axis of symmetry, and the tip line construction (Section IV-K1 and Fig. 8) makes use of this symmetry.

The shape of the COR locus depends *only* on the distance of the tip of the locus from the CM, $a^2/\bar{\alpha} \cdot \bar{c}$, as a multiple of the disc radius a . If COR loci for various tip distances are precomputed, we need only select the appropriate one, scale it by the disc radius a , and tilt it at the appropriate angle α .

Finally, the COR locus can depend only on the force and torque applied by the pusher. Displacing the point of contact \bar{c} perpendicular to the edge angle α (i.e., along the line of action of the applied force) changes neither force nor torque, and therefore cannot change the COR locus. In Fig. 22, the COR loci in sections A and B are identical because the point of contact \bar{c} has been displaced perpendicular to the edge.

M. Summary

We have found the boundary of the COR locus for any choice of \bar{c} and α . Within the disc, the boundary is given by a simple formula relating r and ϵ , the polar coordinates of the boundary (31). Outside of the disc, the polar coordinates of the boundary are found by binary search as outlined in Section IV-K. For most applications it is not necessary to find the entire COR locus boundary, as simple formulas exist for several important points on the boundary. Most important of these is the tip-line construction described in Section IV-K1.

Slightly more discussion of the boundaries of the quotient locus (Section IV-G) is in order. The quotient locus is an intermediate mathematical construction whose boundaries are transformed directly into the boundaries of the COR locus. The boundaries of the quotient locus were found by making an informed guess as to the pressure distributions which give rise to the boundaries. This guess was tested by extensive computer simulation of random pressure distributions. These numerical results suggest that the analytic quotient locus boundaries were indeed correct: no randomly generated pressure distribution ever appeared which landed outside the analytic boundary of the quotient locus. Because of the empirical justification of the boundaries of the quotient locus, however, our derivation of the analytic boundaries of the COR locus is not rigorous. It may well be that it was this step (requiring computer testing) which prevented analytic solution for the COR locus long ago [6], [8], [17].

V. APPLICATION

A useful application of the results found above is to the problem of aligning a workpiece by pushing it. In Fig. 2 a misoriented rectangle is being pushed by a fence. The fence is moving in a direction perpendicular to its front edge. Evidently the rectangle will rotate CW as the fence advances [10], and will cease to rotate when the edge of the rectangle comes into contact with the front edge of the fence [2]. The problem is to find how far the fence must advance to assure that the CW motion is complete.

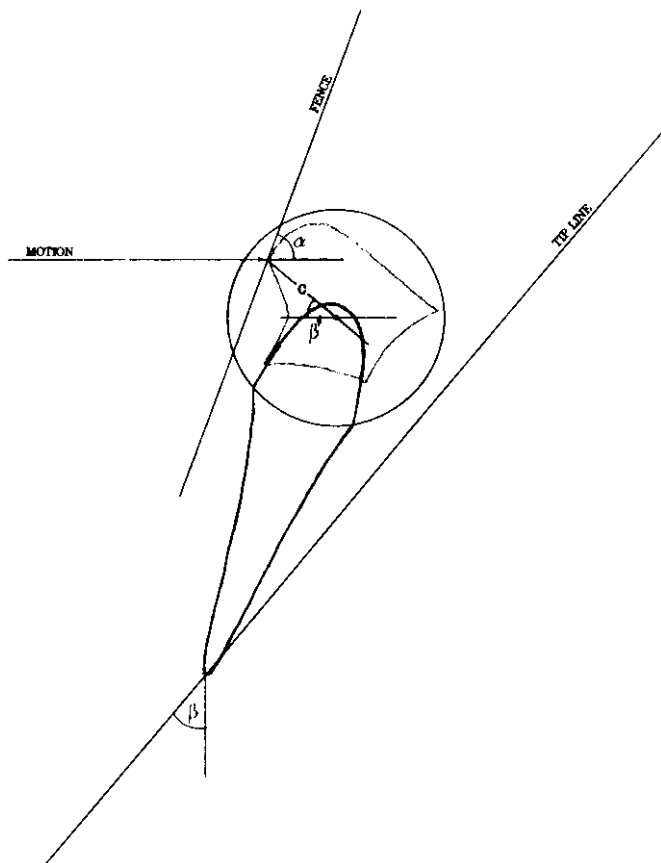


Fig. 23. Initial configuration of workpiece and fence, and resulting COR locus. The fence travels horizontally and contacts the shaded workpiece as shown. As the fence advances the workpiece rotates clockwise at a rate which depends upon the location of the COR. The workpiece is circumscribed by a disc of radius a , since this is the only shape for which we can find exact COR locus boundaries. The ice-cream-cone shaped COR locus boundary is shown. The minimum rate of rotation occurs when the COR is at the tip of the locus.

The geometry of this problem differs from the geometry used in previous sections. Previously, a point pusher made contact with a straight workpiece edge. Here, the straight edge of the pusher makes contact with a point (corner) of the workpiece. But since the coefficient of friction between the pusher and the edge of the workpiece (μ_c) is zero, we know that in either case the force exerted by the pusher on the workpiece is normal to the edge, regardless of whether the edge is that of the pusher or that of the workpiece. Since the motion of the workpiece can depend only on the force applied to it, the angle of the fence takes the place of the angle of the workpiece edge (α), and all the results derived above remain unchanged.

In this section we will generalize the problem slightly, relative to the problem illustrated in Fig. 2:

- The workpiece pushed is arbitrary, not a rectangle.
- The motion of the fence is not necessarily perpendicular to its face.

First we circumscribe a disc of radius a about the workpiece. The disc is centered at the CM of the workpiece (Fig. 23). Note that the contact point need not be on the perimeter of the circumscribed disc.

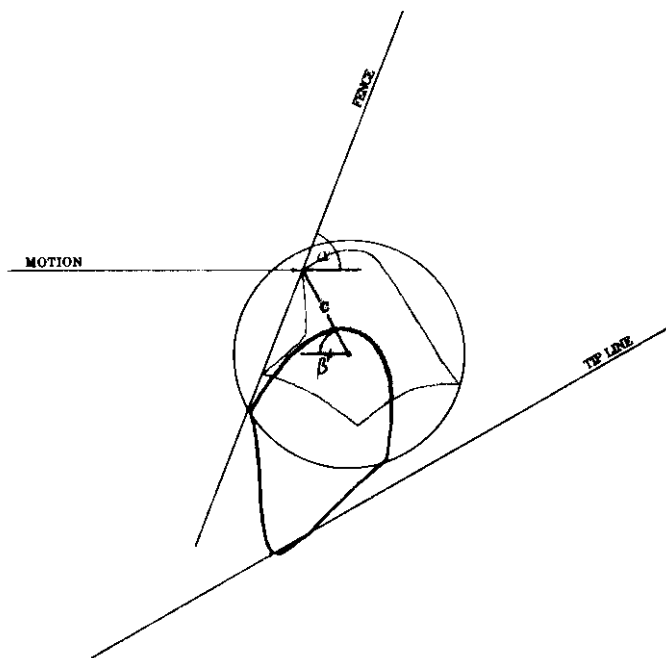


Fig. 24. Final configuration of workpiece and fence, and resulting COR locus. Finally, the workpiece has rotated into alignment with the fence. At the moment before alignment the COR locus boundary is as shown. We want to determine the maximum advance of the fence which could possibly be required to get from the orientation shown in Fig. 23 to the one shown here. So we assume that the COR is always at the tip of the locus, which is the point for which the workpiece rotates most slowly as the fence advances.

We know [10] that the workpiece will rotate CW, and will cease to rotate when the final configuration shown in Fig. 24 is reached.

We now ask the rate of rotation of the workpiece about the COR, with unit advance of the pusher. Let the angle of the CM from the direction of motion of the pusher be β . This is also the angle between the tip line and the perpendicular to the line of motion. (Both angles are indicated in Fig. 23.) From (4) we have

$$\delta x = \frac{d\beta}{\sin \alpha} \bar{\alpha} \cdot (\bar{c} - \bar{r}) \tag{40}$$

where \bar{r} is the distance from the CM to the COR. The rate of rotation per advance of the pusher, $d\beta/dx$, depends on where the COR \bar{r} falls within the COR locus. Since we wish to find the longest push which could possibly be necessary to achieve a certain amount of rotation, we need to know for which \bar{r} in the COR locus $d\beta/dx$ is minimized, i.e., we consider the worst case location for \bar{r} . This occurs when \bar{r} is at the tip of the COR locus. Therefore we have

$$\delta x = \frac{d\beta}{\sin \alpha} \bar{\alpha} \cdot (\bar{c} - \bar{r}_{tip}). \tag{41}$$

Using r_{tip} from (38), this can be integrated to yield the indefinite integral

$$x = \frac{-c \sin(\alpha + \beta)}{\sin \alpha} - \frac{a^2}{2c \sin \alpha} \log \left| \frac{1 + \sin(\alpha + \beta)}{1 - \sin(\alpha + \beta)} \right|. \tag{42}$$

To find the maximum pushing distance Δx , required to cause the workpiece to rotate from its initial configuration shown in Fig. 23 to its final configuration shown in Fig. 24, we simply substitute the initial and final values of β into (42), and take the difference $x_{\text{final}} - x_{\text{initial}}$.

VI. SOLUTION FOR THE COR LOCUS INCLUDING CONTACT FRICTION

Up to now we have assumed that the coefficient of friction between the pusher and the edge of the pushed workpiece was zero, i.e., $\mu_c = 0$. The pushing force was therefore normal to the edge being pushed. Since the motion of the workpiece can depend only on the force applied to it, we will designate the locus we found $\{COR\}_\alpha$ to indicate its dependence on the force angle, which is perpendicular to $\vec{\alpha}$.

We know how to generate the COR locus for a given angle of applied force. Unfortunately, when $\mu_c > 0$, it is not possible to tell what the force angle will be. We will describe angular *limits* on the force angle in Section VI-A, but within those limits the force angle depends on the pressure distribution, which is not known. If we already knew that the COR would be at a certain point, however, it would then be possible to find the force angle.

Our approach to this problem is to seek COR's which are consistent with the force angle which gives rise to them. For each force angle ϕ within the angular limits, we generate $\{COR\}_\phi$. For each COR in $\{COR\}_\phi$ we find the force angle implied. If the force angle implied matches ϕ , that COR is a possible one for the workpiece. This formulation seems to threaten a great deal of computation, which in fact is not required.

We will refer to the set of consistent COR's as the *COR sketch*, to distinguish it from the elementary COR loci $\{COR\}_\phi$ produced for known force angles. Two elementary COR loci will be used in the construction of the COR sketch. In the figures, these COR loci will be left visible in outline, while the actual COR sketch—the consistent COR's—will be shown shaded.

A. Contact Friction and the Friction Cone

Let μ_c be the coefficient of friction between the pusher and the workpiece. If $\mu_c > 0$, two distinct modes of behavior of the system are possible: *sticking* and *slipping*. In Fig. 2, sticking means that the element of the fence in contact with the corner of the workpiece remains invariant as the pusher's motion proceeds. Referring to Fig. 3, sticking means the element of the workpiece edge which is in contact with the pushing point remains invariant as the pusher's motion proceeds. Slipping is simply the case in which either the element of the pusher or the element of the workpiece, which are in contact with each other, changes as the motion proceeds.

Define

$$\nu = \tan^{-1} \mu_c. \quad (43)$$

In Fig. 25 we construct a *friction cone*, of half angle ν , at the point of contact \vec{c} . The cone is centered on the edge normal, at

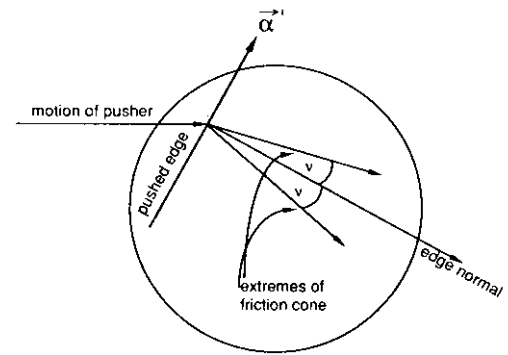


Fig. 25. Construction of the friction cone. The force which the pusher applies to the workpiece edge must lie within the friction cone shown. If we attempt to apply a force at an angle falling outside the friction cone, friction cannot support the component of force tangential to the workpiece edge. The pusher will then slip along the workpiece edge, and the actual force applied will lie along one extreme of the friction cone. If we apply a force which lies within the friction cone, the pusher will not slip relative to the workpiece edge.

angle $\alpha - \pi/2$ relative to horizontal. Note that the edge may be either that of a fence, where it contacts a corner of the workpiece (as in Fig. 2), or an edge of the workpiece, where it is touched by a corner of the pusher (as in Fig. 3). The friction cone is a well-known construction in classical mechanics. (Recently, Erdmann [3] has extended the friction cone to configuration space.)

The component of the applied pushing force tangential to the edge, F_{\parallel} , is supported by friction. Its magnitude cannot exceed $\mu_c F_{\perp}$, where F_{\perp} is the component of force normal to the edge. Therefore, the total applied force vector must lie within the friction cone.

If we attempt to apply a force to the workpiece edge at an angle outside of the friction cone, friction cannot support the tangential component of force. The result is slipping along the edge, and the actual applied force is directed along one extreme of the friction cone. If we apply a force within the friction cone, friction is sufficient to support the tangential component of force, and slipping will not occur: we have sticking.

In short, slipping is only consistent with a force vector at one extreme of the friction cone, while sticking is only consistent with a force vector within the friction cone. It is not usually possible to tell if slipping or sticking will occur: often, depending on the pressure distribution, either may occur.

B. Sticking and Slipping Zones

In this section we presume that the COR is known: a single point is the COR for the workpiece. We divide the plane into three zones, called the *sticking line*, the *up-slipping zone*, and the *down-slipping zone* (Fig. 26). The up-slipping and down-slipping zones are regions of the plane with positive areas, while the sticking line is merely a line, but all three will be collectively designated "sticking and slipping zones." The motion of the workpiece is qualitatively different for the COR falling in each of the three zones.

The sticking line is the line perpendicular to the pusher's line of motion, intersecting the point of contact between

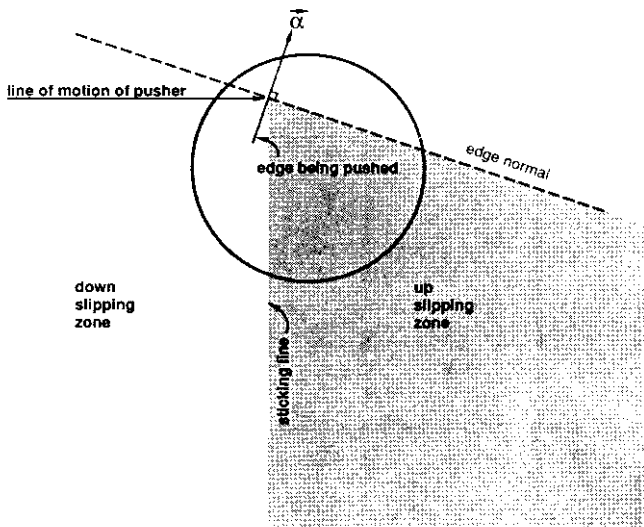


Fig. 26. Construction of zones: up-slipping, down-slipping, and sticking line. The location of the COR has implications for slipping or sticking of the pusher with respect to the workpiece edge. If the COR lies on the sticking line shown, pusher and workpiece edge move along (horizontally) together and there is no slipping of one relative to the other. If the COR falls in the up- or down-slipping zones to either side of the sticking line, then the workpiece has a vertical component of motion and so must slip relative to the pusher (which moves horizontally).

pusher and workpiece (i.e., \vec{r} lies on the sticking line). Since we choose to draw the pusher's line of motion horizontally, the sticking line is vertical. The sticking line divides the down-slipping zone, on its left, from the up-slipping zone, on its right. Also shown in Fig. 26 is the edge normal line. Above this line, the up-slipping and down-slipping designations are reversed. The area above the edge normal will be unimportant, however.

1) *Sticking Line*: First consider the workpiece's motion when the COR is on the sticking line. Recall that the motion of any point of the workpiece is perpendicular to the vector from the COR to that point. If the COR lies on the sticking line, the workpiece's motion at the point of contact is perpendicular to the sticking line, and is therefore parallel to the pusher's line of motion.

Since the pusher's line of motion and the workpiece's motion at the point of contact are parallel, the pusher and the workpiece, at the point of contact, travel along together. There is no need for one to slip relative to the other; the workpiece and the pusher are *sticking* at the point of contact.

2) *Slipping Zones*: Now suppose that the COR is in the down-slipping zone. The workpiece's motion at the point of contact has a downward component, relative to the pusher's line of motion. The pusher-workpiece contact must be *slipping*, with the workpiece moving down relative to the pusher.

Similarly, if the COR is in the up-slipping zone, the workpiece at the point of contact moves up relative to the pusher as the pusher advances.

C. Consistency for Slipping

If we know that the workpiece is slipping relative to the pusher (and whether up or down), then the force angle is

known: it is at one extreme of the friction cone, perpendicular to $\alpha \pm \nu$.

If the COR lies in the down-slipping zone, the workpiece moves *down* as the pusher advances. Therefore, the force angle must be along the upper extreme of the friction cone, at angle $\alpha + \nu - \pi/2$. Similarly, if the COR lies in the up-slipping zone, the workpiece moves *up* as the pusher advances, and the force angle must be along the lower extreme of the friction cone, at angle $\alpha - \nu - \pi/2$.

Combining the above observations, we see that if slipping occurs, the COR must be either in $\{COR\}_{\alpha+\nu}$ and the down-slipping zone, or in $\{COR\}_{\alpha-\nu}$ and the up-slipping zone. These two intersection regions are called the *down-slipping locus* and the *up-slipping locus*. A very similar construction was used by Mason and Brost in [12, figure 5].

The down-slipping and up-slipping loci are two components of the COR sketch, because every COR in either locus is consistent with the force angle that was used to generate it. We construct the down-slipping locus of the COR sketch by intersecting the down-slipping zone (left of the sticking line) with $\{COR\}_{\alpha+\nu}$. We construct the up-slipping locus of the COR sketch by intersecting the up-slipping zone (right of the sticking line) with $\{COR\}_{\alpha-\nu}$.

In Fig. 9, $\{COR\}_{\alpha+\nu}$ and $\{COR\}_{\alpha-\nu}$ are shown in outline. The down-slipping and up-slipping loci are the shaded areas left and right of the sticking line, respectively.

D. The Sticking Locus

The third set of consistent COR's belong to the *sticking locus*. The sticking locus, together with the up-slipping and down-slipping loci whose construction was described above, are all the COR's consistent with the force angle they presume. The three consistent loci constitute the COR sketch.

If the COR lies on the sticking line, sticking occurs. The force angle can be anywhere in the friction cone, i.e., between $\alpha - \nu - \pi/2$ and $\alpha + \nu - \pi/2$. The sticking locus is therefore the intersection of the sticking line with the union, over all ϕ perpendicular to a force angle within the friction cone, of $\{COR\}_{\phi}$. The sticking locus is shown as a bold section of the sticking line in Fig. 9.

As discussed above, the two slipping loci are $\{COR\}_{\alpha\pm\nu}$, possibly cut off by the sticking line. In calculating either slipping locus, the force angle is known: it is $\alpha \pm \nu - \pi/2$. But in calculating the sticking locus (which is just a simple line segment), the force angle is not known, except that it lies within the friction cone. To find the endpoints of the sticking locus exactly, we could form every locus $\{COR\}_{\phi}$, for $\alpha - \nu < \phi < \alpha + \nu$, and intersect each locus with the sticking line. The union of these intersections is the sticking locus. This is not an efficient method.

The lower endpoint of the sticking locus is of particular interest. It is possible to approximate it by using the tip-line construction described in Section IV-K1. The procedure for finding the sticking locus described above is to form every locus $\{COR\}_{\phi}$, for $\alpha - \nu < \phi < \alpha + \nu$, and intersect each locus with the sticking line. As we vary ϕ , $\{COR\}_{\phi}$ varies continuously from $\{COR\}_{\alpha-\nu}$, which is outlined in Fig. 9, to

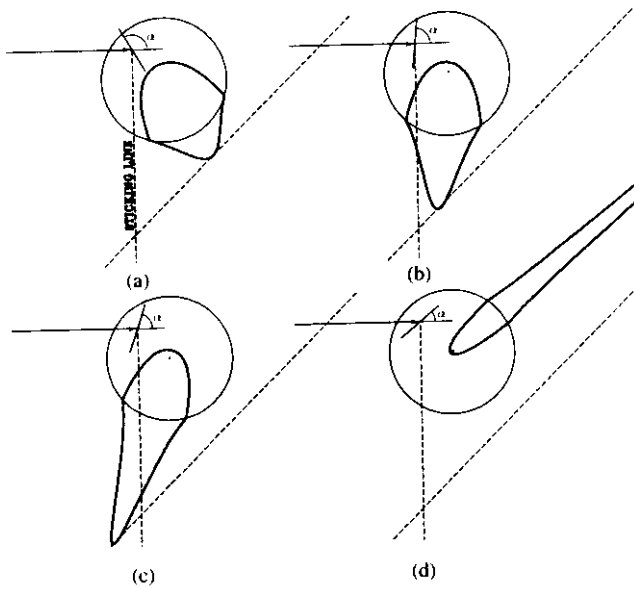


Fig. 27. Possible elementary configurations of the COR locus. (a) Pure slipping. (b) Same-sided split. (c) Opposite-sided split. (d) Wrapped. As the angle α of the pushed edge varies, the COR locus may intersect the three zones in different ways, called distinct "elementary configurations." The entire locus may fall in the down-slipping zone (a), the locus may intersect both slipping zones and the sticking line with the tip of the locus on one side or the other (b) and (c), or the locus may "wrap" through infinity as shown in (d).

$\{COR\}_{\alpha+\nu}$, also shown outlined. The tips of the extreme loci, as well as of all intermediate loci, fall on the tip line. The tip line is shown dotted in Fig. 9.

Were it not for the fact that each $\{COR\}_{\phi}$ locus drawn dips slightly below the tip line, the lower endpoint of the sticking locus would be exactly at the tip line. We will use this approximation. The small error so introduced can be bounded [15], and is usually negligible.

Using the tip line to approximate the lower endpoint of the sticking locus in this way depends on an unstated assumption: that the tip of $\{COR\}_{\alpha-\nu}$ lies to the left of the sticking line while the tip of $\{COR\}_{\alpha+\nu}$ lies to the right of the sticking line. This assumption is necessary so that the tip of some intermediate locus $\{COR\}_{\phi}$ will intersect the sticking line. In Section VI-F, we will deal methodically with this problem.

The shaded slipping loci and the bold sticking locus of Fig. 9 contain all the possible locations of the COR.

E. Possible Configurations of an Elementary COR Locus

The down-slipping, up-slipping, and sticking loci play an important part in the rest of this work. It is worth describing the qualitatively different ways in which an elementary COR locus $\{COR\}_{\alpha}$ can intersect the three zones (down-slipping, up-slipping, and sticking line) in order to form the loci. These qualitatively different types of intersections will be called distinct *elementary configurations*. Later we will describe the qualitatively different COR sketches which can occur; the latter will be called distinct *sketches*. Two COR loci are used in the construction of a COR sketch, so there are more distinct sketches than distinct elementary configurations.

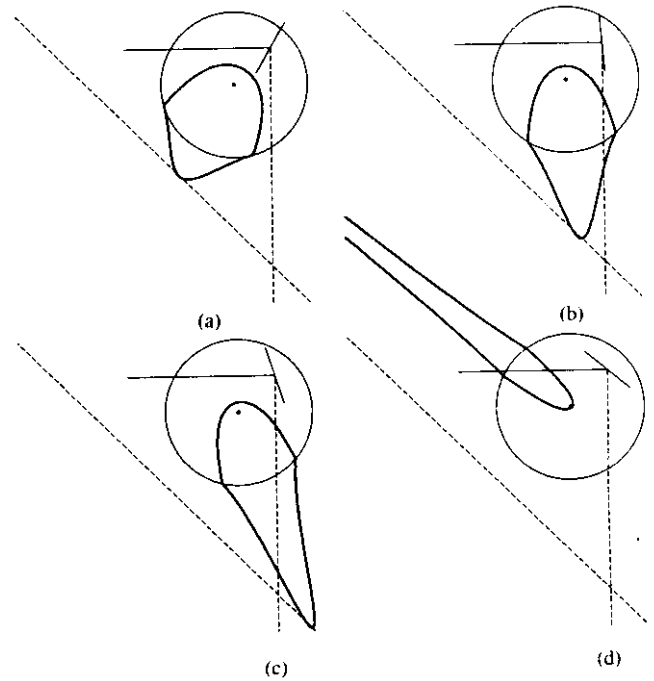


Fig. 28. Possible elementary configurations with sticking line to the right of the CM. The same four elementary configurations can be defined when the sticking line is to the right of the CM. (a) Pure slipping. (b) Same-sided split. (c) Opposite-sided split. (d) Wrapped.

For a given contact point \vec{c} , changing α yields four distinct elementary configurations of the resulting COR loci. In Fig. 27(a), the *pure slipping* elementary configuration, the entire COR locus falls in the up-slipping zone. In Fig. 27(b), the COR intersects all three zones, but the tip of the locus falls on the same side of the sticking line as the CM. This is the *same-sided-split* elementary configuration. As α is further decreased, the tip of the COR locus crosses the sticking line, entering the *opposite-sided-split* elementary configuration, as shown in Fig. 27(c). Finally, when α decreases to the point where the edge normal at \vec{c} intersects the CM, the COR locus goes to infinity [10]. The COR at infinity implies pure translation (with no rotation) of the workpiece as the pusher advances. Beyond this point, the workpiece's sense of rotation switches from clockwise to counterclockwise. For our purposes in constructing a COR sketch, counterclockwise rotation is unphysical [10], and so we will class this, and pure translation as one elementary configuration, the *wrapped* elementary configuration, as shown in Fig. 27(d). No part of a "wrapped" locus will ever contribute to the COR sketch, yet we will continue to draw its outline as shown in the figure.

The same four elementary configurations can be defined (now with increasing α) when the sticking line is to the right of the CM (Fig. 28).

F. Possible Distinct COR Sketches

Depending on α and μ_c , each of the two elementary COR loci $\{COR\}_{\alpha\pm\nu}$ used in constructing the COR sketch may be any of the four elementary configurations described in Section VI-E (pure slipping, same-sided split, opposite-sided split, or wrapped). There are nine possible distinct sketches composed

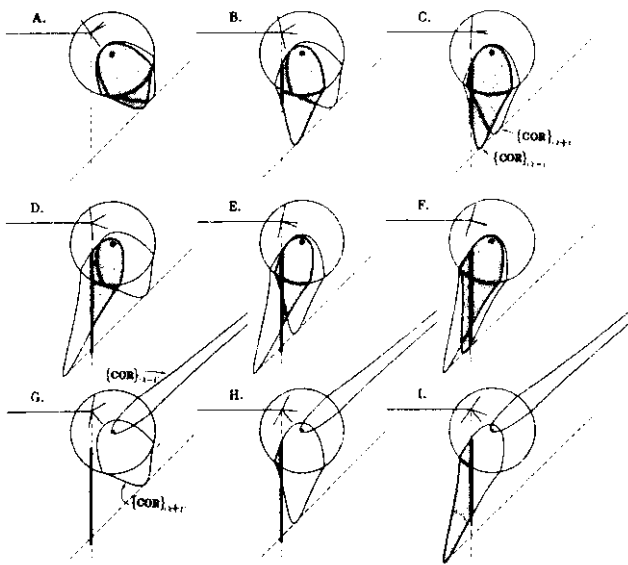


Fig. 29. Nine distinct COR sketches with respect to the sticking line. Depending on the angle α of the pushed edge (not labeled here) and the coefficient of friction μ_c (which determines the width of the friction cones shown), the two elementary COR loci which contribute to a COR sketch may intersect the slipping and sticking zones in nine different ways. Look closely at each distinct sketch to understand the origin of the sticking locus (the bold section of the sticking line). The sticking locus is the intersection of $\{COR\}_\phi$ with the sticking line, as ϕ is swept from $\alpha + \nu$ to $\alpha - \nu$. The sweeping is always *clockwise*. In sketch (G), sweeping clockwise means sweeping from the pure slipping locus, clockwise, to the wrapped locus. The intermediate loci therefore do intersect the sticking line, even though neither locus $\{COR\}_{\alpha \pm \nu}$ does.

of two elementary configurations, as shown in Fig. 29. (Of the 4^2 combinations, 6 are eliminated because the tip of $\{COR\}_{\alpha+\nu}$ cannot be left of the tip of $\{COR\}_{\alpha-\nu}$. The one sketch in which both $\{COR\}_{\alpha \pm \nu}$ are "wrapped" elementary configurations is inconsistent with clockwise rotation of the workpiece.)

It is worth looking carefully at each sketch, in particular to understand the construction of the sticking locus. The sticking locus is the intersection of $\{COR\}_\phi$ with the sticking line, as ϕ is swept from $\alpha + \nu$ to $\alpha - \nu$. The sweeping is always *clockwise*. In sketch (G), sweeping clockwise means sweeping from the pure slipping locus, clockwise, to the wrapped locus. The intermediate loci therefore do intersect the sticking line, even though neither locus $\{COR\}_{\alpha \pm \nu}$ does. Unless this is understood the origin of the sticking locus in sketches (G) and (H) will remain mysterious.

Several of the sketches shown in Fig. 29 have interesting properties. In sketch (A), the workpiece must slip up relative to the pusher. In sketches (B) and (D), the workpiece must stick or slip up. In sketch (G), the workpiece must stick to the pusher. In sketches (H) and (I), the workpiece must stick or slip down. In the remaining sketches (C), (E), and (F), either mode of slipping, or sticking, is possible, depending on the pressure distribution.

Analogous qualitative results are possible when the point of contact \bar{c} is to the right of the CM. The distinct COR sketches for this case can be obtained from those shown in Fig. 29 by reflecting about a vertical axis. (The pusher's motion should still be considered left-to-right, however.) The distinct

sketches for counterclockwise rotation of the workpiece may be obtained by reflecting about a horizontal axis.

VII. FROM INSTANTANEOUS MOTION TO GROSS MOTION

We have shown how to find all possible instantaneous motions of a pushed sliding workpiece, given only the parameters α , \bar{c} , and a . In some cases it is possible to say with certainty that a particular kind of motion, such as sticking, can or cannot occur. The set of possible COR's, as found by constructing the COR sketch, describes completely the possible instantaneous motions of the workpiece as long as those parameters remain in effect. Usually however, the instantaneous motion which results changes the parameters (except the radius a), so that a new COR sketch must be constructed.

Often we wish to calculate not the bounds on the instantaneous direction of motion, as above, but bounds on a gross motion of the workpiece which can occur concurrently with some other gross motion of known magnitude. (For instance, we may wish to find bounds on the displacement of the pusher which occurs while the workpiece rotates 15° .) Our approach to dealing with gross motion follows a definite strategy, which will be illustrated in the sample problems solved in Sections VIII-X.

Suppose we wish to find the greatest possible change in a quantity x , while quantity β changes from β_{initial} to β_{final} . From the geometry of the problem we find an *equation of motion* relating the instantaneous motions dx and $d\beta$. We then construct the COR sketch for each value of β . In each sketch we locate the possible COR which maximizes $dx/d\beta$. Using that COR, we integrate the equation of motion from β_{initial} to β_{final} , yielding an upper bound for the quantity x .

Sometimes the possible COR which maximizes $dx/d\beta$ can be found analytically, or at least approximated analytically, and sometimes it must be found numerically. When an analytical solution is found, it may or may not be possible to integrate the equation of motion in closed form using that analytical solution. The examples which follow illustrate all of these situations.

VIII. EXAMPLE: ALIGNING A WORKPIECE BY PUSHING WITH A FENCE

In this example, we wish to find the maximum distance a fence must advance after first contacting a workpiece, in order to assure that an edge of the pushed workpiece has rotated into contact with the fence. A typical initial configuration is shown in Fig. 30, with the workpiece shown shaded. (Note that the fence does not advance perpendicular to its front edge.) The final configuration is shown in Fig. 31. (In Section V we have solved this problem for the case where $\mu_c = 0$.)

Also shown in Fig. 30 is the COR sketch for the initial configuration, and the angle β between the line of motion and the line from the point of contact to the CM. β is also the angle between the tip line and the sticking line. Angle β changes from 45° initially in Fig. 30 to 80° in the final configuration, Fig. 31. Note that a 1° rotation of the workpiece about the COR will produce a 1° change in β as well. We wish to find the advance x of the pusher (fence) required to change β by 35° .

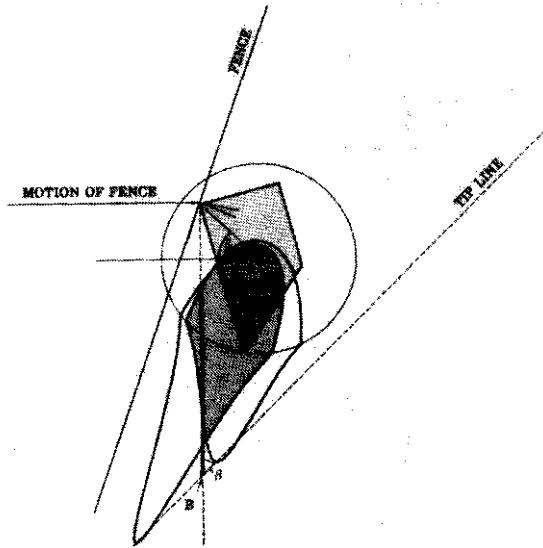


Fig. 30. Initial orientation of the fence and pushed workpiece. As the fence advances horizontally the four-sided workpiece rotates clockwise. The COR sketch is the shaded portion, plus the bold section of the sticking line called the sticking locus. The two elementary ($\mu_c = 0$) COR loci which were used to generate the COR sketch are shown in outline. We need to find the COR responsible for slowest rotation of the workpiece. This turns out to be at the lowest point of the sticking locus (marked "B"), not at the tip of one of the $\mu_c = 0$ loci as in the frictionless case considered in Section V.

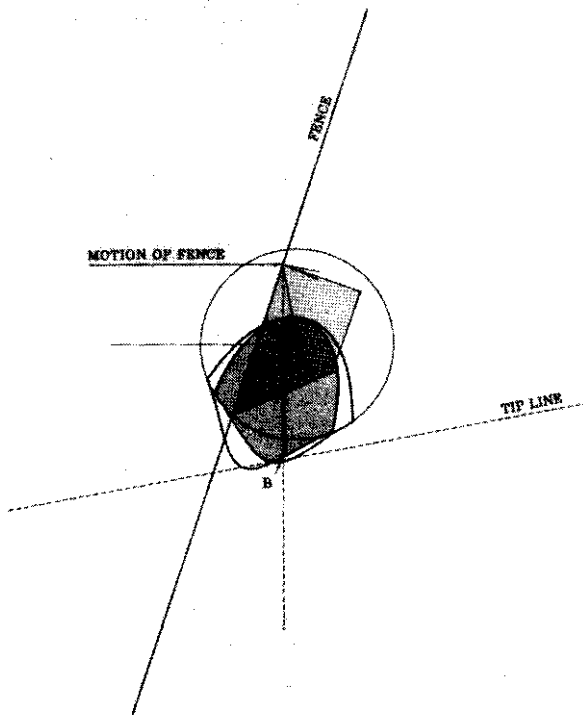


Fig. 31. Final (aligned) orientation of the fence and pushed workpiece. Here we show the COR sketch at the moment before the conclusion of the workpiece's clockwise rotation into alignment with the fence. By this time the COR responsible for slowest rotation of the workpiece is no longer at the bottom of the sticking locus but rather at the point marked "B" which is the tip of one of the elementary ($\mu_c = 0$) COR loci

The workpiece's rate of rotation about the COR $d\beta$, for advance of the pusher dx , is given by

$$dx = \frac{d\beta}{\sin \alpha} \vec{\alpha} \cdot (\vec{c} - \vec{r}). \quad (44)$$

To find the maximum required pushing distance, we must find the maximum value of $\vec{\alpha} \cdot \vec{r}$ for any possible COR \vec{r} in the COR sketch. This will be the *slowest* COR; the one for which the rotation of the workpiece with advance of the pusher is slowest.

Reviewing the nine distinct COR sketches in Fig. 29, we see that the slowest COR is at the lower endpoint of the sticking locus in sketches (D), (E), (G), and (H). We will call this behavior *sticking-slowest*. It occurs when the tips of the two loci $\{COR\}_{\alpha \pm \nu}$ fall on opposite sides of the sticking line.

In sketches (A), (B), (C), (F), and (I), the slowest COR is an element of one of the slipping loci $\{COR\}_{\alpha \pm \nu}$. We will call this behavior *slipping-slowest*. It occurs when the tips of the two loci $\{COR\}_{\alpha \pm \nu}$ fall on the same side of the sticking line. (For the purposes of the rule given here, the "wrapped" loci in sketches (G), (H), and (I) count as having their tip to the left of the sticking line.) In fact, the slowest COR in the slipping-slowest regime is very nearly the COR at the tip of one of the loci $\{COR\}_{\alpha \pm \nu}$. It is only because the angle of symmetry $\alpha \pm \nu$ differs from α that the tip is *not* the slowest COR. We will use the tip of one of the loci $\{COR\}_{\alpha \pm \nu}$ as an approximation to the slowest COR. The error introduced by this approximation can be bounded [15] in terms of the radius of curvature of the tip of the COR loci, but for practical purposes is negligible.

It is possible to have a transition from slipping-slowest behavior to sticking-slowest behavior within a pushing operation, as β increases. Such a transition occurs when the tip of one of the loci $\{COR\}_{\alpha \pm \nu}$ passes through the sticking line. In Fig. 32, for example, it is $\{COR\}_{\alpha - \nu}$ which passes through the sticking line. We may derive the condition for intersection

$$a^2 + c^2 = -a^2 \tan \beta \tan (\alpha \pm \nu + \beta). \quad (45)$$

The tip of locus $\{COR\}_{\alpha + \nu}$ is on the same side of the sticking line as the CM when the left side of (45) is less than the the right side. The value of β at which the tip crosses the sticking line may be found by solving (45) for β

$$\tan \beta_{\text{transition}} = \frac{c^2 \tan (\alpha \pm \nu) \pm (c^4 \tan^2 (\alpha \pm \nu) - 4a^2(a^2 + c^2))^{1/2}}{2a^2}. \quad (46)$$

The pushing distances required to advance β from its initial value to the transition, and from the transition to the final value, must be evaluated separately. In our example, the locus $\{COR\}_{\alpha + \nu}$ is type same-sided split initially, but changes to type opposite-sided split. Using (46) we find $\beta_{\text{transition}} = 69.4^\circ$, as shown in Fig. 32.

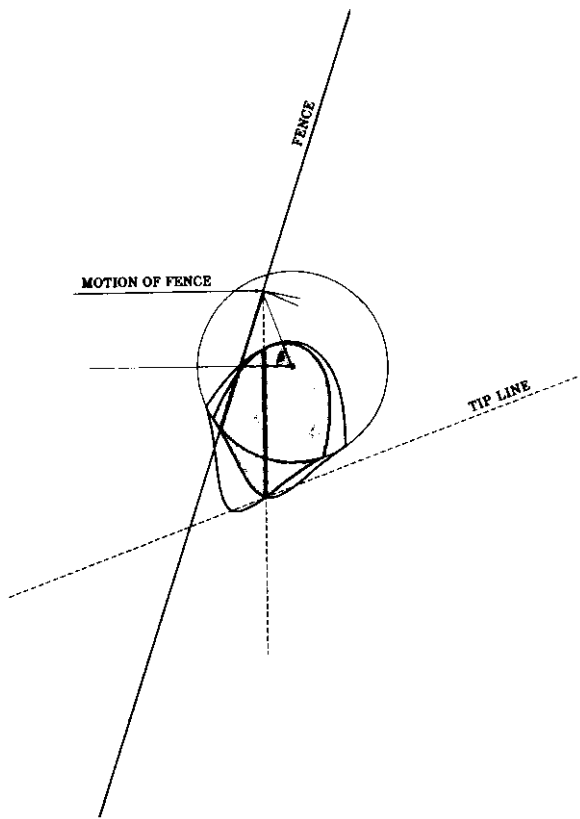


Fig. 32. Transition from sticking-slowest to slipping-slowest behavior. This is the moment of "transition" from the COR responsible for slowest possible rotation of the workpiece being at the bottom of the sticking locus as in Fig. 30 to being at the tip of one of the elementary ($\mu_c = 0$) COR loci as in Fig. 31.

A. Slipping-Slowest Regime

If the slowest COR is at the tip of one of the loci $\{COR\}_{\alpha \pm \nu}$ we have

$$dx = \frac{d\beta}{\sin \alpha} \bar{\alpha} \cdot (\bar{c} - \bar{r}_{tip}) \tag{47}$$

where

$$r_{tip} = \frac{a^2}{(\bar{d} \pm \bar{\nu}) \cdot \bar{c}}$$

which can be integrated to yield the indefinite integral

$$x = \frac{-c \sin(\alpha \pm \nu + \beta)}{\sin \alpha} - \frac{a^2}{2c \sin \alpha} \log \left| \frac{1 + \sin(\alpha \pm \nu + \beta)}{1 - \sin(\alpha \pm \nu + \beta)} \right| \tag{48}$$

Since, in the example being considered, the motion from $\beta_{transition} = 69.4^\circ$ until $\beta_{final} = 80^\circ$ falls in the slipping-slowest behavior regime, we simply evaluate x at these two angles and subtract. Here the "-" sign in " $\alpha \pm \nu$ " is used. The distance Δx obtained is one component of the maximum required pushing distance to align the workpiece.

B. Sticking-Slowest Regime

In Fig. 30 the slowest COR is the lowest point of the sticking locus, labeled "B." When the COR is at point "B" $\bar{c} - \bar{r}$ may be easily approximated as

$$|\bar{c} - \bar{r}| = \frac{c^2 + a^2}{c \sin \beta} \tag{49}$$

(If the radius of curvature of the tip of the COR locus boundary were zero this approximation would be exact. As it is not zero, the bottom of the sticking locus drops slightly below the tip line. This is a negligible effect, bounded in [15]. We will neglect it here.)

Note the absence of any dependence on the friction cone angle ν . This is because when the pusher and workpiece are already sticking, further increase in μ_c has no physical effect. To find the maximum required pushing distance it is only necessary to integrate (47) with $\bar{c} - \bar{r}$ as given here. We obtain the indefinite integral

$$x = \frac{c^2 + a^2}{2c} \log \left| \frac{1 - \cos \beta}{1 + \cos \beta} \right| \tag{50}$$

In our example, motion from $\beta_{initial} = 45^\circ$ until $\beta_{transition} = 69.4^\circ$ falls in the sticking-slowest behavior regime, so we simply evaluate x at these two angles and subtract. The distance Δx obtained is the second component of the maximum required pushing distance to align the workpiece. The total required pushing distance to align the workpiece is the sum of the two partial results obtained from (48) and (50).

IX. EXAMPLE: MOVING POINT PUSHING ASIDE A DISC

In this example we consider a disc being pushed not by a fence, but by a point moving in a straight line. The point may be a corner of a polygonal pusher, as long as it is only a corner of the pusher that touches the disc, and not an edge.

In all cases the outcome of the collision is the same: the disc is pushed aside by the pusher, and contact is broken. The disc ceases to move at the instant the pusher loses contact with it (we assume slow motion), so the disc will be left tangent to the pusher's path when contact is broken. The initial and final configurations of the disc are shown in Fig. 33. We wish to calculate the minimum and maximum length of the encounter, $x_{encounter}$, in terms of the collision parameter, β , as indicated in Fig. 33. We might also wish to know the minimum and maximum angles through which the disc may rotate during the collision.

A. Length of the Encounter

In Fig. 34, the variables of interest are x , which parametrizes the advance of the pusher along its path, and β , which completely characterizes the collision. β will vary from $\beta_{initial}$, its value at first contact, to $\beta_{final} = \pi/2$ when contact is broken. $x_{encounter}$ is the corresponding change in x , as β changes from $\beta_{initial}$ to $\pi/2$.

If the instantaneous COR is known, the direction of motion of the CM of the disc is known: it makes an angle θ with the

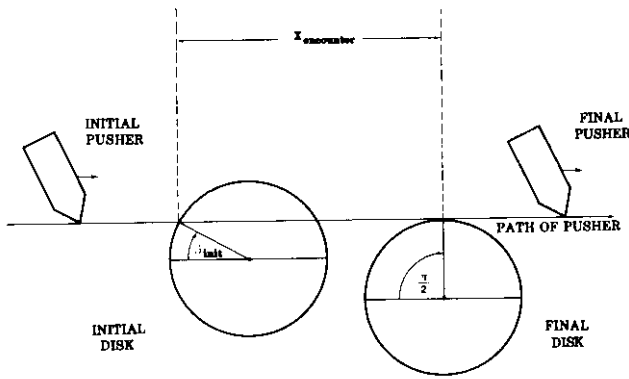


Fig. 33. Configuration of the disc and the path of the pusher, before and after collision. A point pusher in linear motion encounters a disc. The collision is characterized by an initial value of the "collision parameter" β_{initial} . After the pusher has translated a distance $x_{\text{encounter}}$, the disc has become tangent to the path of the pusher and the two break contact, ending the collision. β_{final} is $\pi/2$. During the collision the disc rotates an angle ξ . We wish to place bounds on $x_{\text{encounter}}$ and on ξ .

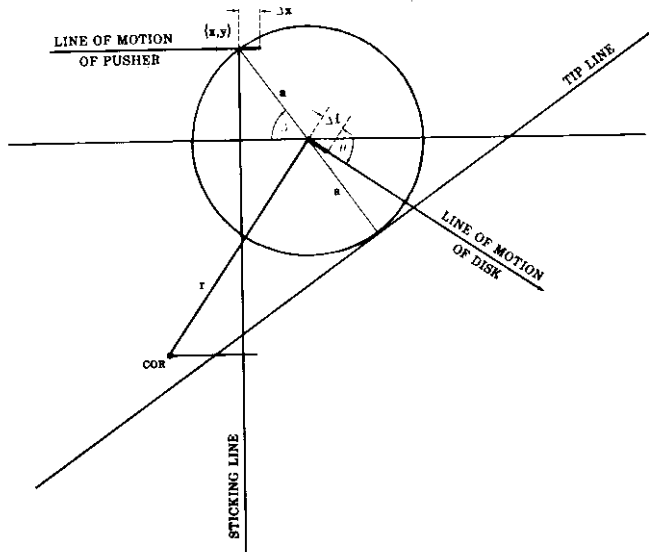


Fig. 34. Finding equation of motion (51). If the COR were known, we could find relations among: a) the motion of the CM of the disk Δl , b) the change in the collision parameter $\Delta\beta$, and c) the advance of the pusher Δx .

horizontal, as shown in Fig. 34. If the CM of the disc moves a distance Δl along its line of motion, we can find the resulting values of $\Delta\beta$ and Δx , and thereby relate $\Delta\beta$ and Δx to each other.

The pusher advances a distance

$$\Delta x = \Delta l \cos \theta + \Delta l \sin \theta \tan \beta \quad (51)$$

due to Δl . At all times β can be found from

$$a \sin \beta = y + \Delta l \sin \theta \quad (52)$$

where (x, y) are the coordinates of the point of contact.

Substituting Δl from (51), and evaluating the change in $\sin \beta$ due to Δl , we find

$$a \Delta(\sin \beta) = \frac{\Delta x \sin \theta}{\cos \theta + \sin \theta \tan \beta} \quad (53)$$

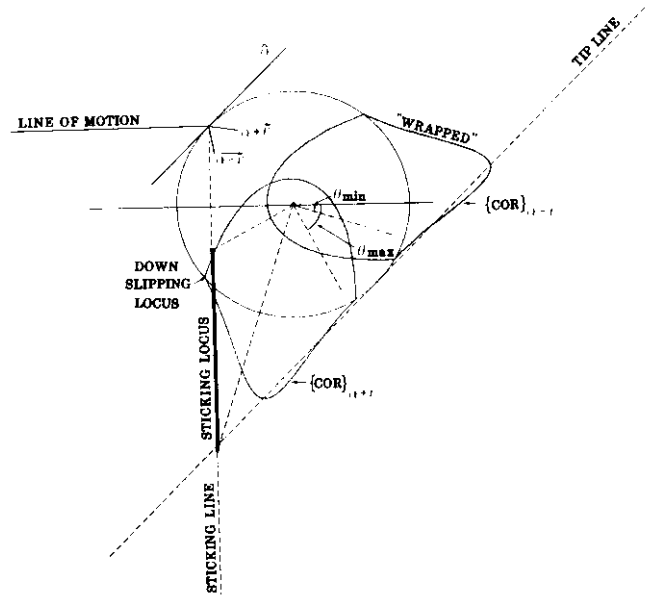


Fig. 35. COR sketch for a point pushing a disc. The COR sketch for the collision between pusher and disc. The angle of the edge being pushed, α , is the tangent to the disc at the point of contact \bar{c} . Therefore one of the two elementary COR loci which compose the COR sketch is "wrapped" (Fig. 27). The COR sketch consists of only a down-slipping locus (left of the sticking line) and a sticking locus. This is reasonable: it would be surprising if the disc should slip up relative to the pusher.

For infinitesimal motions, $\Delta\beta$ and Δx become $d\beta$ and dx . Using $d(\sin \beta) = \cos \beta d\beta$, we find an equation of motion

$$dx = a d\beta \left(\sin \beta + \frac{\cos \beta}{\tan \theta} \right) \quad (54)$$

Since it will turn out that $\tan \theta > 0$, the largest and smallest values of $dx/d\beta$ will result when θ assumes its smallest and largest values, respectively.

Now we construct the COR sketch, shown in Fig. 35. Since the edge normal at \bar{c} passes through the CM, the extremes of the friction cone pass to either side of the CM, for any $\mu_c > 0$. $\{COR\}_{\alpha-\beta}$ is a "wrapped" locus (as described in Section VI-E), so the COR sketch must be that of Fig. 29 sketch (G), (H), or (I). In any case there must be a sticking locus, there cannot be an up-slipping locus, and there may or may not be a down-slipping locus. In Fig. 35 we have shown a down-slipping locus.

In Fig. 35 (and in general when the COR sketch is any one of distinct types (G), (H) or (I)), the smallest and largest values of θ (Fig. 34) occur when the COR is at the lower or upper endpoints, respectively, of the the sticking locus. For sketches (G) and (H) the lower endpoint of the sticking locus is well approximated by the intersection of the sticking line with the tip line, and we will use this approximation (neglecting the small effect of the curvature of the tip, though this could be included). For the lower endpoint of the sticking locus in sketch (I), and for the top of the sticking locus in all three sketches, numerical methods would have to be used. We will not find these numerical results here.

1) *Greatest Length of Encounter:* As in Section VIII-B, we will neglect the slight dip of the sticking locus below the tip

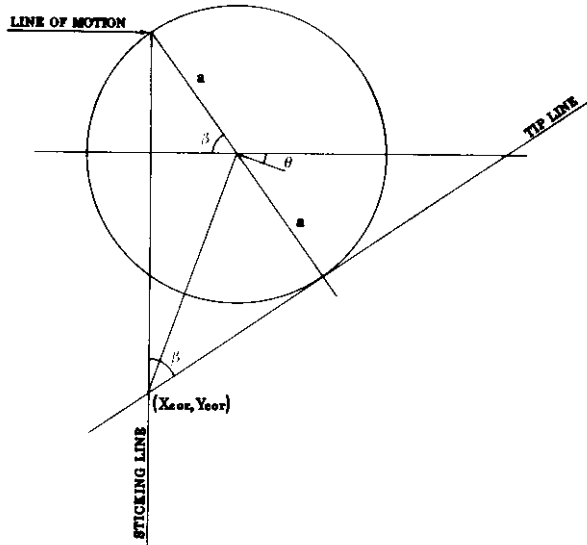


Fig. 36. Finding the smallest θ (55). The length of the encounter between pusher and disc is greatest if the COR is at such a location that θ is minimal. In most cases the bottom of the sticking locus is the location of the COR which minimizes θ . Using the tip line construction we can find the minimum value of θ as shown here.

line, which results from the nonzero radius of curvature of the tip of the COR locus boundary. We will also assume that the COR sketch is of type (G) or (H), not (I), so that the lower endpoint of the sticking locus can be approximated by the intersection of the sticking line with the tip line. This assumption will be addressed in Section IX-A2 below.

If the COR is at the intersection of the sticking line with the tip line, we find from Fig. 36

$$\tan \theta = \frac{x_{COR}}{y_{COR}}$$

$$x_{COR} = -a \cos \beta \tag{55}$$

and

$$y_{COR} = a \frac{\sin^2 \beta - 2}{\sin \beta}$$

where y_{COR} is found from the construction of Fig. 36. Using $c = a$, (55) can be simplified to

$$\tan \theta = \frac{\cos \beta \sin \beta}{1 + \cos^2 \beta} \tag{56}$$

Using this value of $\tan \theta$ in the equation of motion (54) results in

$$dx = a d\beta (\sin \beta) + \frac{1 + \cos^2 \beta}{\sin \beta} \tag{57}$$

which, integrated, yields the indefinite integral

$$x_{encounter} = a \left(\ln \frac{1 - \cos \beta}{1 + \cos \beta} \right) \tag{58}$$

The maximum value of $x_{encounter}$ can be obtained by evaluating

(58) at $\beta_{initial}$ and $\beta_{final} = \pi/2$, and subtracting. The value at $\pi/2$ is zero.

2) *Condition for Sketch Type (I)*: The above derivation of maximum $x_{encounter}$ assumed that the lower endpoint of the sticking locus is at the tip line. This is not true when the COR sketch is of type (I), in Fig. 29.

The COR sketch is of type (I) when the tip of $\{COR\}_{\alpha+\nu}$ is left of the sticking line. Simplifying (45) for $a = c$ and $\alpha + \beta = \pi/2$, we find the condition for sketch (I) to be

$$\tan \beta > 2 \tan \nu = 2\mu_c \tag{59}$$

This means that the COR sketch will always become type (I) as $\beta \rightarrow \pi/2$, unless $\mu_c = \infty$. ($\mu_c = \infty$ can occur, for example, in pushing a gear, if a tooth is engaged by the pusher.) In every case of pushing aside a disc, sketch (I) is entered eventually.

By using the tip line as the lower endpoint of the sticking locus, despite the fact that this is a poor approximation in sketch (I), we find too low a value for the minimum θ . Our calculated maximum for $x_{encounter}$ (58) is unnecessarily high. We could in principle refine the upper bound by finding the lower endpoint of the sticking locus more accurately by numerical methods.

As mentioned above, we are also neglecting the slight dip of the sticking locus below the tip line (in sketches (G) and (H)), which causes us to underestimate the maximum possible value of $x_{encounter}$. Here too we could refine $x_{encounter}$ by numerical methods.

Neglect of sketch (I), and neglect of the dip due to tip curvature, cause errors of opposite sign in calculating the maximum $x_{encounter}$. The latter is a smaller error. Neither error will be addressed here.

3) *Least Length of Encounter*: The minimum possible value of $x_{encounter}$ occurs when the COR is at the top of the sticking locus. We do not have an analytical method of finding or approximating the upper endpoint of the sticking locus, as we have for the lower endpoint. The lower endpoint is similarly hard to analyze if the COR sketch is of type (I) in Fig. 29. In these cases it is necessary to find the endpoints numerically for all β in the range of interest, calculate θ for each β , and then integrate (54) numerically to find $x_{encounter}$.

B. Rotation of the Pushed Disc During Encounter

1) *Maximum Rotation*: In Section IX-A both the largest and smallest possible values of $x_{encounter}$ resulted from COR's on the sticking line. If the COR remains on the sticking line, the pusher does not slip relative to the surface of the disc, and so evaluation of the rotation of the disc during the encounter, $\xi_{encounter}$, is trivial. We have

$$\xi_{encounter} = a(\pi/2 - \beta_{initial}) \tag{60}$$

Since only up-slipping of the pusher is possible, (60) is an exact upper bound for $\xi_{encounter}$; any slipping will only serve to reduce the rotation of the disc.

Maximal slipping is obtained if $\mu_c = 0$. The pushing force is directed through the CM of the disc, so the disc can only

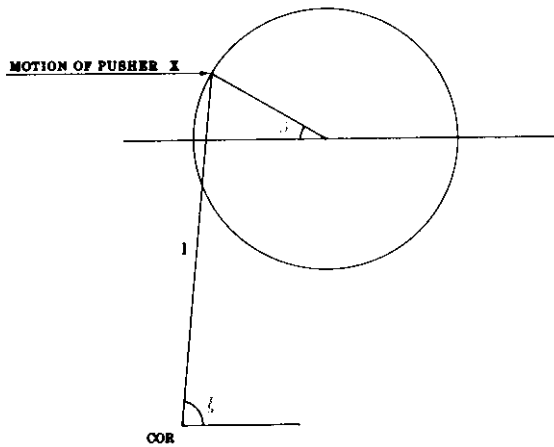


Fig. 37. Finding equation of motion (61). If the location of the COR is known, the rotation of the disc ξ can be related to the advance of the pusher Δx .

translate and not rotate [10]. So if $\mu_c = 0$, we have $\xi_{\text{encounter}} = 0$ as both maximum and minimum rotation.

2) *Minimum Rotation:* We found in Section IX-A that extreme values of $dx/d\beta$ occur when θ takes on extreme values. Having constructed the COR sketch, we found that the extreme values of θ for possible COR's are assumed when the COR falls at the top or bottom of the locus. In this section we will not be able to find a single geometric variable, analogous to θ , whose extremes correspond to extremes of the rate of rotation.

Rotation of the disc will be measured by the angle ξ , measured at the COR, as shown in Fig. 37. We can relate $\Delta\xi$ to advance of the pusher Δx

$$\Delta x = l \sin \xi d\xi. \quad (61)$$

Combining (61) with (54) which relates $\Delta\beta$ to Δx , we find

$$\Delta x = \frac{a d\beta \left(\sin \beta + \frac{\cos \beta}{\tan \theta} \right)}{l \sin \xi} d\beta. \quad (62)$$

We can eliminate θ and $l \sin \xi$ in favor of the coordinates of the COR

$$\tan \theta = \frac{x_{\text{COR}}}{y_{\text{COR}}} \quad (63)$$

$$l \sin \xi = a \sin \beta - y$$

yielding

$$\frac{d\xi}{d\beta} = \frac{a(y_{\text{COR}} \cos \beta + x_{\text{COR}} \sin \beta)}{x_{\text{COR}}(a \sin \beta - y_{\text{COR}})}. \quad (64)$$

This has no simple geometric interpretation. Contours of constant $d\xi/d\beta$ are plotted in Fig. 38 for $\beta = 45^\circ$. Minimum rotation occurs at minimum $d\xi/d\beta$. The COR sketch for $\beta = 45^\circ$ is superimposed on Fig. 38. The possible value of the COR which is responsible for minimum rate of rotation is the point of the COR locus which intersects the slowest valued

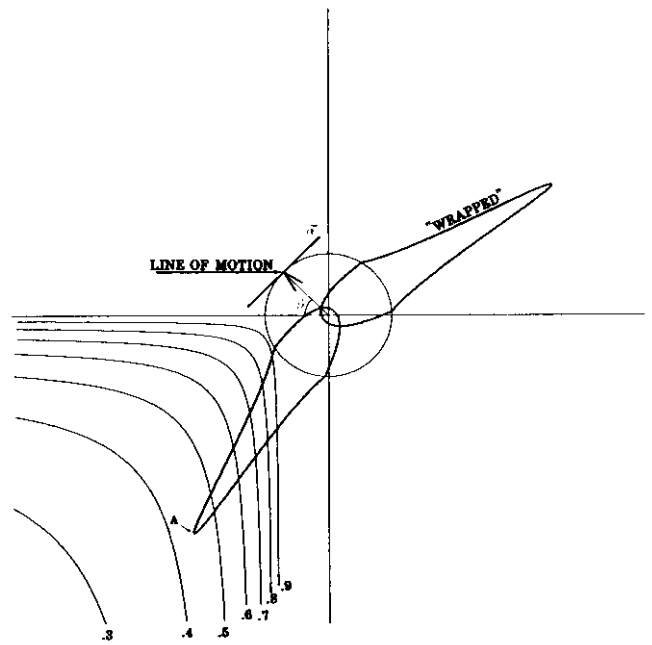


Fig. 38. Contours of constant $d\xi/d\beta$, and the COR sketch. To find the minimum possible rotation of the disc ξ during its encounter with the pusher we seek that location of the COR which minimizes ξ for unit increase in the collision parameter β , i.e., which minimizes $\delta\xi/\delta\beta$. Plotted are contours of constant $\delta\xi/\delta\beta$. We must find numerically the point in the COR locus which intersects the least contour. For the COR locus plotted, the least contour intersected is about 0.46, and the COR which intersects it is, once again, very near the tip of the COR locus.

contour line, indicated in the figure as point *A* (in this case very close to the tip). Having obtained numerically the minimum possible value of $d\xi/d\beta$, as a function of β , we can numerically find the indefinite integral

$$\xi_{\min} = \int \left(\frac{d\xi}{d\beta} \right)_{\min}(\beta) d\beta. \quad (65)$$

Minimum rotation in a given collision can then be evaluated by subtracting $\xi_{\min}(\beta_{\text{initial}})$ from $\xi_{\min}(\beta_{\text{final}} = \pi/2)$.

X. EXAMPLE: SPIRAL LOCALIZATION OF A DISC

In this example we analyze an unusual robot motion by which the position of a disc (a washer, say), free to slide on a tabletop, can be localized without sensing. If the disc is known initially to be located in some bounded area of radius b_1 , we begin by moving a point-like pusher in a circle of radius b_1 . Then we reduce the pusher's radius of turning by an amount Δb with each revolution, so that the pusher's motion describes a spiral. Eventually the spiral will intersect the disc (of radius a), bumping it. We wish the disc to be bumped toward the center of the spiral, so that it will be bumped again on the pusher's next revolution. If the spiral is shrinking too fast, however, the disc may be bumped *out* of the spiral instead of toward its center, and so the disc will be lost and not localized.

We wish to find the maximum shrinkage parameter Δb consistent with guaranteeing that the disc is bumped into the spiral, and not out. (Δb will be a function of the present spiral radius.) We also wish to find the number of revolutions that will be required to localize the disc to some radius b , with $a <$

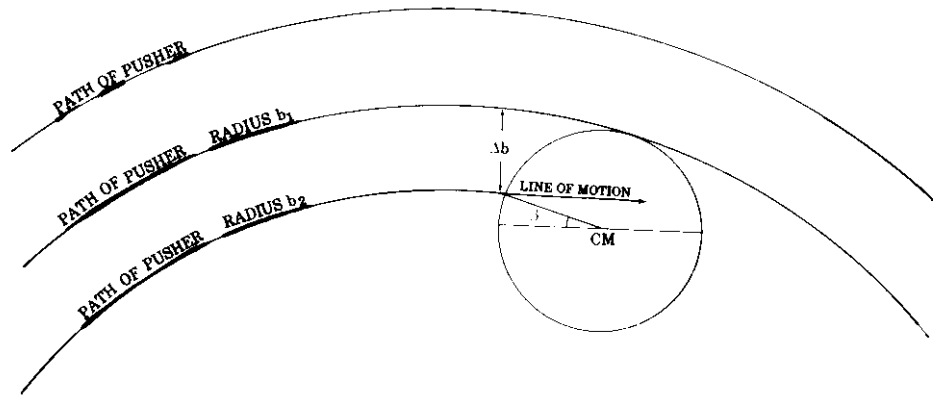


Fig. 39. Geometry at the moment of the second collision of pusher and disc. A point pusher describes a decreasing spiral about a region of radius a , within which a disc of radius a is known to be. As the spiral decreases in radius the disc is pushed towards the center and never out of the spiral. It turns out there is a limiting radius of the spiral below which further confinement of the disc cannot be guaranteed, no matter how slowly the spiral decreases in radius. In this figure the disc was first struck by the pusher when it was at radius b_1 , and was pushed towards the interior of the spiral. The disc was left tangent to the path of the pusher, and is about to be struck again by the pusher, which is now at radius b_2 . $\Delta b = b_1 - b_2$ is the shrinkage rate of the spiral. Notice the collision parameter β which results.

$b < b_1$, and the limiting value of b , called b_∞ , below which it will not be possible to guarantee localization, regardless of number of revolutions.

A. Analysis

Suppose the pushing point has just made contact with the disc. Since the previous revolution had radius only Δb greater than the current revolution, the pusher must contact the disc at a distance at most Δb from the edge of the disc, as shown in Fig. 39. We will consider only the worst case, where the distance of the pusher from the edge is the full Δb .

We know that if $\Delta b < a$ the disc will move downward [10]. This is not sufficient to assure that the disc will be pushed into the spiral (rather than out of the spiral), because the pushing point will also move down, as it continues along its path (Fig. 39). To guarantee that the disc will be pushed into the spiral, we must make sure that it moves down *faster* than does the pushing point.

Note that we will continue to draw the pusher's motion as horizontal, even though the pusher must turn as it follows the spiral. This is done to maintain the convention for COR sketches used in previous sections. At every moment we simply choose to view the system from such an angle that the pusher's motion is horizontal.

One way of comparing rates of moving down is by considering the increase or decrease in the angle β , called the *collision parameter* in Fig. 39. If, as the pusher's motion along its spiral progresses, β increases, then the disc is being pushed *into* the spiral; localization is succeeding. When β reaches $\pi/2$, the pusher grazes the disc and leaves it behind. The disc is then left tangent to the spiral. If, as the pusher's motion progresses, β decreases, the disc is being pushed *out* of the spiral; localization is failing.

B. Critical Case: Pusher Chasing the Disc Around a Circular Path

In the critical case the angle β does not change with advance of the pusher. The pusher "chases" the disc around the spiral,

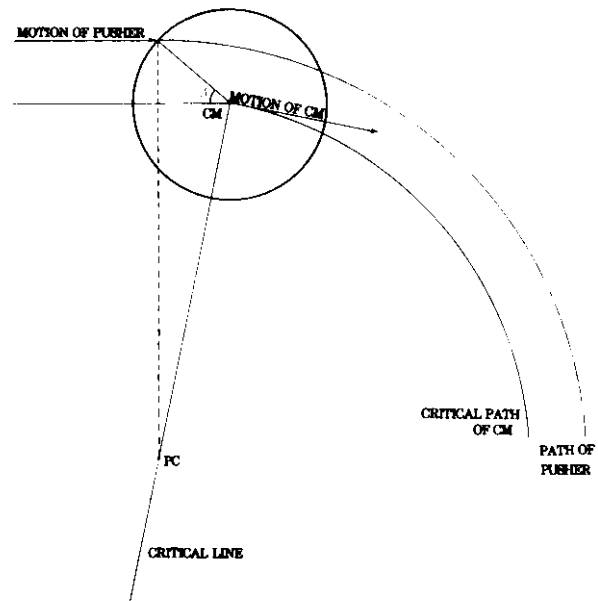


Fig. 40. Critical case: pusher "chasing" disc around a circular path. If the shrinkage of the spiral Δb is too great, the disc can be pushed *out* of the spiral. To find the critical value of Δb below which the disc is guaranteed to be pushed *into* the spiral, we consider the marginal case where it is possible for the pusher to "chase" the disc, with the collision parameter β neither increasing (meaning the disc is going towards the interior of the spiral) nor decreasing (meaning that the disc is going towards the exterior of the spiral).

neither pushing it in nor out. In this section we will take the spiral to be a circle (i.e., $\Delta b = 0$), to simplify analysis. The critical case, shown in Fig. 40, is highly unstable. The pusher's motion is shown as an arc of a circle, labeled path of pusher. (Underlined names refer to elements of Fig. 40). The center of that circle is labeled PC (for pusher-center). Point PC is directly below the point of contact, in keeping with our convention of drawing the pusher's line of motion horizontal.

To maintain the critical case, the path followed by the CM of the disc (labeled critical path of CM) must be as shown in the figure: an arc of a circle, concentric with the arc path of

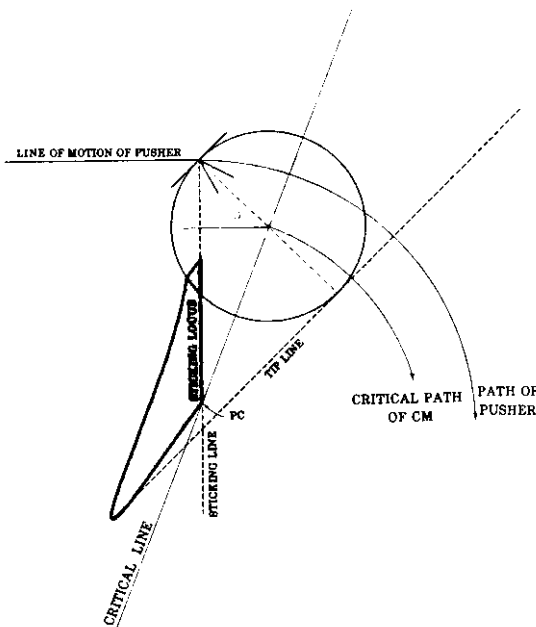


Fig. 41. COR sketch for critical case, and solution for location of PC . We wish to find a condition on the radius of the pusher circle which guarantees that the disc will always be pushed *into* the circle. We will construct the COR sketch, and then find positions for PC such that all possible COR's are to the left of the critical line. To make sure that the whole COR locus falls to the left of critical line, we need only place the center of the pusher motion (PC) *below* the lower endpoint of the sticking locus.

pusher. Instantaneously, the direction of motion of the CM must be along the line labeled motion of CM, tangent to the critical path of CM. The critical line, drawn through PC and CM , is by construction perpendicular to motion of CM. The COR of the disc must fall on the critical line, in order that the instantaneous motion along the line motion of CM be tangent to the critical path of CM.

We have just seen that the COR of the disc must fall on critical line for the instantaneous motion of the CM to be consistent with the CM following the critical path of CM. If the COR falls to the left of the critical line, the CM diverges from the critical path of CM by moving *inside* the arc. Therefore, β will increase with advance of the pusher, and localization is succeeding. If the COR falls to the right of the critical line, the CM diverges from the critical path of CM by moving *outside* the arc. Therefore, β will decrease with advance of the pusher, and localization is failing. The critical line divides the plane into two zones: if the COR falls in the left zone, the disc is pushed into the pusher circle, while if the COR falls in the right zone, the disc is pushed out of the pusher circle.

We wish to find a condition on the radius of the pusher circle which guarantees that the disc will always be pushed *into* the circle. We will construct the COR sketch, and then find positions for PC such that all possible COR's are to the left of the critical line.

In Fig. 41 we have constructed the COR sketch with collision parameter β . Since the edge normal at \vec{c} passes through the CM, the extremes of the friction cone pass to either side of the CM, for any $\mu_c > 0$. $\{COR\}_{\alpha-\nu}$ is a

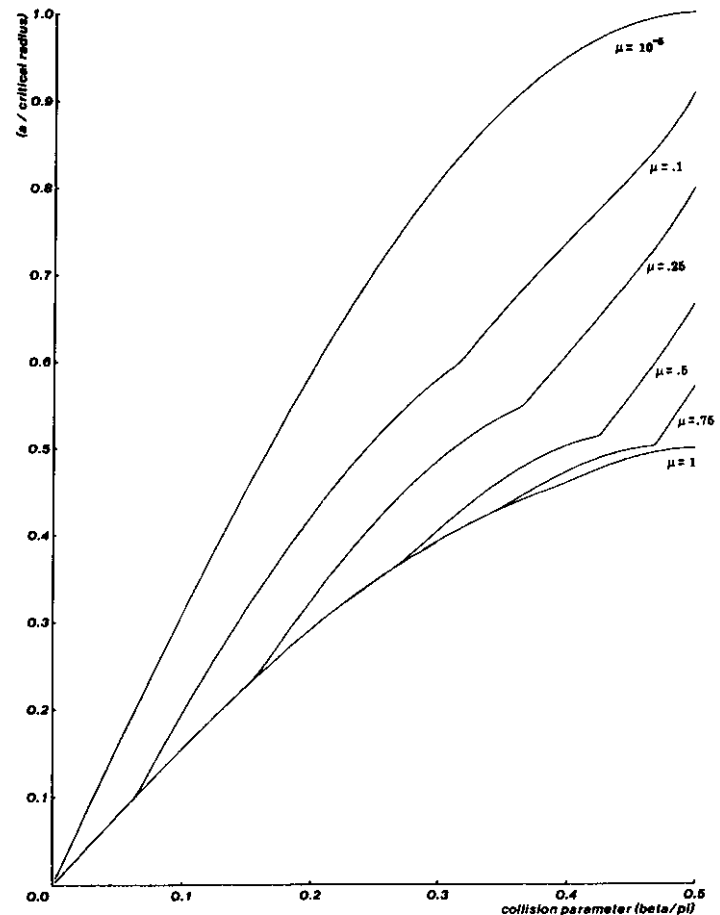


Fig. 42. Radius $r^*(\beta)$ of the critical circle as a function of collision parameter β . For every collision parameter β (here plotted as β/π), there is a tightest radius r^* which the pusher can describe still maintaining the guarantee that the disc can be chased or pushed inward, but never be pushed outward. For a variety of coefficients of friction μ_c we plot here the *inverse* of that tightest (critical) radius, a/r^* .

“wrapped” locus (Section VI-E), and the COR sketch must be that of Fig. 29 (G), (H), or (I). In any case, there must be a sticking locus, there cannot be an up-slipping locus, and there may or may not be a down-slipping locus. In Fig. 41 we have shown a down-slipping locus.

To make sure that the whole COR locus falls to the left of critical line, we need only place the center of the pusher motion (PC) *below* the lower endpoint of the sticking locus. (Point PC is required to have the same x coordinate as the point of contact, in keeping with our convention of drawing the pusher's line of motion horizontal.)

C. Critical Radius versus Collision Parameter

For every value of β (the collision parameter), we compute the distance from the pusher's line of motion to the lower endpoint of the sticking locus. This defines a critical radius $r^*(\beta)$. For each collision parameter β , $r^*(\beta)$ is the radius the tightest circle that the pusher can describe with the guarantee that the disc will be pushed into the circle, or at worst be “chased” around the circle indefinitely, but not be pushed out of the circle. In Fig. 42, $1/r^*(\beta)$ is plotted as a function of collision parameter β for each of several values of μ_c . (The

discontinuity in slope results from the discontinuity in slope of the COR locus boundary at $r = a$.)

The inverse of the function $r^*(\beta)$ will be denoted $\beta^*(r)$, representing the smallest value of β for which a pusher motion of radius r still results in guaranteed localization. In terms of the pusher's distance from the top edge of the disc, d (Fig. 41), we can use the relationship

$$a(1 - \sin \beta) = d \quad (66)$$

to define the *critical distance from grazing* $d^*(r)$ as a function of r . $d^*(r)$ is the largest distance of the pusher from the top edge of the disc for which a pusher motion of radius r still results in guaranteed localization.

D. Limiting Radius for Localization

If there is a limiting radius b_∞ of the spiral motion below which localization cannot be guaranteed, then as the spiral approaches radius b_∞ the motion must become circular. $\Delta b \rightarrow 0$ as b_∞ is approached, so collisions become grazing collisions, and we have the distance from grazing $d \rightarrow 0$. (In terms of the collision parameter β , we have $\beta \rightarrow \pi/2$.) The COR sketch for $\beta = \pi/2$ is shown in Fig. 43. If the disc is not to be bumped out of the spiral, we must have $b_\infty = r^*(\beta = \pi/2)$. b_∞ is indicated in the figure, and can be shown analytically to be

$$\begin{aligned} b_\infty &= a(\mu_c + 1), & \text{for } \mu_c \leq 1 \\ b_\infty &= 2a, & \text{for } \mu_c \geq 1. \end{aligned} \quad (67)$$

Only at $\mu_c = 0$ can a disc be localized completely, i.e., localized to within a circle the same radius as the disc. Otherwise, the tightest circle within which the disc can be localized is given by (67).

E. Computing the Fastest Guaranteed Spiral

Let b_n be the radius of the n th revolution of the pusher, so that we have initially radius b_1 , and b_∞ is the limiting radius as $n \rightarrow \infty$. (In specifying but a single radius for each revolution of the spiral, we will not truly specify the spiral completely, but this will be sufficient to characterize the number of revolutions required to achieve a desired degree of localization.)

To excellent approximation we can define the fastest spiral recursively by

$$b_n = b_{n-1} - d^*(b_n). \quad (68)$$

The difference between the radii of consecutive turns of the spiral $n - 1$ and n is therefore $\Delta b = d^*(b_n)$. Equation (68) thus enforces the condition that on the n th revolution, the value of d is exactly the critical value for circular pushing motion of radius b_n . At worst, the disc is pushed neither in nor out of the spiral. A slightly slower spiral would guarantee that the disc cannot be chased in this way for long, but is pushed into the spiral. However, the difference between our spiral and the "slightly slower" one is so slight that it is not worth dealing with here [15].

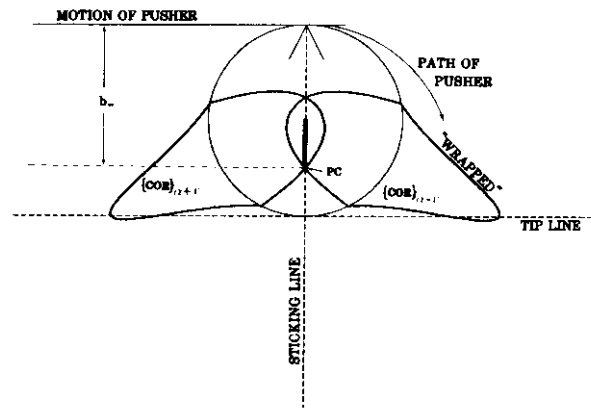


Fig. 43. COR sketch at the limiting radius, showing b_∞ . There is a limiting radius of the spiral b_∞ , below which we cannot guarantee that the disc will be pushed inward, no matter how slowly the spiral is decreasing in radius, i.e., no matter how small Δb . As the spiral approaches this radius it must more and more accurately approximate a circle, since it cannot go below radius b_∞ . Thus the collision parameter β becomes $\pi/2$ as radius b_∞ is approached, and all collisions become grazing collisions. Drawing the COR sketch for a grazing collision we find that $b_\infty = a(\mu_c + 1)$, a general kinematic limitation on the success this herding strategy can achieve.

Fig. 44 shows the fractional deviation of spiral radius b_n above b_∞ , versus number of turns n , on logarithmic and on linear scales. We start (arbitrarily) with $b_1 = 100a$. The spiral radius was computed numerically for $\mu_c = 0.25$, using the results for $\beta^*(r)$ shown in Fig. 42 and (68).

Fig. 44 shows that when the spiral radius is large compared to the disk radius a (which is taken to be 1 in the figure), we can reduce the radius of the spiral by almost a with each revolution. As the limiting radius is approached, the spiral reduces its radius more and more slowly, approaching the limiting radius b_∞ as about $n^{-1.6}$, where n is the number of revolutions. Fig. 44 demonstrates the best performance that the "herding" strategy can achieve.

XI. CONCLUSION

We have solved for the possible instantaneous motions of a sliding workpiece as it is pushed, in the presence of unknown frictional forces between workpiece and table, and between workpiece and pusher. We have characterized the qualitatively different kinds of sliding motion which are possible, and found the conditions under which each can occur. Using these results it is possible to find bounds for *gross* motions of a pushed workpiece as well. This is done by integrating the possible instantaneous motions.

As an example, we have found the maximum distance a polygonal sliding workpiece must be pushed by a fence in order to guarantee that a side of the workpiece has aligned itself with the fence. Using the useful *tip line construction* described here, approximate results are obtained both for the alignment problem and several others. Strict upper bounds for the maximum required pushing distance are found by using slightly more sophisticated methods, but the difference between the upper bounds and the approximate results are so slight that the effort seems hardly justified.

In a second example, we have taken the pushed workpiece to be a disc, and the pusher to be a point, or the corner of a

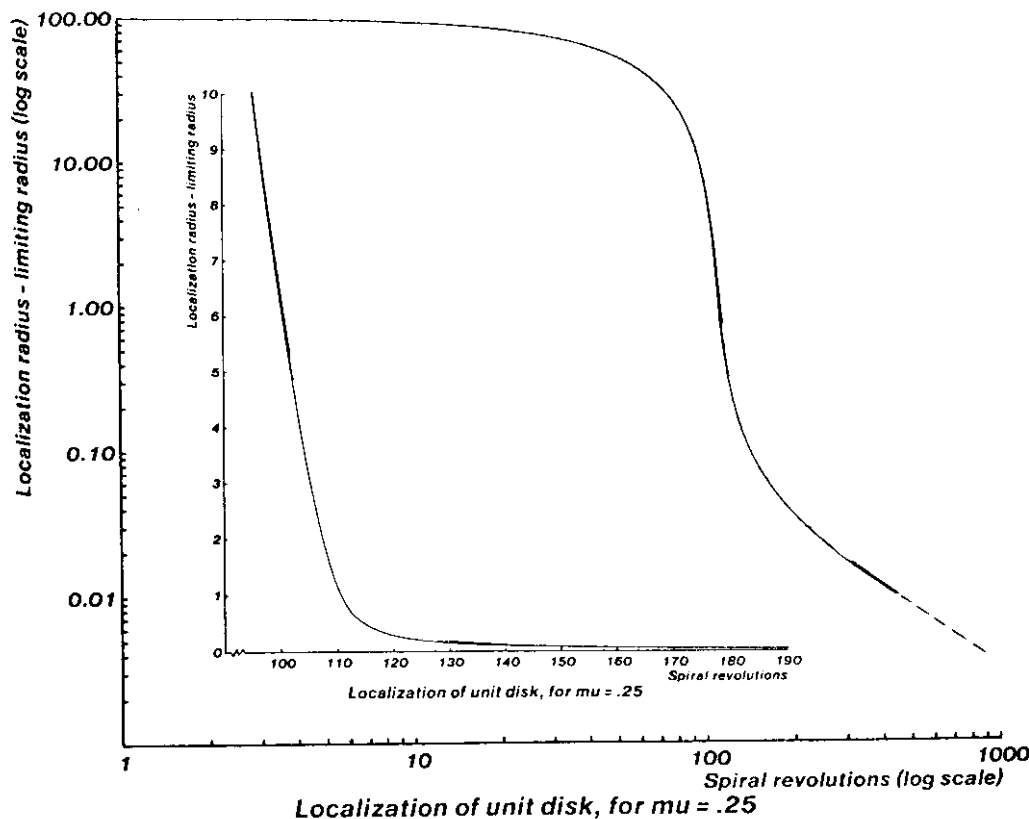


Fig. 44. Performance of the optimal spiral. For $\mu_c = 0.25$ we plot the optimal spiral. This is the fastest decreasing spiral which still guarantees that the disc is pushed into the spiral and cannot be pushed out, i.e., localizes the disc as quickly as possible. We found that the spiral cannot decrease below a radius b_∞ while maintaining the guarantee, so that value has been subtracted from the vertical (spiral radius) axis, leaving only the difference between the spiral radius and its limiting value. In the linear plot, we can see that the radius of the optimal spiral decreases swiftly by almost the disc's radius a with each revolution until quite close to the limiting radius. It is then more instructive to look at the log-log plot to see how the spiral radius approaches the limiting radius.

polygon, moving in a straight line. We have found the maximum distance that the pusher and the disc may be in contact, before the disc is "pushed aside" by the moving workpiece. Bounds on the rotation of the disc during its interaction with the pusher are also found.

Finally, we have analyzed an unusual robot maneuver, in which a disc known to be within a certain circular area can be "localized" to a much smaller circular area by a pusher which, perhaps under robot control, describes a decreasing spiral around the disc. Thus the disc can be located by a robot without sensors. We found the ultimate limiting radius below which the disc cannot be localized further, no matter how slowly the spiral decreases in radius. We also found (to within tight bounds) the "optimal spiral": the spiral which localizes the disc with the fewest number of revolutions, while guaranteeing that the disc is not lost from the spiral.

XII. SUGGESTIONS FOR FURTHER WORK

A. Other Models of Friction

An important assumption used in deriving the COR loci is that of a coefficient of sliding friction μ_s which is uniform over the sliding surface and velocity-independent: simple Coulomb friction. Friction is rarely so well behaved.

Velocity dependence of μ_s will have only moderate conse-

quences for the COR loci. The sense of rotation (CW or CCW) is not affected by velocity dependence, because pure translation of the workpiece is the marginal case dividing the senses of rotation. In pure translation, all parts of the workpiece move with the same velocity, so velocity dependence of μ_s is unseen by the workpiece. If μ_s decreases with increasing velocity (the usual case), we can predict that COR's will lie closer to center of mass (i.e., rotation rates will be faster) than they would with constant μ_s . The side of the workpiece towards which it turns has a lower velocity, therefore higher μ_s , and therefore more drag, causing the workpiece to turn still faster towards that side.

Spatial nonuniformity of μ_s is more serious. In our experimental work [15] a nonuniformly worn surface caused a 5° offset in the marginal pushing direction dividing CW from CCW rotation. It would be hard to control such a major effect analytically. Instead, sliding surfaces must be kept uniform.

When it is the surface of the sliding part, rather than the surface of the table, which is nonuniform, we may hope to find simple analytic adjustments to the COR locus to compensate. The distinction between *center of friction (COF)* and *center of mass* becomes important [8], [10]. If the composition of the part surface is understood and some information about the pressure distribution is available, a COF distinct from the CM can be calculated for the part. Then the sense of rotation (at

least) will be predictable. It is not known what effect a COF distinct from the CM will have on the COR locus.

B. Pushing Above the Plane

We assumed that the point of contact between pusher and pushed workpiece is not far (relative to the radius of the workpiece) above the sliding surface. In the extreme case of pushing far above the plane, the workpiece will tip over instead of sliding. For small heights, the effect creates a center of friction (COF) distinct from the center of mass (CM). The effect on the COR locus is unknown.

C. Non-Quasi-Static Velocities

The results of Sections V and VI depend on the quasi-static assumption, discussed in Section II. We assume that dissipative effects due to friction between a workpiece and the surface it slides on overwhelm inertial effects. In the real world, both effects are present, and become of comparable importance at characteristic speeds considered in Section I here, and in [15] and [11]. The results of Sections V and VI may be considered to be the $v \rightarrow 0$ limit.

In the opposite extreme, we may neglect sliding friction altogether, and only consider inertial effects. The motion is then independent of speed, so we may consider this case to be the $v \rightarrow \infty$ limit. The details of the contact between the sliding workpiece and the surface it slides on (the pressure distribution, Section II-E) no longer have any effect on the motion. For given initial conditions then, a *single* resulting motion can be calculated, rather than the *locus* of possible motion calculated for slow motions.

Drawing on the work of Routh [18], Wang [19] has calculated the motion of a pushed workpiece in the $v \rightarrow \infty$ limit (the "impact" limit). The motion is a function of the coefficient of friction between the pusher and workpiece μ_c as in the quasi-static case, and of the geometry of pushing, but it also depends on the elasticity of the materials in contact. Elasticity ranges from the plastic limit $e = 0$ (e.g., modeling clay) to the elastic limit $e = 1$ (e.g., spring steel).

The instantaneous motion on impact can be described by a center of rotation (COR) somewhere in the plane. Wang finds [20] that when $e = 0$ or $\mu_c = 0$, the COR falls along the axis of symmetry of the quasi-static COR locus derived in Section V, and at a distance r_{impact} from the CM given by

$$r_{\text{impact}} = \frac{\rho^2}{\bar{\alpha} \cdot \bar{c}} \quad (69)$$

where ρ is the radius of gyration of the workpiece. Equation (69) is the same as (38) (which gives the tip of the COR locus in the quasi-static case) when the workpiece pushed is a circular rim, for which $\rho = a$. For all other workpieces, $\rho < a$, so we may conclude that the COR for impact lies within the COR locus for quasi-static pushing if $e = 0$ or $\mu_c = 0$.

If $e > 0$ and $\mu_c > 0$, Wang finds that the sense of rotation (CW or CCW) does not necessarily agree with Mason's results for quasi-static motion [10]. This means that in realistic cases where $e > 0$, a given sliding operation which results in CW

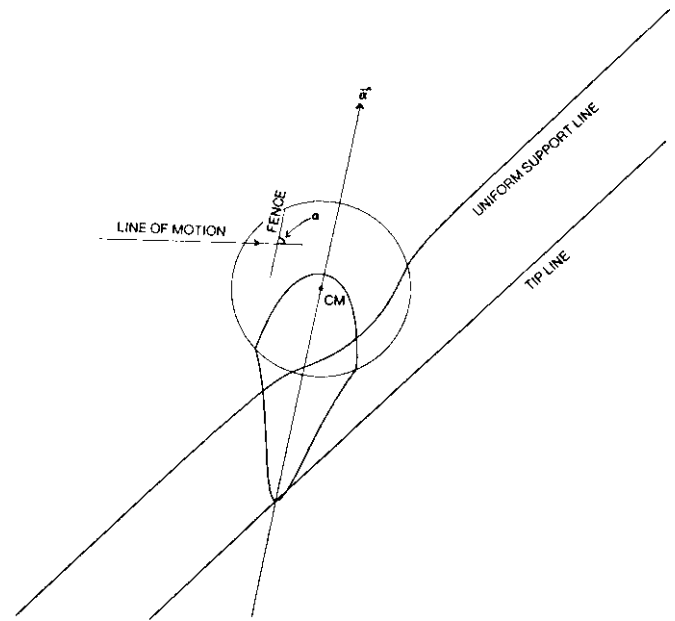


Fig. 45. Tip line and line of COR's for uniform pressure distribution. Shown is the tip line for all α . This is the curve traced out by the tip of the COR locus as α is changed. The tip is the farthest the COR can fall from the CM, no matter what pressure distribution exists beneath the disc. If we assume a *uniform* pressure distribution beneath the disc, then rather than a locus of COR's a single COR must be the result. For comparison with the tip line, we also plot here the curve traced out by the COR for uniform pressure distribution, as α is changed. For a given α such as the one shown, the COR locus is shown, the tip of the COR locus falls at the intersection of the vector $\bar{\alpha}$ with the tip line, and the COR for uniform pressure distribution lies at the intersection of the vector $\bar{\alpha}$ with the "uniform support line."

rotation of the pushed workpiece in the quasi-static limit may change over to CCW rotation as velocity is increased.

For fixed elasticity e and coefficients of friction μ_c and μ_s , as velocity is increased the locus of COR's describing the motion must change continuously from the quasi-static locus at $v = 0$ to the single point (sometimes outside the quasi-static locus) which is Wang's result at $v = \infty$. If the COR loci for intermediate velocities could be found or bounded, motion planning algorithms based on sliding friction (e.g., [14], [2], [9]) could be extended to non-quasi-static velocities.

D. Bounds on the COR Locus for Other than Discs

The COR loci found in Section V are exact if the sliding workpiece is a disc. Any COR in the locus could occur for some combination of bumps on the bottom of a disc, i.e., for some pressure distribution. The COR locus for a disc necessarily encloses the COR locus for any workpiece which could be enclosed in that disc, with the same center of mass. The COR locus for the inscribed workpiece may be considerably smaller than that for the disc, especially when the area of the inscribed workpiece is considerably less than that of the disc. The COR locus for a square, found numerically is shown in Fig. 6.

For comparison, the line of COR's for a *uniform* pressure distribution on a disk is shown in Fig. 45. In the uniform case, for each α (related to the force angle), there is of course only one COR, as the pressure distribution is completely specified.

Shown in the figure is a particular α for illustration, and the COR locus outline for all pressure distributions for that α . The tip line for all α is shown. The point of intersection of the $\vec{\alpha}$ vector through the CM and the tip line is the COR locus for α . The tip of the COR locus for any α lies at the intersection of the $\vec{\alpha}$ vector through the CM and the tip line. Similarly, the COR for uniform pressure for α lies at the intersection of the $\vec{\alpha}$ vector through the CM and the uniform pressure line, as indicated by a dot. The COR for uniform pressure for any α lies at the intersection of the $\vec{\alpha}$ vector through the CM and the line of uniform pressure.

Using the COR loci of discs in planning manipulation strategies for other shapes results in unnecessarily conservative strategies. It is even possible that no strategy might be found when one exists. This problem could be alleviated if exact COR loci for arbitrarily shaped workpieces could be found. In finding the COR locus for a disc we discovered two classes of "dipods" (pressure distributions consisting of only two points of support, Section IV-E) which were responsible for the boundary of the COR locus. For workpieces other than discs, the boundary is not described by dipods, and finding the COR locus becomes considerably harder.

ACKNOWLEDGMENT

The authors wish to acknowledge useful discussions with R. Brost and M. Mason, both of whom also contributed many helpful suggestions for improving this paper. Several equations were obtained or simplified using MACSYMA.

REFERENCES

- [1] J. Barber, R. A. Volz, R. Desai, R. Rubinfeld, B. Schipper, and J. Wolter, "Automatic two-fingered grip selection," presented at the IEEE 1986 Int. Conf. on Robotics and Automation, Apr. 1986.
- [2] R. Brost, "Automatic grasp planning in the presence of uncertainty," *Int. J. Robotics Res.*, vol. 7, no. 1, 1988.
- [3] M. A. Erdmann, "On motion planning with uncertainty," Master thesis, Mass. Inst. Technol., 1984, Tech. Rep. AI-TR-810.
- [4] M. A. Erdmann and M. T. Mason, "An exploration of sensorless manipulation," this issue, pp. 000-000.
- [5] S. Goyal and A. Ruina, "The load-motion relation for rigid bodies sliding on planar surfaces with dry friction," draft.

- [6] J. H. Jellett, *A Treatise on the Theory of Friction*. London, UK: MacMillan, 1872.
- [7] T. Lozano-Pérez, "Motion planning and the design of orienting devices for vibratory parts feeders," to be published.
- [8] W. D. MacMillan, *Dynamics of Rigid Bodies*. New York, NY: Dover, 1936.
- [9] M. Mani and W. R. D. Wilson, "A programmable orienting system for flat parts," in *Proc. NAMRII XIII*, 1985.
- [10] M. T. Mason, "Mechanics and planning of manipulator planning operations," *Int. J. Robotics Res.*, vol. 5, no. 3, 1986. Also in *Robot Hands and the Mechanics of Manipulation*. Cambridge, MA: MIT Press, 1985.
- [11] - , "On the scope of quasi-static pushing," in *Proc. 3rd Int. Symp. on Robotics Res.*, Oct. 1985.
- [12] M. T. Mason and R. Brost, "Automatic grasp planning: An operation space approach," in *Proc. 6th Symp. on the Theory and Practice of Robots and Manipulators* (Cracow, Poland, Sept. 1986).
- [13] M. A. Peshkin and A. C. Sanderson, "Manipulation of a sliding object," in *Proc. IEEE 1986 Int. Conf. on Robotics and Automation* (Apr. 1986), pp. 233-239.
- [14] - , "Planning robotic manipulation strategies for sliding objects," presented at the IEEE 1987 Int. Conf. on Robotics and Automation, Raleigh, NC, Apr. 1987; submitted to *IEEE J. Robotics Automat.*
- [15] M. A. Peshkin, "Planning robotic manipulation strategies for sliding objects," Ph.D. dissertation, Physics Dep., Carnegie-Mellon Univ., Oct. 1986.
- [16] K. Pingle, R. Paul, and R. Bolles, "Programmable Assembly, Three Short Examples," Film, Stanford AI Lab., 1974.
- [17] J. Prescott, *Mechanics of Particles and Rigid Bodies*. London, UK: Longmans, Green and Co., 1923.
- [18] E. J. Routh, *Dynamics of a System of Rigid Bodies*, 7th ed. New York, NY: Dover, 1960.
- [19] Y. Wang and M. T. Mason, "Modeling impact dynamics for robotic operations," in *Proc. 1987 IEEE Int. Conf. on Robotics and Automation* (Raleigh, NC), pp. 678-685.
- [20] - , personal communication.
- [21] M. A. Peshkin and A. C. Sanderson, "Minimization of energy in quasistatic manipulation," in *Proc. IEEE 1988 Int. Conf. on Robotics and Automation* (Philadelphia, PA); submitted to *IEEE J. Robotics Automat.*

Michael A. Peshkin (S'86-M'86), for a photograph and biography please see page 531 of the October 1988 issue of this JOURNAL.

Arthur C. Sanderson (S'66-M'68-M'74-SM'86), for a photograph and biography please see page 531 of the October 1988 issue of this JOURNAL.

The Motion of a Pushed, Sliding Workpiece

M. A. Peshkin* and A. C. Sanderson+
Robotics Institute
Carnegie-Mellon University
Pittsburgh, PA 15213

ABSTRACT: It occurs frequently in robotic applications that a robot manipulates a workpiece which is free to slide on a work surface. Because the pressure distribution supporting the workpiece on the work surface cannot in general be known, the motion of the workpiece cannot be calculated uniquely. Yet despite this indeterminacy, several researchers have shown that sliding motions can be employed to accurately align workpieces without visual or other feedback.

Here we find the locus of centers of rotation of a workpiece for *all* possible pressure distributions. The results allow a quantitative understanding of open-loop robot motions which guarantee the alignment of a workpiece. Several sample problems are solved using the results, including the distance that a flat "fence" or robot finger must push a polygonal workpiece to assure that a facet of the workpiece comes into alignment with the fence.

KEYWORDS: Center of rotation, sliding, slipping, pushing, grasping, manipulation, friction.

This work was supported by a grant from Xerox Corporation and by the Robotics Institute, Carnegie Mellon University.

* current address: Mechanical Engineering, Northwestern University, Evanston, IL 60201

+ current address: Electrical, Computer, and Systems Engineering, Rensselaer Polytechnic Institute,
Troy, NY 12180

1. Motivation

Sliding operations are encountered frequently in robotics. It is almost inevitable that when the position of a workpiece that is to be acquired by a robot is not perfectly known, a sliding phase will occur before the robot can acquire the workpiece. Mason [10] was the first to identify sliding operations as *fundamental* to manipulation, and especially to grasping.

The sliding phase need not be considered an undesirable but unavoidable fact of life. In the examples which follow sliding operations are used constructively to manipulate and acquire workpieces, without sensing, and despite uncertainty in the initial orientation and position of the workpiece. Yet in each example quantitative information about the motion of the workpiece, which would be needed to guarantee the success of the operation, is lacking. It is the objective of this paper to solve completely for the motion of a sliding workpiece, thus allowing proof of the success of operations which rely on sliding, and facilitating the design of such operations.

1.1. Automatic Feeders

Sliding occurs when a workpiece on a moving belt interacts with a fence across the belt. (An equivalent interaction occurs when the workpiece is stationary on a work surface, and a fence or gripper under control of a robot pushes it.) And similar interactions occur in bowl feeders, as parts interact with fences as the parts move along a ramp.

One of the many possible behaviors of the workpiece when it hits a fence is to rotate until a flat edge is flush against the fence, and then to slide along the fence (if the fence is sufficiently slanted.) Another behavior is to roll along the fence instead of sliding. Or the workpiece may stop rotating and simply stick to the fence.

To design feeders the behavior of the workpiece must be understood. This problem has been considered explicitly by Mani and Wilson [9] and also by Brost [2]. (Related work includes [7] and [4].) Mani and Wilson developed strategies for manipulation which can orient a workpiece on a table by a carefully planned sequence of pushes with a fence. Each push aligns a facet of the workpiece with the fence, until an initially randomly oriented workpiece is reduced to a unique final orientation.

In the case of Mani and Wilson's fence-pushing aligner, the quantitative information needed is the distance a polygonal workpiece must be pushed to align a given facet with the pushing fence. Sometimes a workpiece may have to be pushed a great distance before it will align with the fence pushing it. To make Mani and Wilson's manipulation strategies into guaranteed strategies we need an upper bound on the distance a workpiece must be pushed to align.

1.2. Grasping Strategies

In a typical grasping operation, the robot opens a two-jaw gripper wide enough to accommodate both the workpiece to be grasped, and any uncertainty in the workpiece's position. Then the gripper begins to close. Generally the workpiece will be closer initially to one jaw than to the other, and the closer jaw will make contact first.

There follows a sliding phase until the second jaw makes contact. During the sliding phase the workpiece is likely to rotate, especially if the face of the jaw is in contact with a corner of the workpiece rather than a flat facet. The behavior of the workpiece during grasping is discussed by Brost [2], who finds grasp strategies which bring the workpiece into a unique orientation in the gripper, despite substantial uncertainty in its initial orientation and position.

To fully characterize the configuration of the workpiece in the gripper when a grasping operation is complete, we need more complete information about the motion of the workpiece than was available to Brost. Bounds can be obtained for the translation of the workpiece (perpendicular to the direction it is pushed by the gripper) as well as for its rotation as it is pushed.

R. P. Paul invented [16], and Mason later analyzed [10], a clever grasping sequence on a hinge plate. (Figure 1-1.) The strategy makes use of sliding to simultaneously reduce the uncertainty of a hinge plate's configuration to zero, and then to grasp it.

The hinge grasp works only for a certain range of initial hinge orientations. For orientations outside of this range, the jaws will be closing too fast for the hinge plate to complete its clockwise rotation into alignment, before the jaws close. To find the range of orientations for which this grasp will work, for a given convergence angle of the jaws, we need to know the slowest possible rotation rate of the hinge plate as it is pushed.

1.3. Grasp Strength

Barber et. al. [1] have analyzed the resistance of a two-fingered robot grasp of a workpiece to applied torques and forces. A grasped workpiece slides relative to the gripper fingers as the grasp fails, and the resistance of a grasp to this failure can be used as a measure of the quality of the grasp in automated grasp selection algorithms.

In order to determine the force or torque which is needed to cause a grasp to slip, Barber et. al. assumed a linear variation of pressure over the grasped surface of the workpiece. The utility of this measure of grasp quality could be extended if the assumption of linear pressure variation could be removed, since in

Figure 1-1: Hinge grasp strategy (Paul [16] and Mason [10])

The robot fingers follow the trajectory indicated by the dotted lines, closing as they translate. On contact with the hinge-plate the trajectory causes the plate to rotate into alignment with the gripper and then to self-center. This open-loop strategy requires no sensing and succeeds despite some uncertainty in the initial configuration of the plate.

general the pressure distribution is unknown.

1.4. Statement of "The Sliding Problem"

The prototypical sliding problem is to solve for the motion of a workpiece on a planar surface with friction, when a force is applied to it at a known point. This is a problem in classical mechanics, indeed in quasistatic mechanics. It was recognized but never solved in the heyday of classical mechanics [6] [8] [17], although the answers turn out to be simple and of analytical form. The sliding problem is difficult because the pressure distribution beneath the workpiece is in general unknown. The 19th and early 20th century classical mechanicians (cited above) assumed a particular form of the pressure distribution, either uniform or with linear variation over the bottom surface of the workpiece, and solved the difficult mechanics problem which resulted.

Mason realized the only useful result would be one which applied for all pressure distributions, as the pressure distribution is unknown. Mason was able to find the direction (clockwise or counterclockwise) of rotation of a pushed, sliding workpiece, when the pressure distribution is unknown [10]. His result is remarkable in that the direction turns out to be independent of the pressure distribution. Mason's results are used extensively in Mani and Wilson's work [9], Brost's work [2], and also here.

Our work solves the "other half" of the sliding problem. We determine the motion of the sliding workpiece completely. The motion is most conveniently expressed as a center of rotation (COR) of the sliding workpiece. (The COR lies somewhere in the plane of sliding.) Unlike Mason's sense of rotation result, the COR does depend on the pressure distribution supporting the workpiece, and that pressure distribution is in general unknown. But we are able to find the locus of centers of rotation (that is, the set of all possible motions) for all pressure distributions.

Using our results manipulation and grasping strategies can be designed which are guaranteed to succeed [13], because all the possible motions of the pushed workpiece are predictable.

2. Range of Applicability

2.1. Workpiece shape

In this paper we will treat the workpiece as a two-dimensional rigid body, since we are only concerned with the interaction of the workpiece with the table on which it is sliding. All pushing forces will be restricted to lie in the plane of the table. The results may be applied to three-dimensional workpieces, so long as the vertical component of the pushing force is negligible, and so long as the point of contact is near the table.

2.2. Point of contact between workpiece and pusher

In the general case, when a workpiece is being pushed there is only one point of contact between the workpiece and the pusher. The contact may be where the flat edge of a pushing fence or robot finger touches a corner of the workpiece (figure 2-1), or it may be where a pushing point touches an edge of the workpiece (figure 2-2). In most of this paper we will assume that the pusher is a point in contact with a flat facet of the workpiece, but the analysis applies equally well if the pusher is a flat surface in contact with a corner of the workpiece.

Motion of a workpiece when there are two or more points of contact between pusher and workpiece has been considered by Brost [2] and by Mani and Wilson [9].

Figure 2-1: The edge of an advancing fence pushing a corner of a sliding workpiece

The motion of the workpiece depends on the angle (α) of the front edge of the fence, measured relative to its line of motion, which in this case is horizontal.

Figure 2-2: A corner of an advancing pusher pushing an edge of a sliding workpiece

The motion of the workpiece depends on the angle (α) of the edge being pushed, measured relative to the line of motion of the pusher, which in this case is horizontal. Compare to the meaning of α in figure 2-1. The analysis done in this paper applies equally well to either figure.

2.3. Position controlled pusher

It is assumed the pusher will move along a predetermined path in the plane, i.e., it is under position control. Equivalently, the surface on which the workpiece slides may move, carrying the workpiece relative to a fixed pusher, for example on a conveyor belt. The workpiece has two degrees of freedom, with the third degree of freedom of its motion fixed by the contact maintained between the pusher and the workpiece. Our results may be easily converted to the case where the pusher exerts a known force on the workpiece rather than following a known path.

2.4. Center of rotation (COR)

The two degrees of freedom of the workpiece are most conveniently expressed as the coordinates of a point in the plane called the *center of rotation* (COR). Any infinitesimal motion of the workpiece can be expressed as a rotation $\delta\theta$ about some COR, chosen so that the infinitesimal motion of each point \vec{r} of the workpiece is perpendicular to the vector from the COR to the point \vec{r} . If the workpiece is a disk, and the motion it performs is pure rotation in place, the COR is at the center of the disk. Motions we might describe as "mostly translation" correspond to CORs far from the point of contact. In the extreme case, pure translation occurs when the COR is at infinity.

All kinematic results can be obtained once the COR is found.

2.5. Pressure distribution between workpiece and table

The weight of a workpiece is supported by a collection of contact points between the workpiece and the table. The pressure distribution may change as the workpiece moves relative to the table. Finding the COR is complicated by the fact that changes in the pressure distribution under the workpiece substantially affect the motion, i.e., such changes affect the location of the COR. Intuitively, if pressure is concentrated

near the center of mass (CM), the workpiece will tend to rotate more and translate less than if the pressure is uniformly distributed over the entire bottom surface of the workpiece.

The pressure distribution may be changed dramatically by tiny deviations from flatness in the workpiece's bottom surface (or of the surface it is sliding on.) Indeed, if the workpiece and the table are sufficiently rigid and not perfectly flat, they may be expected to make contact at only three points. The three points may be located anywhere on the workpiece's bottom surface, but like the legs of a three-legged stool, the triangle formed by the points of support always encloses the projection of the CM onto the surface.

Since any assumption we could make about the form of the pressure distribution (for instance that it is uniform under the workpiece as in [17]) would not be justified in practice, our goal is to find the locus of CORs under *all* possible pressure distributions.

Let the CM be at the origin, and \vec{r} be a point in the plane. All that is known about the pressure distribution

$P(\vec{r})$ is that

- $P(\vec{r})$ is zero outside the workpiece. The workpiece can be entirely contained within a circle of radius a centered at the CM.
- $P(\vec{r}) \geq 0$ everywhere,
- the total pressure $\int P(\vec{r}) d\vec{r} = Mg$, the weight of the workpiece, and
- the first moment of the distribution, $\int P(\vec{r}) \vec{r} d\vec{r} = 0$. This means that the centroid of the distribution is at the CM of the workpiece, which is at the origin.

2.6. Coulomb friction

It turns out that the coefficient of friction of the workpiece with the supporting surface (called μ_s for "sliding friction") does not affect the motion of the workpiece if we use a simple model of friction. We assume that μ_s is constant over the work surface, that it is independent of normal force magnitude and tangential force magnitude and direction (isotropic), and that it is velocity independent. In short, we assume Coulomb friction.

There is another coefficient of friction in the problem, μ_c (for "contact friction"), at the point of contact between the edge of the workpiece and pusher. This is distinct from the coefficient μ_s between workpiece and table, discussed above. Initially we consider only $\mu_c=0$. This assumption is relaxed in section 6.

2.7. Quasi-static motion

It is assumed that all motions are slow. This *quasi-static approximation* requires that frictional forces on the workpiece (due to the coefficient of friction with the surface μ_s) quickly dissipate any kinetic energy of the workpiece:

$$v^2 \ll Xg\mu_s \tag{1}$$

where v is the velocity of the workpiece, g is the acceleration due to gravity, and X is the precision with which it is desired to calculate distances. The high-speed limit is discussed in section 12.3.

Characteristic speeds for quasistatic motion are discussed in [15] and [11].

2.8. Bounding the workpiece by a disk

We will take the workpiece being pushed to be a disk with its CM at the center. Given another workpiece of interest we can consider a disk centered at the CM of the workpiece, big enough to enclose it. The radius a of the disk is the maximum distance (from the CM) of the workpiece to any point of the workpiece. Since any pressure distribution on the workpiece could also be a pressure distribution on the disk, the COR locus of the disk must enclose the COR locus of the workpiece. The locus for the disk provides useful bounds on the locus for the real workpiece.

2.9. Geometric parameters

Geometric parameters of the problem are the point of contact \vec{c} between the pusher and the workpiece, and the angle α between the edge being pushed and the line of pushing, as shown in figure 2-3. The values of α and \vec{c} shown are useful in considering the motion of the five-sided workpiece shown inscribed in the disk. We do not require the point of contact to be on the perimeter of the disk, as this would eliminate applicability of the results to workpieces inscribed in the disk. Indeed, for generality we do not even require the point of contact to be within the disk. Similarly, we will not require α to be such that the edge being pushed is perpendicular to vector \vec{c} , as it would be if the workpiece were truly a disk. The disk (with radius a), α , \vec{c} , and the CM, are shown in figure 2-3. A particularly simple pressure distribution $P(\vec{r})$, in which the support is concentrated at just a "tripod" of points $(\vec{r}_1, \vec{r}_2, \vec{r}_3)$ is indicated, along with the COR which might result for that pressure distribution.

Figure 2-3: Parameters of the pushing problem

Important geometric parameters are the angle α of the edge being pushed relative to the line of motion of the pusher, the vector \vec{r} from the center of mass (CM) to the point of contact between pusher and workpiece, and the radius a of the disk which circumscribes the workpiece. When these parameters are given the locus of centers of rotation for all possible pressure distributions can be found.

3. Overview

In this paper we wish to find not the *sense* of rotation (CW or CCW) as Mason did, but the motion itself, expressed as a COR somewhere in the plane.

First we approach the problem numerically. A formulation of Newton's laws of motion which we call "minimum power mechanics" suggests that for a given pressure distribution $P(\vec{r})$ and advance of the pusher dx , the COR is at that point which minimizes the energy lost to sliding friction. Figures 3-1 and 3-2 show the CORs so found for hundreds of thousands of randomly selected pressure distributions, for a pushed disk and a pushed square respectively. In these figures the point of contact between pusher and workpiece is unphysically chosen to be *outside* the perimeter of the workpiece to ease problems of numerical convergence.

Note that if the centers of mass of the disk and the square are superimposed the COR locus for the disk will entirely cover the COR locus for the square. As discussed in section 2.8, this is because the disk entirely covers the square, so any pressure distribution on the square could be a pressure distribution on the disk. The COR which results from any pressure distribution on the square therefore must also be a possible COR for the disk. To bound the COR locus for any workpiece it is therefore only necessary to find the COR locus for a disk which circumscribes the workpiece of interest.

Next we approach the problem analytically. We express the energy lost to sliding friction for a fixed advance of the pusher dx as an integral of the pressure distribution $P(\vec{r})$. The disk will seek that COR which minimizes the energy lost to sliding friction. Minimizing this energy with respect to the location of the COR, we find an intrinsic solution for the COR in terms of two moments of the unknown pressure

Figure 3-1: COR locus for a disk found by iterative minimization (dots)

The disk shown encloses the workpiece of interest. The pusher moves horizontally along the line indicated, and contacts the edge of the workpiece at the arrowhead. (In reality this point of contact would always fall within the disk bounding the workpiece, but numerical convergence is simplified for this unrealistic case.) The angle α of the edge which the pusher contacts is indicated. Dots indicate the locations of the center of rotation for 500,000 randomly chosen pressure distributions supporting the workpiece.

Figure 3-2: COR locus for a square found by iterative minimization.

Now the workpiece is taken to be a square rather than a disk. (Again we unrealistically choose a point of contact not on the perimeter of the workpiece.) Note that the locus of possible CORs (dots) can be entirely contained within the locus calculated for a disk (figure 3-1).

distribution $P(\vec{r})$. The COR is related to the ratio of these moments. When the pushed workpiece is a disk, we are able to identify two classes of pressure distributions which are responsible for extremal values of the moment ratio, and therefore also are responsible for extremal values of the COR. These special pressure distributions are simply dipods: pressure distributions consisting of just two points of support. In one class of dipods, one point of support is anywhere on the perimeter of the disk and the other diametrically opposite it. The second class is only slightly more complicated. By solving for the COR analytically for these special classes of pressure distributions, the boundary of the COR locus is found.

In figure 3-3 we show a typical pushing problem and the boundary of the locus of all possible centers of rotation of the pushed workpiece.

Note that the COR locus is symmetric about the angle of the pushed edge α , which is drawn as a vector $\vec{\alpha}$ in figure 3-4. The farthest point of the COR locus from the CM falls on $\vec{\alpha}$. For most applications this "tip" of the COR locus is of particular importance, as it specifies the slowest possible rotation of the workpiece as it is pushed, regardless of the pressure distribution. The distance r_{tip} from the center of the disk to the tip of the COR locus has a simple relation to the parameters of the problem:

$$r_{tip} = \frac{a^2}{\alpha \cdot \vec{c}} \quad (2)$$

This formula has an interesting geometric interpretation. As the edge angle α is varied, the tip of the COR locus traces out a straight line called the "tip line", and shown in figure 3-4. The tip line is perpendicular to \vec{c} and a distance a^2/c from the CM. Simple formulae exist for the curvature of the boundary of the COR locus at the tip (and at the interior end as well), and for the points of intersection of the boundary of the COR locus with the perimeter of the disk. For most purposes the formulae for these

Figure 3-3: A typical pushing problem and the boundary of the COR locus found.

A point pusher is advancing horizontally, and is pushing the edge of a workpiece. The circle represents the circumscribing disk for which the center of rotation locus can be found. The bold outline is the boundary of the COR locus for this pushing operation; regardless of the actual pressure distribution supporting the workpiece the center of rotation will lie somewhere in this boundary. Any kinematic result can be obtained once the COR locus has been found.

points of the COR locus suffice, and it is unnecessary to find the entire locus.

As an application of the results so far, we can calculate the maximum distance it is necessary to push a polygonal workpiece with a frictionless fence, in order to guarantee alignment of an edge of the workpiece with the fence, regardless of the pressure distribution beneath the workpiece (equation 42.)

As noted, the COR loci discussed above apply only when μ_c , the coefficient of "contact friction" between the pusher and the pushed workpiece, is zero. In section 6 we generalize to $\mu_c > 0$. The COR locus for $\mu_c > 0$ turns out to be a combination of two of the COR loci calculated for $\mu_c = 0$. The two COR loci used are those with "effective" edge angles $\alpha \pm \tan^{-1}\mu_c$. Part of each of these two loci, plus a linear segment just above the tip line, constitute all the possible centers of rotation for $\mu_c > 0$. In figure 3-5 the shaded and bold sections are the resulting COR locus for $\mu_c > 0$. (Similar "effective angles" were shown in Mason and Brost's figure 5 [12].)

As examples of the $\mu_c > 0$ results we find the distance a polygonal workpiece must be pushed by a fence to assure alignment of an edge of the workpiece with the fence, now with $\mu_c > 0$. We also analyze the motion of a sliding disk as it is pushed aside by the corner of a workpiece in linear motion. Finally, we study the effectiveness of an open-loop manipulation strategy based on "herding" a disk toward a central goal by moving a pusher in a decreasing spiral about the goal.

3.1. Minimum power mechanics

Suppose that the geometry of a pushing operation is specified; that is, the radius a of the disk enclosing the workpiece, the point \vec{c} at which the workpiece is being pushed, and the angle α of the flat surface involved in the push. If we suppose further that a single pressure distribution is specified, then a unique

Figure 3-4: $r_{tip}(\alpha)$ vs. α , and construction of the tip line

The most useful point on the COR locus boundary seems to be the tip, as this is the COR for which rotation of the workpiece is slowest. The distance to the tip (from the CM) is given by the simple formula $r_{tip} = a^2 / \bar{\alpha} \cdot \vec{c}$. As the angle of the pushed edge α is varied, the tip of the COR locus sweeps out a straight line called the tip line.

Figure 3-5: Construction of the COR sketch

When the coefficient of friction between pusher and edge of workpiece $\mu_c > 0$, the locus of possible CORs can be constructed from two of the simpler COR loci which we calculated for $\mu_c = 0$. The two $\mu_c = 0$ loci are shown in outline, while the COR "sketch" for a non-zero μ_c is shown shaded. Depending on where the COR falls in the COR sketch, slipping of the workpiece (either up or down) relative to the pusher, or sticking, may be predicted.

COR at a single point must be the result.

Our system is *constrained* because the pusher and the workpiece are in contact, the pusher is advancing a distance dx in a given instant, and the workpiece must slide enough to accommodate the advance of the pusher. The COR could be at almost any point in the plane, and still allow the workpiece to accommodate the advance of the pusher. However, some of these locations will require a greater rotation of the workpiece (about the COR) to accommodate the advance of the pusher than do others.

To solve for the COR we use a formulation of Newton's laws for constrained motions which we call minimum power mechanics [15]. Minimum power mechanics expresses the intuitively appealing idea that the motion a system makes (e.g. the COR about which the workpiece actually *does* choose to rotate) will be the one for which the energy dissipated to sliding friction is minimized.

We have proven that minimum power mechanics is correct under some fairly restrictive conditions [15]: slow (quasistatic) motion is required, and the only dissipative forces which may occur in the system are (slightly generalized) analogues of Coulomb friction. The present system qualifies. (Minimum power mechanics should not be confused with the principle of virtual work, which applies to static systems without dissipation, and sets energy to zero rather than minimizing it.) Recently Goyal and Ruina have done further work on minimization principles in quasistatic mechanics [5].

3.2. Notation

- Vectors are indicated by an arrow, e.g., \vec{v} .
- \vec{r} is the vector from the CM to the COR. r is the magnitude of that vector, i.e., the distance from the CM to the COR.
- A Greek letter is used to represent both an *angle* and a *unit vector* which makes that angle with respect to the x-axis (measured CCW). An arrow is used to indicate the unit vector: $\vec{\alpha} = (\cos \alpha, \sin \alpha)$.
- We indicate functional dependence with subscripts. E_r is a function of \vec{r} (the COR).

- All integrals are over the area of the disk.
- Curly brackets indicate a locus of values of a quantity.

4. Solution for the COR locus

In this section we compute the energy that is dissipated due to friction when the pusher advances a distance δx , as a function of the center of rotation \vec{r} , and for a given pressure distribution $P(\vec{r})$. We will then minimize the energy with respect to \vec{r} to find the COR about which the workpiece actually *does* choose to rotate.

It may help to imagine the disk "pinned" at the COR. This is not difficult to imagine if the COR happens to fall inside the perimeter of the disk, and one's intuition can be extended to include the case where the COR is outside the perimeter. Either way, the disk is free to rotate *only about the COR*, and the COR itself stays stationary.

Given the COR, the motion of the disk is fully determined when we apply our constraint: the edge being pushed (at \vec{c}) must move out of the way of the advancing pusher, but stay in contact.

4.1. Relation between motion of the pusher and rotation of the workpiece

In order to accommodate the advance δx of the pusher, the disk will rotate an amount $\delta\theta$ about the center of rotation \vec{r} . A rotation of $\delta\theta$ allows an advance of the pusher δx consisting of two parts, as shown in figure 4-1.

$$\begin{aligned}\delta x_1 &= \delta\theta |\vec{c} - \vec{r}| \cos \theta = \delta\theta (c_y - r_y) \\ \delta x_2 &= \delta x_1 \frac{\tan \theta}{\tan \alpha} = \delta\theta \frac{c_x - r_x}{\tan \alpha}\end{aligned}\tag{3}$$

Note that δx_2 corresponds to slipping of the point of contact along the workpiece edge.

Figure 4-1: Relation between advance of pusher (δx) and rotation about the COR ($\delta\theta$)

For fixed COR the pusher may advance a distance dx while the workpiece rotates an angle $d\theta$ about the COR. dx consists of two parts: movement of the workpiece edge (dx_1), and slipping of the pusher along the edge (dx_2).

Defining the unit vector $\alpha = (\cos \alpha, \sin \alpha)$ we can write

$$\delta x = \delta x_1 + \delta x_2 = \frac{\delta \theta}{\sin \alpha} \alpha \cdot (\vec{c} - \vec{r}). \quad (4)$$

To avoid proliferation of absolute value signs, henceforth $\alpha \cdot (\vec{c} - \vec{r})$ will be taken to be positive.

Considerations of symmetry will allow application of the results to cases where $\alpha \cdot (\vec{c} - \vec{r})$ is negative.

Physically, $\alpha \cdot (\vec{c} - \vec{r}) > 0$ corresponds to clockwise rotation of the workpiece as it is pushed.

4.2. Energy lost to friction with the table

An area element of the disk at \vec{w} supports a force $P(\vec{w}) d\vec{w}$ normal to the table. The element will slide a distance

$$\delta \theta |\vec{w} - \vec{r}| \quad (5)$$

due to the rotation $\delta \theta$ about the center of rotation \vec{r} , and in the process will dissipate an amount of energy

$$dE_r = \mu_s P(\vec{w}) d\vec{w} \delta \theta |\vec{w} - \vec{r}|. \quad (6)$$

Integrating over the area of the disk, the total energy dissipated due to rotation $\delta \theta$ is

$$E_r = \delta \theta \mu_s \int P(\vec{w}) |\vec{w} - \vec{r}| d\vec{w} \quad (7)$$

where we write E_r to remind ourselves that the energy is a function of the presumed location of the center of rotation \vec{r} . Substituting for $\delta \theta$, we have

$$E_r = \frac{\delta x \mu_s \sin \alpha}{\alpha \cdot (\vec{c} - \vec{r})} \int P(\vec{w}) |\vec{w} - \vec{r}| d\vec{w}. \quad (8)$$

The system will find a location for \vec{r} which minimizes E_r . At this minimum the derivatives of E_r with respect to both \vec{r}_x and \vec{r}_y must be zero. Evaluating the derivative of E_r with respect to \vec{r} and setting it equal to zero we find

$$\nabla E_r = \delta x \mu_s \sin \alpha \frac{[d_r \alpha - \vec{v}_r \alpha \cdot (\vec{c} - \vec{r})]}{[\alpha \cdot (\vec{c} - \vec{r})]^2} = 0 \quad (9)$$

where

$$d_r = \int P(\vec{w}) |\vec{w} - \vec{r}| d\vec{w} \quad (10)$$

a scalar, can be physically interpreted as the weighted *distance* from the COR to the pressure distribution,

and

$$\vec{v}_r = \int P(\vec{w}) \frac{\vec{w} - \vec{r}}{|\vec{w} - \vec{r}|} d\vec{w} \quad (11)$$

a vector, can be interpreted as the weighted *direction* from the COR to the pressure distribution.

4.3. A digression: Iterative numerical solution

Minimization of E_r can be carried out in an iterative manner to find the COR for a given pressure distribution $P(\vec{w})$. Figure 3-1 shows the locus of CORs obtained in this manner. Each point is the COR for a randomly chosen three-point pressure distribution. Only pressure distributions consisting of three points (a tripod) need be considered since according to Mason's theorem 5 [10] three points are sufficient. Weights were computed for the three points in such a way as to satisfy the constraint that the CM be at the center of the disk. (If this required any of the weights to be negative, the tripod was discarded.) An initial guess was made for the location of the center of rotation \vec{r} , and ∇E_r evaluated at that point.

The minimization technique used requires computation of $\nabla(\nabla E_r)$, the second derivative of E_r , (a two-by-two matrix,) which can be obtained analytically. A new guess for \vec{r} is then made by adding to the old guess

$$\Delta \vec{r} = \frac{-\nabla E_r}{\nabla(\nabla E_r)}. \quad (12)$$

This method usually converged quickly if the initial guess was sufficiently close to the correct answer. By moving only one leg of the tripod at a time, and by only a small amount, the value of \vec{r} found for one tripod could be used as an initial guess for the next. Figure 3-1 represents 590000 tripods, taking 4 CPU

hours on a VAX-780. Similar figures done with four points of support instead of tripods are identical, numerically validating Mason's theorem 5 [10].

4.4. Analytic solution

Resuming our analytical discussion from section 4.2, we set $\nabla E_r = 0$ in equation 9. The constant terms drop out leaving

$$r^2 \bar{\alpha} = \bar{q}_r [\bar{\alpha} \cdot (\bar{c} - \bar{r})] \quad (13)$$

where we define the *quotient moment*, a vector, as

$$\bar{q}_r = r^2 \frac{\bar{v}_r}{d_r} . \quad (14)$$

with \bar{v}_r and d_r given in equations 10 and 11. \bar{q}_r is a function of the COR \bar{r} and the pressure distribution $P(\bar{w})$, and has units of distance. In this section we *hold the center of rotation \bar{r} fixed*, and analyze the quotient moment for all pressure distributions $P(\bar{w})$.

The *quotient locus* $\{\bar{q}_r\}$ is the set of \bar{q}_r for all possible choices of the pressure distribution $P(\bar{w})$ consistent with the requirements listed in section 2.5. It is still a function of \bar{r} , but the dependence on $P(\bar{w})$ has been removed. Unfortunately we have been unable to develop any physical intuition about the meaning of the quotient locus. We regard it merely as an intermediate mathematical construction, more tractable than the COR locus to which it is related.

We will always plot the quotient locus displaced by \bar{r} , i.e., based at the COR. $\{\bar{q}_r\}$ may be plotted as a region of space, if we remember that a given $\bar{q} \in \{\bar{q}_r\}$ is a *vector* with its tail at the COR and its head anywhere in that region.

We will find the boundary of the quotient locus. The results will allow us to find the boundary of the COR

locus in section 4.9.

To simplify discussion, we take the total weight of the workpiece $Mg = 1$, that is

$$Mg = \int P(\vec{w}) d\vec{w} = 1 . \quad (15)$$

Since multiplying the pressure distribution P by a constant factor changes both numerator and denominator of \vec{q}_r by that same factor, the assumption is harmless. Physically, the mass of the disk has no effect on the motion, so we can choose it arbitrarily.

4.5. Extrema of the Quotient Locus

Since \vec{v}_r (equation 11) can be interpreted as a weighted average of *unit vectors* from the COR to the pressure distribution, the greatest magnitude \vec{v}_r can have will be 1, and will be attained when the pressure distribution is concentrated at the CM. In all other cases the direction to elements of the pressure distribution varies, and so some cancellation is inevitable. When the magnitude of \vec{v}_r is maximal, it must be directed from the COR to the CM.

The smallest magnitude \vec{v}_r can achieve depends on whether the COR is inside or outside the disk, i.e., on whether $r > a$ or $r < a$, where a is the radius of the disk. In either case we wish to achieve the maximum amount of cancellation of direction possible. If $r > a$ this occurs when the pressure distribution consists of two points at opposite edges of the disk, providing the minimum possible agreement on direction between the two vectors, as shown in figure 4-2.

If $r < a$, we can arrange for \vec{v}_r to be zero. Indeed we can arrange for \vec{v}_r to point from the COR maximally away from the CM by making a two-point pressure distribution as shown in figure 4-3. (In the figure the distance from w_2 to the COR is infinitesimal.) The two vectors \vec{w}_1 and \vec{w}_2 point in opposite directions. To

Figure 4-2: Dipod responsible for the smallest value of \vec{v}_r , for $r > a$

We study extrema of the moments \vec{v}_r and d_r of the pressure distribution to find extrema of the "quotient moment" $\vec{q}_r = \vec{v}_r / d_r$. We study extrema of the quotient moment \vec{q}_r to obtain bounds on the COR to which it is related.

\vec{v}_r is the weighted unit vector from the COR (\vec{r}) to the pressure distribution. It is maximized when the pressure distribution supporting the workpiece is concentrated at the CM. When $r > a$, \vec{v}_r is minimized by the pressure distribution shown here: half the weight of the workpiece is concentrated at each of the two points of support \vec{w}_1 and \vec{w}_2 , which are chosen to provide as little agreement in direction from the COR as possible.

Figure 4-3: Dipod responsible for a negative value of \bar{v}_r , for $r < a$

If the COR is within the disk ($r < a$), it is even possible to arrange for \bar{v}_r to point from \bar{r} away from the CM, by choosing the pressure distribution to be a dipod such as this one. As w_2 is closer to the CM than w_1 , it bears more than half of the weight of the disk.

maintain the centroid of the pressure distribution at the CM, we find the weights of \bar{w}_1 and \bar{w}_2 are

$$P_1 = \frac{r}{r+a}, \text{ and} \quad (16)$$

$$P_2 = \frac{a}{r+a}.$$

Therefore \bar{w}_2 is more heavily weighted than \bar{w}_1 , and

$$\bar{v}_r = P_1 \bar{v}_1 + P_2 \bar{v}_2 = (P_2 - P_1) \bar{v}_2 = \frac{a-r}{a+r} \bar{v}_2 \quad (17)$$

points from the COR away from CM.

Now consider d_r (equation 10). Clearly if the pressure distribution is concentrated at the CM, the weighted distance from the COR to the pressure distribution is just r . In fact r is the smallest value which d_r can attain. In the configuration shown in figure 4-3,

$$d_r = P_1 \cdot (a+r) + P_2 \cdot 0 = r. \quad (18)$$

d_r takes on its maximum value when the pressure distribution consists of two points as in figure 4-2.

That value is

$$d_r = (r^2 + a^2)^{1/2}. \quad (19)$$

Since \bar{q}_r is the quotient of \bar{v}_r and d_r , extreme values of $|\bar{q}_r|$ occur when \bar{v}_r is maximal and d_r minimal, and when \bar{v}_r is minimal and d_r maximal. Figures 4-2 and 4-3 illustrate the pressure distributions which (simultaneously) minimize \bar{v}_r and maximize d_r , for $r > a$ and $r < a$ respectively.

4.6. Numerical explorartion of the Quotient Locus

We can find the locus of all possible quotients numerically. It is much easier to find the $\{\bar{q}_r\}$ locus (for a given value of \bar{r}) than it is to find the COR locus. No iteration is required; for a given tripod, the moments \bar{v}_r and d_r can be calculated immediately. Figures 4-4 and 4-5 show typical $\{\bar{q}_r\}$ loci for $r < a$ and $r > a$, respectively. The dots are values of \bar{q}_r found numerically, while the solid curve is the empirical boundary

of the locus as described below.

The dots in figures 4-4 and 4-5 represent over 3,000,000 and 500,000 randomly chosen tripods, respectively. The solid curves which appear to bound the dots are generated by two classes of dipods, discussed below. On the basis of numerical studies such as shown in these figures, we believe that no value of \vec{q}_r generated by a tripod or any other pressure distribution falls outside the dipod curve. Therefore the dipod curve is the exact boundary of $\{\vec{q}_r\}$. We have not been able to prove analytically that no value of \vec{q}_r falls outside the dipod curve, so the boundaries should be considered empirically justified only.

4.7. Boundary for $|\text{COR}| < a$

We observe that for $r < a$ the boundary of the locus is a circle. This empirical boundary can be generated by two-point pressure distributions (dipods) of the type shown in figure 4-6, where the angle ω can vary. These dipods are a generalization of the one shown in figure 4-3 . (The distance from \vec{r} to \vec{w}_2 is infinitesimal.) We can then calculate a parametric form for the boundary in terms of ω :

$$\vec{q}_r = \vec{\omega} \frac{r}{r+a} (a\vec{\omega} - \vec{r}) \quad (20)$$

where $\vec{\omega} = (\cos \omega, \sin \omega)$

This generates a circle of radius

$$b = \frac{a r}{r+a} . \quad (21)$$

Figure 4-4: Quotient locus $\{\vec{q}_r\}$ (dots), and empirical boundary (solid), for $r < a$

Hundreds of thousands of randomly selected pressure distributions were chosen, and for each the quotient moment was evaluated and plotted (dots). All the observed values of the quotient moment fall within the boundary (solid curve) generated by quotient moments of special pressure distributions consisting of just two points of support: dipods. In fact, the boundary turns out to be a circle, the radius of which can be determined analytically.

Figure 4-5: Quotient locus $\{\vec{q}_r\}$ (dots), and empirical boundary (solid), for $r > a$

As in figure 4-4, the quotient moments for randomly generated pressure distributions all fall within the boundary generated by quotient moments of a special group of dipods. Here $r > a$, and the bean-shaped boundary does not have a simply named shape such as the circle we found for $r < a$. However it is still described by analytic formulae.

Figure 4-6: Dipods contributing to the boundary of $\{\vec{q}_r\}$, for $r < a$

When $r < a$, i.e. when the COR turns out to be within the disk, these are the pressure distributions which are responsible for the boundary of the quotient locus, and thus also are responsible for the boundary of the COR locus. They are simply dipods, in which one point of contact between workpiece and sliding surface is at the periphery of the disk, and the other point is internal to the disk, near what turns out to be the COR. More than half the weight is supported by the internal contact, as it is nearer to the CM. It is not surprising that the workpiece rotates about a COR essentially coincident with a point supporting most of the weight of the workpiece [5]. As the internal point of support is moved in an infinitesimal circle parametrized by angle ω , the corresponding COR traces out the boundary of the COR locus inside the disk.

4.8. Boundary for $|\text{COR}| > a$

For $r > a$, the empirical boundary of the locus $\{\bar{q}_r\}$ is generated by dipods of the type shown in figure 4-7, where ω is allowed to vary. These dipods are a generalization of the dipod shown in figure 4-2. Again,

the boundary can be calculated parametrically from ω (via intermediate terms d^+ , d^- , γ^+ , and γ^-) as

$$d^\pm = (r^2 + a^2 \pm 2 a r \cos \omega)^{1/2} \quad (22)$$

$$\sin \gamma^\pm = \frac{a \sin \omega}{d^\pm}$$

$$\cos \gamma^\pm = (1 - \sin^2 \gamma^\pm)^{1/2}$$

$$\bar{v}_r = \left(\frac{\cos \gamma^+ + \cos \gamma^-}{2}, \frac{\sin \gamma^+ - \sin \gamma^-}{2} \right)$$

$$d_r = \frac{d^+ + d^-}{2}$$

$$\bar{q}_r = r^2 \frac{\bar{v}_r}{d_r}.$$

It is the boundaries of $\{\bar{q}_r\}$ that will be used (in section 4.9) to determine the boundaries of the COR locus. Therefore the boundaries of the COR locus, too, can be found by considering only dipods. This is a stronger statement than Mason's theorem 5, which requires tripods. Additionally, we have found the two points constituting the dipods. However, it should be noted that the sufficiency of tripods holds for any workpiece, whereas dipods are sufficient only for a disk.

Figures 4-4 and 4-5 demonstrate that the two classes of dipods considered above, and illustrated in figures 4-6 and 4-7, generate extremal quotient moments. In other words, the locus $\{\bar{q}_r\}$ of values of \bar{q}_r for all pressure distributions $P(\bar{v})$ satisfying the conditions of section 2.5 fall inside the empirical boundary generated by the above dipods. The boundaries themselves are, of course, part of $\{\bar{q}_r\}$ since the boundaries are generated by acceptable pressure distributions.

Figure 4-7: Dipods contributing to the boundary of $\{\vec{q}_r\}$, for $r > a$

When $r > a$, i.e. when the COR turns out to be outside the disk, these are the pressure distributions which are responsible for the boundary of the quotient locus, and thus also are responsible for the boundary of the COR locus. Again they are simply dipods, but now in each dipod both points of contact with the sliding surface are at the periphery of the disk, and so each supports half the weight of the workpiece. As the dipod system rotates around the CM (parametrized by angle ω), the corresponding COR traces out the boundary of the COR locus outside the disk.

4.9. Analytic form of the COR locus

Having found a parametric representation of the $\{\vec{q}_r\}$ locus, we can find the COR locus. Recall the requirement for minimizing the energy lost to friction (equation 13):

$$r^2 \vec{\alpha} = \vec{q}_r [\vec{\alpha} \cdot (\vec{c} - \vec{r})]. \quad (23)$$

The COR locus is the set of all \vec{r} for which there exists a $\vec{q}_r \in \{\vec{q}_r\}$ satisfying equation 23.

Equation 23 is a vector equation. The left side obtains its direction from $\vec{\alpha}$. The right side obtains its direction from \vec{q}_r , since $\vec{\alpha} \cdot (\vec{c} - \vec{r})$ is a scalar. To satisfy the vector equation \vec{q}_r must have direction $\vec{\alpha}$.

We can rewrite equation 23 in scalar form, retaining the direction constraint on \vec{q}_r separately:

$$r^2 = |\vec{q}_r| [\vec{\alpha} \cdot (\vec{c} - \vec{r})] \quad (24)$$

where $\vec{q}_r \in \{\vec{q}_r\}$

and $\vec{q}_r \parallel \vec{\alpha}$

We wish to find the locus of \vec{r} for all distributions $P(\vec{w})$. It is best to imagine \vec{r} to be an independent variable. Each value of \vec{r} yields a locus $\{\vec{q}_r\}$, with one element $\vec{q}_r \in \{\vec{q}_r\}$ corresponding to each acceptable pressure distribution $P(\vec{w})$. For some values of \vec{r} the value of \vec{q}_r required to satisfy equation 24 is in $\{\vec{q}_r\}$; for other values it is not. The former values constitute the COR locus.

It is confusing, but unavoidable, that the locus $\{\vec{q}_r\}$ shifts as we consider different locations of the center of rotation \vec{r} . In figure 4-8 we have plotted several $\{\vec{q}_r\}$ loci for different values of \vec{r} . Note that varying the *magnitude* of \vec{r} continuously changes the shape or size of the $\{\vec{q}_r\}$ loci. But changing the *direction* of \vec{r} only causes a corresponding rotation of the $\{\vec{q}_r\}$ locus.

The variables of equation 24 are shown geometrically in figures 4-9, 4-10, and 4-11. In each figure we have plotted a value of \vec{r} and the locus $\{\vec{q}_r\}$ for that \vec{r} . We then calculate and plot the value of \vec{q}_r

Figure 4-8: Boundaries of quotient loci $\{\vec{q}_r\}$ for various \vec{r}

As \vec{r} is changed, the boundary of the quotient locus changes continuously. Sweeping \vec{r} around the CM causes a corresponding rotation of the quotient locus boundary. Changing the distance of \vec{r} from the CM changes the shape and size of the quotient locus boundary.

required to satisfy equation 24. In figure 4-9, the value of \vec{q}_r required does not fall in $\{\vec{q}_r\}$, so the value of \vec{r} shown is not in the COR locus. In figure 4-10, the value of \vec{q}_r required *does* fall in $\{\vec{q}_r\}$, so the value of \vec{r} shown is in the COR locus. In figure 4-11, the value of \vec{q}_r required to satisfy equation 24 happens to be on the boundary of the $\{\vec{q}_r\}$ locus. The boundary of the COR locus is generated by such cases. Interior points of the COR locus are generated when the \vec{q}_r required is interior to the $\{\vec{q}_r\}$ locus, as in figure 4-10. Since we are interested only in the boundary of the COR locus, we will consider only values of \vec{q}_r which are on the boundary of the $\{\vec{q}_r\}$ locus, as shown.

4.10. Solution for the $|\text{COR}| < a$ part of the COR locus

It will be convenient to represent the COR by its polar coordinates (r, ε) , and to define the relative angle

η . Both angles are shown in figure 4-11. We have

$$\varepsilon = \pi + \alpha - \eta . \quad (25)$$

If $r < a$, the boundary of $\{\vec{q}_r\}$ is a circle. The condition that \vec{q}_r lie on the circle can be expressed

$$| |\vec{q}_r| - \vec{a} + (r - b)\hat{\varepsilon} | = b . \quad (26)$$

where b is the radius of the circle, from equation 21. Equation 26 can be expressed in terms of the angle

η as

$$(|\vec{q}_r| - (r - b) \cos \eta)^2 + ((r - b) \sin \eta)^2 = b^2 . \quad (27)$$

Solving this quadratic equation for $|\vec{q}_r|$ we find

$$|\vec{q}_r| = (r - b) \cos \eta \pm (b^2 - ((r - b) \sin \eta)^2)^{1/2} . \quad (28)$$

Inserting this value of $|\vec{q}_r|$ into equation 24 and eliminating the square root we obtain

$$\left(\frac{r^2}{\alpha \cdot (\vec{c} - \vec{r})} - (r - b) \cos \eta \right)^2 = b^2 - ((r - b) \sin \eta)^2 . \quad (29)$$

Substituting b from equation 21 and simplifying we find

Figure 4-9: Variables of equation 24, for a value of \vec{r} not in the COR locus

Is a proposed value of \vec{r} the COR of the workpiece for some pressure distribution? First generate the quotient locus boundary for the proposed \vec{r} . In this case it is a circle, because \vec{r} falls within the disk. Now compute the value of \vec{q}_r , which would be required to satisfy energy minimization (equation 24). Plot it too. If \vec{q}_r falls within the quotient locus boundary (which it does not here), then \vec{r} is the COR of the workpiece for some pressure distribution. \vec{q}_r points to a quotient moment in the locus, so the pressure distribution which led to that quotient moment is the one which causes the COR to be at \vec{r} .

Figure 4-10: Variables of equation 24, for a value of \bar{r} in the COR locus

Here \vec{q}_r does fall within the quotient locus boundary, so the COR is at \bar{r} for some pressure distribution.

Figure 4-11: Variables of equation 24, for a value of \vec{r} on the boundary of the COR locus

Here \vec{q}_r falls on the boundary of the quotient locus, so \vec{r} is on the boundary of the COR locus. We could test all values of \vec{r} to see if they fall on the boundary in this way. Instead, we generate the boundary of the quotient locus (parametrized by an angle ω in the dipods) and solve for the value of \vec{r} which gives rise to a \vec{q}_r satisfying this figure.

$$r^2(a+r)+(r-a)[\alpha \cdot (\vec{c}-\vec{r})]^2-2r^2[\alpha \cdot (\vec{c}-\vec{r})]\cos\eta=0 \quad (30)$$

where $[\alpha \cdot (\vec{c}-\vec{r})] = \alpha \cdot \vec{c} + r \cos \eta$.

Equation 30 is cubic in r and quadratic in $\cos \eta$. The solution for $\cos \eta$ is

$$\cos \eta = \frac{r((r+a)^2+(\alpha \cdot \vec{c})^2)^{1/2}-a(\alpha \cdot \vec{c})}{r(r+a)}. \quad (31)$$

The other quadratic root is invalid. Since η is related by equation 25 to the polar angle ε , equation 31 describes the boundary of the COR locus in the polar coordinates r, ε , for $r < a$. A typical COR locus boundary generated using equation 31 is shown in figure 4-12.

4.10.1. Extremal radius of the COR locus boundary for $|\text{COR}| < a$

The minimum radius of the COR locus boundary occurs at $\varepsilon = \alpha$, which corresponds to $\eta = \pi$. From equation 30 we find

$$r_{min} = \frac{a(\alpha \cdot \vec{c})}{2a+(\alpha \cdot \vec{c})}. \quad (32)$$

Note that r_{min} is not the minimum distance from the CM to an *element* of the COR locus; that distance is zero. r_{min} is the minimum distance from the CM to the *boundary* of the COR locus. r_{min} is indicated in figure 4-12.

It will also be useful to have the angles at which the COR locus boundary intersects the disk boundary.

From equation 31 we obtain

$$\cos \eta_{r=a} = \frac{((\alpha \cdot \vec{c})^2+4a^2)^{1/2}-(\alpha \cdot \vec{c})}{2a} \quad (33)$$

>From equation 30 we can find the radius of curvature of the COR locus boundary at r_{min} to be

$$s = \frac{a(\alpha \cdot \vec{c})((\alpha \cdot \vec{c})+2a)^2}{(\alpha \cdot \vec{c})^3+4a(\alpha \cdot \vec{c})^2+8a^2(\alpha \cdot \vec{c})+4a^3}. \quad (34)$$

Figure 4-12: COR locus boundary for $r < a$

Shown is the part of the COR locus boundary internal to the disk. The pressure distributions which give rise to CORs on the bold boundary are dipods, with one point of support at the COR and the other on the periphery of the disk as far as possible from the COR.

r_{min} is the minimum distance from the CM to the boundary of the COR locus. Note that r_{min} is not the minimum distance from the CM to an *element* of the COR locus; that distance is zero.

4.11. Solution for the $|\text{COR}| > a$ part of the COR locus

If $r > a$, we cannot find a simple equation analogous to equation 26 constraining \vec{q}_r to the boundary of $\{\vec{q}_r\}$. An effective approach is to parametrize the boundary of the $\{\vec{q}_r\}$ locus by the angle ω of equation 22, and solve for both ε and r by binary search.

For each ω the following procedure is used: We guess a value of r , in the range $a < r < r_{tip}$, where r_{tip} is an upper bound to be found in section 4.11.1. Equation 22 is then used to calculate a value of \vec{q}_r . Angle η is related to the terms of equation 22 by

$$\eta = \arctan \frac{-\vec{v}_x}{\vec{v}_y} \quad (35)$$

and so can be computed from ω . Equation 24 can be written in terms of the angle η as

$$r^2 = |\vec{q}_r| (\alpha \cdot \vec{c} + r \cos \eta) \quad (36)$$

which is easily tested. If it is satisfied, we have found angle η and magnitude r describing a point on the boundary of the COR locus. ε is then obtained from η using equation 25.

If the left-hand side of equation 36 is greater (resp. less) than the right-hand side, we increase (resp. decrease) the value of r guessed above. In this way we perform a binary search, quickly converging on a solution for r and ε .

Figure 4-13 shows the boundary of the COR locus for various \vec{c} and α . The part of the boundary inside the disk was computed using equation 31, while the part outside the disk was found by binary search as outlined here. Calculation of each locus required about 2 CPU seconds on a VAX-780.

Figure 4-13: Boundaries of COR loci for various \vec{r} and α

The pressure distributions which give rise to CORs on the boundary of the COR locus external to the disk are dipods, with both points of support on the periphery of the disk diametrically opposite each other. The boundary is generated as the angle ω parametrizing the dipods is varied (figure 4-7).

In the figures the point at which the workpiece is being pushed is indicated by an arrowhead, and the angle (α) of the edge being pushed is indicated by the line the arrowhead contacts. (In several cases the arrowhead is outside the disk; this is unrealistic.)

4.11.1. Tip Line

We can calculate the extremum of the COR locus analytically. For many purposes this may be all that is required. Additionally, it gives us a range within which to conduct the binary search discussed in section 4.11 . By symmetry, r takes on an extremal value when $\eta = 0$. In figure 4-7 this corresponds to $\vec{v}_x = 0$, which in turn occurs only when $\omega = 0$ or $\omega = \frac{\pi}{2}$.

The extremum at $\omega=0$ has no apparent meaning. At $\omega = \frac{\pi}{2}$ we find from equation 22

$$\bar{q}_r = \alpha \frac{r^3}{r^2 + a^2}. \quad (37)$$

At this value equation 24 yields

$$r_{tip} = \frac{a^2}{\alpha \cdot \bar{c}}. \quad (38)$$

This is the greatest distance \vec{r} may be from the CM, and it occurs at polar angle $\varepsilon = \pi + \alpha$. In figure 3-4 we plot r_{tip} vs. contact angle α , for a given value of \bar{c} . As α is varied, the tip of the COR locus at distance r_{tip} from the CM traces out straight line, the *tip line*.

The use of this graphical construction is illustrated in figure 3-4. For a given value of α , as shown, r_{tip} is at the intersection of the tip line described above with a ray from the CM at angle $\pi + \alpha$.

An interesting case occurs when α becomes perpendicular to \bar{c} . (Note that this does not require $\alpha = \frac{\pi}{2}$.)

As $\alpha \cdot \bar{c} \rightarrow 0$, we have $r_{tip} \rightarrow \infty$. The COR at infinity corresponds to pure translation perpendicular to \bar{c} .

Figure 4-13 c shows a case in which α is almost perpendicular to \bar{c} . Note that $r_{tip} \rightarrow \infty$ does not mean that pure translation is assured; only that it is possible. The COR may fall at any distance less than r_{tip} .

The radius of curvature of the COR locus boundary at the tip can be found analytically to be

$$s = \frac{r_{tip}}{\frac{1}{2} + \frac{r_{tip}}{a^4}}. \quad (39)$$

4.12. Symmetries of the COR locus

We now have the ability to quickly compute the COR locus for any \vec{c} and α .

The COR locus is a function of four parameters: the disk radius a , the edge angle α (which may be the angle of the pushing fence or of the workpiece edge pushed, measured with respect to the line of motion of the pusher), and the two components of the point of contact \vec{c} between pusher and pushed workpiece. However the COR locus is really much simpler in functional dependence than the existence of four parameters would seem to imply.

The most obvious symmetry is one of total size: if both \vec{c} and a are changed by a factor of γ , the COR locus will be scaled by a factor of γ as well.

Note that the COR locus has an axis of symmetry through the CM at angle $\bar{\alpha}$. The "tip" of the locus falls on this axis of symmetry, and the tip line construction (section 4.11.1, and figure 3-4) makes use of this symmetry.

The shape of the COR locus depends *only* on the distance of the tip of the locus from the CM, $a^2/\bar{\alpha}\vec{c}$, as a multiple of the disk radius a . If COR loci for various tip distances are precomputed, we need only select the appropriate one, scale it by the disk radius a , and tilt it at the appropriate angle α .

Finally, the COR locus can depend only on the force and torque applied by the pusher. Displacing the point of contact \vec{c} perpendicular to the edge angle α (i.e. along the line of action of the applied force)

changes neither force nor torque, and therefore cannot change the COR locus. In figure 4-13, the COR loci in sections a and b are identical because the point of contact \vec{c} has been displaced perpendicular to the edge.

4.13. Summary

We have found the boundary of the COR locus for any choice of \vec{c} and α . Within the disk the boundary is given by a simple formula relating r and ε , the polar coordinates of the boundary (equation 31). Outside of the disk, the polar coordinates of the boundary are found by binary search as outlined in section 4.11. For most applications it is not necessary to find the entire COR locus boundary, as simple formulae exist for several important points on the boundary. Most important of these is the tip-line construction described in section 4.11.1.

Slightly more discussion of the boundaries of the quotient locus (section 4.7) is in order. The quotient locus is an intermediate mathematical construction whose boundaries are transformed directly into the boundaries of the COR locus. The boundaries of the quotient locus were found by making an informed guess as to the pressure distributions which give rise to the boundaries. Then this guess was tested by extensive computer simulation of random pressure distributions. These numerical results suggest that the analytic quotient locus boundaries were indeed correct: no randomly generated pressure distribution ever appeared which landed outside the analytic boundary of the quotient locus. Because of the empirical justification of the boundaries of the quotient locus, however, our derivation of the analytic boundaries of the COR locus is not rigorous. It may well be that it was this step (requiring computer testing) which prevented analytic solution for the COR locus long ago [6] [8] [17].

5. Application

A useful application of the results found above is to the problem of aligning a workpiece by pushing it. In figure 2-1 a misoriented rectangle is being pushed by a fence. The fence is moving in a direction perpendicular to its front edge. Evidently the rectangle will rotate CW as the fence advances [10], and will cease to rotate when the edge of the rectangle comes into contact with the front edge of the fence [2]. The problem is to find how far the fence must advance to assure that the CW motion is complete.

The geometry of this problem differs from the geometry used in previous sections. Previously a point pusher made contact with a straight workpiece edge. Here the straight edge of the pusher makes contact with a point (corner) of the workpiece. But since the coefficient of friction between the pusher and the edge of the workpiece (μ_c) is zero, we know that in either case the force exerted by the pusher on the workpiece is normal to the edge, regardless of whether the edge is that of the pusher or that of the workpiece. Since the motion of the workpiece can depend only on the force applied to it, the angle of the fence takes the place of the angle of the workpiece edge (α), and all the results derived above remain unchanged.

In this section we will generalize the problem slightly, relative to the problem illustrated in figure 2-1 :

- The workpiece pushed is arbitrary, not a rectangle.
- The motion of the fence is not necessarily perpendicular to its face.

First we circumscribe a disk of radius a about the workpiece. The disk is centered at the CM of the workpiece (figure 5-1). Note that the contact point need not be on the perimeter of circumscribed disk.

We know [10] that the workpiece will rotate CW, and will cease to rotate when the final configuration shown in figure 5-2 is reached.

Figure 5-1: Initial configuration of workpiece and fence, and resulting COR locus

The fence travels horizontally and contacts the shaded workpiece as shown. As the fence advances the workpiece rotates clockwise at a rate which depends upon the location of the COR. The workpiece is circumscribed by a disk of radius a , since this is the only shape for we can find exact COR locus boundaries. The ice-cream-cone shaped COR locus boundary is shown. The minimum rate of rotation occurs when the COR is at the tip of the locus.

Figure 5-2: Final configuration of workpiece and fence, and resulting COR locus

Finally the workpiece has rotated into alignment with the fence. At the moment before alignment the COR locus boundary is as shown. We want to determine the maximum advance of the fence which could possibly be required to get from the orientation shown in figure 5-1 to the one shown here. So we assume that the COR is always at the tip of the locus, which is the point for which the workpiece rotates most slowly as the fence advances.

We now ask the rate of rotation of the workpiece about the COR, with unit advance of the pusher. Let the angle of the CM from the direction of motion of the pusher be β . This is also the angle between the tip line and the perpendicular to the line of motion. (Both angles are indicated in figure 5-1). From equation 4 we have

$$\delta x = \frac{d\beta}{\sin \alpha} \alpha \cdot (\bar{c} - \bar{r}) . \quad (40)$$

where \bar{r} is the distance from the CM to the COR. The rate of rotation per advance of the pusher, $d\beta/dx$, depends on where the COR \bar{r} falls within the COR locus. Since we wish to find the *longest* push which could possibly be necessary to achieve a certain amount of rotation, we need to know for which \bar{r} in the COR locus $d\beta/dx$ is minimized, i.e. we consider the worst case location for \bar{r} . This occurs when \bar{r} is at the tip of the COR locus. Therefore we have

$$\delta x = \frac{d\beta}{\sin \alpha} \alpha \cdot (\bar{c} - \bar{r}_{tip}) . \quad (41)$$

Using r_{tip} from equation 38, this can be integrated to yield the indefinite integral

$$x = \frac{-c \sin(\alpha+\beta)}{\sin \alpha} - \frac{a^2}{2c \sin \alpha} \log \left| \frac{1 + \sin(\alpha+\beta)}{1 - \sin(\alpha+\beta)} \right| . \quad (42)$$

To find the maximum pushing distance, Δx , required to cause the workpiece to rotate from its initial configuration shown in figure 5-1 to its final configuration shown in figure 5-2, we simply substitute the initial and final values of β into equation 42, and take the difference $x_{final} - x_{initial}$.

6. Solution for the COR locus including contact friction

Up to now we have assumed that the coefficient of friction between the pusher and the edge of the pushed workpiece was zero, i.e. $\mu_c=0$. The pushing force was therefore normal to the edge being pushed. Since the motion of the workpiece can depend only on the force applied to it, we will designate the locus we found $\{COR\}_\alpha$ to indicate its dependence on the force angle, which is perpendicular to α .

We know how to generate the COR locus for a given angle of applied force. Unfortunately, when $\mu_c > 0$, it is not possible to tell what the force angle will be. We will describe angular *limits* on the force angle in section 6.1, but within those limits the force angle depends on the pressure distribution, which is not known. If we already knew that the COR would be at a certain point, however, it would then be possible to find the force angle.

Our approach to this problem is to seek CORs which are consistent with the force angle which gives rise to them. For each force angle ϕ within the angular limits, we generate $\{COR\}_\phi$. For each COR in $\{COR\}_\phi$ we find the force angle implied. If the force angle implied matches ϕ , that COR is a possible one for the workpiece. This formulation seems to threaten a great deal of computation, which in fact is not required.

We will refer to the set of consistent CORs as the *COR sketch*, to distinguish it from the elementary COR loci $\{COR\}_\phi$ produced for known force angles. Two elementary COR loci will be used in the construction of the COR sketch. In the figures, these COR loci will be left visible in outline, while the actual COR sketch – the consistent CORs – will be shown shaded.

6.1. Contact Friction and the Friction Cone

Let μ_c be the coefficient of friction between the pusher and the workpiece. If $\mu_c > 0$, two distinct modes of behavior of the system are possible: *sticking* and *slipping*. In figure 2-1, sticking means that the element of the fence in contact with the corner of the workpiece remains invariant as the pusher's motion proceeds. Referring to figure 2-2, sticking means the element of the workpiece edge which is in contact with the pushing point remains invariant as the pusher's motion proceeds. Slipping is simply the case in which either the element of the pusher or the element of the workpiece, which are in contact with each other, changes as the motion proceeds.

Define

$$\nu = \tan^{-1} \mu_c \quad (43)$$

In figure 6-1 we construct a *friction cone*, of half angle ν , at the point of contact \vec{c} . The cone is centered on the edge normal, at angle $\alpha - \pi/2$ relative to horizontal. Note that the edge may be either that of a fence, where it contacts a corner of the workpiece (as in figure 2-1), or an edge of the workpiece, where it is touched by a corner of the pusher (as in figure 2-2). The friction cone is a well-known construction in classical mechanics. (Recently Erdmann [3] has extended the friction cone to configuration space.)

The component of the applied pushing force tangential to the edge, F_{\parallel} , is supported by friction. Its magnitude cannot exceed $\mu_c F_{\perp}$, where F_{\perp} is the component of force normal to the edge. Therefore the total applied force vector must lie within the friction cone.

If we attempt to apply a force to the workpiece edge at an angle outside of the friction cone, friction cannot support the tangential component of force. The result is slipping along the edge, and the actual applied force is directed along one extreme of the friction cone. If we apply a force within the friction cone, friction is sufficient to support the tangential component of force, and slipping will not occur: we have sticking.

In short, slipping is only consistent with a force vector at one extreme of the friction cone, while sticking is only consistent with a force vector within the friction cone. It is not usually possible to tell if slipping or sticking will occur: often, depending on the pressure distribution, either may occur.

Figure 6-1: Construction of the friction cone

The force which the pusher applies to the workpiece edge must lie within the friction cone shown. If we attempt to apply a force at an angle falling outside the friction cone, friction cannot support the component of force tangential to the workpiece edge. The pusher will then slip along the workpiece edge, and the actual force applied will lie along one extreme of the friction cone. If we apply a force which lies within the friction cone, the pusher will not slip relative to the workpiece edge.

6.2. Sticking and Slipping zones

In this section we presume that the COR is known: a single point is the COR for the workpiece. We divide the plane into three zones, called the *sticking line*, the *up-slipping zone* and the *down-slipping zone*. (Figure 6-2). The up-slipping and down-slipping zones are regions of the plane with positive areas, while the sticking line is merely a line, but all three will be collectively designated "sticking and slipping zones." The motion of the workpiece is qualitatively different for the COR falling in each of the three zones.

The sticking line is the line perpendicular to the pusher's line of motion, intersecting the point of contact between pusher and workpiece, (i.e. \vec{r} lies on the sticking line). Since we choose to draw the pusher's line of motion horizontally, the sticking line is vertical. The sticking line divides the down-slipping zone, on its left, from the up-slipping zone, on its right. Also shown in figure 6-2 is the edge normal line. Above this line, the up-slipping and down-slipping designations are reversed. The area above the edge normal will be unimportant, however.

6.2.1. Sticking Line

First consider the workpiece's motion when the COR is on the sticking line. Recall that the motion of any point of the workpiece is perpendicular to the vector from the COR to that point. If the COR lies on the sticking line, the workpiece's motion at the point of contact is perpendicular to the sticking line, and is therefore parallel to the pusher's line of motion.

Since the pusher's line of motion and the workpiece's motion at the point of contact are parallel, the pusher and the workpiece, at the point of contact, travel along together. There is no need for one to slip relative to the other; the workpiece and the pusher are *sticking* at the point of contact.

Figure 6-2: Construction of zones: up-slipping, down-slipping, and sticking line

The location of the COR has implications for slipping or sticking of the pusher with respect to the workpiece edge. If the COR lies on the sticking line shown, pusher and workpiece edge move along (horizontally) together and there is no slipping of one relative to the other. If the COR falls in the up- or down-slipping zones to either side of the sticking line, then the workpiece has a vertical component of motion and so must slip relative to the pusher (which moves horizontally).

6.2.2. Slipping Zones

Now suppose that the COR is in the down-slipping zone. The workpiece's motion at the point of contact has a downward component, relative to the pusher's line of motion. The pusher-workpiece contact must be *slipping*, with the workpiece moving down relative to the pusher.

Similarly, if the COR is in the up-slipping zone, the workpiece at the point of contact moves up relative to the pusher as the pusher advances.

6.3. Consistency for slipping

If we know that the workpiece is slipping relative to the pusher (and whether up or down), then the force angle is known: it is at one extreme of the friction cone, perpendicular to $\alpha \pm v$.

If the COR lies in the down-slipping zone, the workpiece moves *down* as the pusher advances. Therefore the force angle must be along the upper extreme of the friction cone, at angle $\alpha + v - \pi/2$. Similarly, if the COR lies in the up-slipping zone, the workpiece moves *up* as the pusher advances, and the force angle must be along the lower extreme of the friction cone, at angle $\alpha - v - \pi/2$.

Combining the above observations, we see that if slipping occurs, the COR must be either in $\{COR\}_{\alpha+v}$ and the down-slipping zone, or in $\{COR\}_{\alpha-v}$ and the up-slipping zone. These two intersection regions are called the *down-slipping locus* and the *up-slipping locus*. A very similar construction was used by Mason and Brost in figure 5 of [12].

The down-slipping and up-slipping loci are two components of the COR sketch, because every COR in either locus is consistent with the force angle that was used to generate it. We construct the down-slipping locus of the COR sketch by intersecting the down-slipping zone (left of the sticking line) with

$\{COR\}_{\alpha+v}$. We construct the up-slipping locus of the COR sketch by intersecting the up-slipping zone (right of the sticking line) with $\{COR\}_{\alpha-v}$.

In figure 3-5, $\{COR\}_{\alpha+v}$ and $\{COR\}_{\alpha-v}$ are shown in outline. The down-slipping and up-slipping loci are the shaded areas left and right of the sticking line respectively.

6.4. The Sticking Locus

The third set of consistent CORs belong to the *sticking locus*. The sticking locus, together with the up-slipping and down-slipping loci whose construction was described above, are all the CORs consistent with the force angle they presume. The three consistent loci constitute the COR sketch.

If the COR lies on the sticking line, sticking occurs. The force angle can be anywhere in the friction cone, i.e., between $\alpha-v-\pi/2$ and $\alpha+v-\pi/2$. The sticking locus is therefore the intersection of the sticking line with the union, over all ϕ perpendicular to a force angle within the friction cone, of $\{COR\}_{\phi}$. The sticking locus is shown as a bold section of the sticking line in figure 3-5.

As discussed above, the two slipping loci are $\{COR\}_{\alpha\pm v}$, possibly cut off by the sticking line. In calculating either slipping locus, the force angle is known: it is $\alpha\pm v-\pi/2$. But in calculating the sticking locus, (which is just a simple line segment), the force angle is not known, except that it lies within the friction cone. To find the endpoints of the sticking locus exactly, we could form every locus $\{COR\}_{\phi}$, for $\alpha-v < \phi < \alpha+v$, and intersect each locus with the sticking line. The union of these intersections is the sticking locus. This is not an efficient method.

The lower endpoint of the sticking locus is of particular interest. It is possible to approximate it by using the tip-line construction described in section 4.11.1. The procedure for finding the sticking locus

described above is to form every locus $\{COR\}_\phi$, for $\alpha-v < \phi < \alpha+v$, and intersect each locus with the sticking line. As we vary ϕ , $\{COR\}_\phi$ varies continuously from $\{COR\}_{\alpha-v}$, which is outlined in figure 3-5, to $\{COR\}_{\alpha+v}$, also shown outlined. The tip of the extreme loci, as well as of all intermediate loci, fall on the tip line. The tip line is shown dotted in figure 3-5.

Were it not for the fact that each $\{COR\}_\phi$ locus drawn dips slightly below the tip line, the lower endpoint of the sticking locus would be exactly at the tip line. We will use this approximation. The small error so introduced can be bounded [15], and is usually negligible.

Using the tip line to approximate the lower endpoint of the sticking locus in this way depends on an unstated assumption: that the tip of $\{COR\}_{\alpha-v}$ lies to the left of the sticking line while the tip of $\{COR\}_{\alpha+v}$ lies to the right of the sticking line. This assumption is necessary so that the tip of some intermediate locus $\{COR\}_\phi$ will intersect the sticking line. In section 6.6, we will deal methodically with this problem.

The shaded slipping loci and the bold sticking locus of figure 3-5 contain all the possible locations of the COR.

6.5. Possible configurations of an elementary COR locus

The down-slipping, up-slipping, and sticking *loci* play an important part in the rest of this work. It is worth describing the qualitatively different ways in which an elementary COR locus $\{COR\}_\alpha$ can intersect the three *zones* (down-slipping, up-slipping, and sticking line) in order to form the loci. These qualitatively different types of intersections will be called distinct *elementary configurations*. Later we will describe the qualitatively different COR sketches which can occur; the latter will be called distinct *sketches*. Two COR loci are used in the construction of a COR sketch, so there are more distinct sketches than distinct

elementary configurations.

For a given contact point \vec{c} , changing α yields four distinct elementary configurations of the resulting COR loci. In figure 6-3(A), the *pure slipping* elementary configuration, the entire COR locus falls in the up-slipping zone. In figure 6-3(B), the COR intersects all three zones, but the tip of the locus falls on the same side of the sticking line as the CM. This is the *same-sided-split* elementary configuration. As α is further decreased, the tip of the COR locus crosses the sticking line, entering the *opposite-sided-split* elementary configuration, as shown in figure 6-3(C). Finally, when α decreases to the point where the edge normal at \vec{c} intersects the CM, the COR locus goes to infinity [10]. The COR at infinity implies pure translation (with no rotation) of the workpiece as the pusher advances. Beyond this point the workpiece's sense of rotation switches from clockwise to counterclockwise. For our purposes in constructing a COR sketch, counterclockwise rotation is unphysical [10], and so we will class this, and pure translation as one elementary configuration, the *wrapped* elementary configuration, as shown in figure 6-3(D). No part of a "wrapped" locus will ever contribute to the COR sketch, yet we will continue to draw its outline as shown in the figure.

The same four elementary configurations can be defined (now with increasing α) when the sticking line is to the right of the CM (Figure 6-4).

6.6. Possible distinct COR sketches

Depending on α and μ_c , each of the two elementary COR loci $\{COR\}_{\alpha \pm v}$ used in constructing the COR sketch may be any of the four elementary configurations described in section 6.5, (pure slipping, same-sided split, opposite-sided split, or wrapped). There are nine possible distinct sketches composed of two elementary configurations, as shown in figure 6-5. (Of the 4^2 combinations, 6 are eliminated because the

Figure 6-3: Possible elementary configurations of the COR locus

As the angle α of the pushed edge varies, the COR locus may intersect the three zones in different ways, called distinct "elementary configurations". The entire locus may fall in the down-slipping zone (part A), the locus may intersect both slipping zones and the sticking line with the tip of the locus on one side or the other (parts B and C), or the locus may "wrap" through infinity as shown in part D.

Figure 6-4: Possible elementary configurations with sticking line to the right of the CM
The same four elementary configurations can be defined when the sticking line is to the right of the CM.

tip of $\{COR\}_{\alpha+v}$ cannot be left of the tip of $\{COR\}_{\alpha-v}$. The one sketch in which both $\{COR\}_{\alpha\pm v}$ are "wrapped" elementary configurations is inconsistent with clockwise rotation of the workpiece.)

It is worth looking carefully at each sketch, in particular to understand the construction of the sticking locus. The sticking locus is the intersection of $\{COR\}_{\phi}$ with the sticking line, as ϕ is swept from $\alpha+v$ to $\alpha-v$. The sweeping is always *clockwise*. In sketch (G), sweeping clockwise means sweeping from the pure slipping locus, clockwise, to the wrapped locus. The intermediate loci therefore do intersect the sticking line, even though neither locus $\{COR\}_{\alpha\pm v}$ does. Unless this is understood the origin of the sticking locus in sketches (G) and (H) will remain mysterious.

Several of the sketches shown in figure 6-5 have interesting properties. In sketch (A), the workpiece must slip up relative to the pusher. In sketches (B) and (D), the workpiece must stick or slip up. In sketch (G), the workpiece must stick to the pusher. In sketches (H) and (I), the workpiece must stick or slip down. In the remaining sketches (C), (E), and (F), either mode of slipping, or sticking, is possible, depending on the pressure distribution.

Analogous qualitative results are possible when the point of contact \vec{c} is to the right of the CM. The distinct COR sketches for this case can be obtained from those shown in figure 6-5 by reflecting about a vertical axis. (The pusher's motion should still be considered left-to-right, however.) The distinct sketches for counterclockwise rotation of the workpiece may be obtained by reflecting about a horizontal axis.

Figure 6-5: Nine distinct COR sketches with respect to the sticking line

Depending on the angle α of the pushed edge (not labeled here) and the coefficient of friction μ_c (which determines the width of the friction cones shown), the two elementary COR loci which contribute to a COR sketch may intersect the slipping and sticking zones in nine different ways.

Look closely at each distinct sketch to understand the origin of the sticking locus (the bold section of the sticking line.) The sticking locus is the intersection of $\{COR\}_\phi$ with the sticking line, as ϕ is swept from $\alpha + \nu$ to $\alpha - \nu$. The sweeping is always *clockwise*. In sketch (G), sweeping clockwise means sweeping from the pure slipping locus, clockwise, to the wrapped locus. The intermediate loci therefore do intersect the sticking line, even though neither locus $\{COR\}_{\alpha \pm \nu}$ does.

7. From instantaneous motion to gross motion

We have shown how to find all possible instantaneous motions of a pushed sliding workpiece, given only the parameters α , \vec{c} , and a . In some cases it is possible to say with certainty that a particular kind of motion, such as sticking, can or cannot occur. The set of possible CORs, as found by constructing the COR sketch, describes completely the possible instantaneous motions of the workpiece as long as those parameters remain in effect. Usually however, the instantaneous motion which results changes the parameters (except the radius a), so that a new COR sketch must be constructed.

Often we wish to calculate not the bounds on the instantaneous direction of motion, as above, but bounds on a gross motion of the workpiece which can occur concurrently with some other gross motion of known magnitude. (For instance, we may wish to find bounds on the displacement of the pusher which occurs while the workpiece rotates 15 degrees.) Our approach to dealing with gross motion follows a definite strategy, which will be illustrated in the sample problems solved in sections 8, 9, and 10.

Suppose we wish to find the greatest possible change in a quantity x , while quantity β changes from $\beta_{initial}$ to β_{final} . From the geometry of the problem we find a *equation of motion* relating the instantaneous motions dx and $d\beta$. We then construct the COR sketch for each value of β . In each sketch we locate the possible COR which maximizes $dx/d\beta$. Using that COR, we integrate the equation of motion from $\beta_{initial}$ to β_{final} , yielding an upper bound for the quantity x .

Sometimes the possible COR which maximizes $dx/d\beta$ can be found analytically, or at least approximated analytically, and sometimes it must be found numerically. When an analytical solution is found, it may or may not be possible to integrate the equation of motion in closed form using that analytical solution. The

examples which follow illustrate all of these situations.

8. Example: Aligning a workpiece by pushing with a fence

In this example, we wish to find the maximum distance a fence must advance after first contacting a workpiece, in order to assure that an edge of the pushed workpiece has rotated into contact with the fence. A typical initial configuration is shown in figure 8-1, with the workpiece shown shaded. (Note that the fence does not advance perpendicular to its front edge.) The final configuration is shown in figure 8-2. (In section 5 we have solved this problem for the case where $\mu_c = 0$.)

Also shown in figure 8-1 is the COR sketch for the initial configuration, and the angle β between the line of motion and the line from the point of contact to the CM. β is also the angle between the tip line and the sticking line. Angle β changes from 45 degrees initially in figure 8-1 to 80 degrees in the final configuration, figure 8-2. Note that a one degree rotation of the workpiece about the COR will produce a one degree change in β as well. We wish to find the advance x of the pusher (fence) required to change β by 35 degrees.

The workpiece's rate of rotation about the COR $d\beta$, for advance of the pusher dx , is given by

$$\delta x = \frac{d\beta}{\sin \alpha} \alpha \cdot (\bar{c} - \bar{r}) . \quad (44)$$

To find the maximum required pushing distance, we must find the maximum value of $\alpha \cdot \bar{r}$ for any possible COR \bar{r} in the COR sketch. This will be the *slowest* COR; the one for which the rotation of the workpiece with advance of the pusher is slowest.

Reviewing the nine distinct COR sketches in figure 6-5, we see that the slowest COR is at the lower endpoint of the sticking locus in sketches (D), (E), (G), and (H). We will call this behavior

Figure 8-1: Initial orientation of the fence and pushed workpiece

As the fence advances horizontally the four-sided workpiece rotates clockwise. The COR sketch is the shaded portion, plus the bold section of the sticking line called the sticking locus. The two elementary ($\mu_c=0$) COR loci which were used to generate the COR sketch are shown in outline. We need to find the COR responsible for slowest rotation of the workpiece. This turns out to be at the lowest point of the sticking locus (marked "B"), not at the tip of one of the $\mu_c=0$ loci as in the frictionless case considered in section 5.

Figure 8-2: Final (aligned) orientation of the fence and pushed workpiece

Here we show the COR sketch at the moment before the conclusion of the workpiece's clockwise rotation into alignment with the fence. By this time the COR responsible for slowest rotation of the workpiece is no longer at the bottom of the sticking locus but rather at the point marked "B" which is the tip of one of the elementary ($\mu_c = 0$) COR loci.

sticking-slowest. It occurs when the tips of the two loci $\{COR\}_{\alpha \pm \nu}$ fall on opposite sides of the sticking line.

In sketches (A), (B), (C), (F), and (I), the slowest COR is an element of one of the slipping loci $\{COR\}_{\alpha \pm \nu}$. We will call this behavior *slipping-slowest*. It occurs when the tips of the two loci $\{COR\}_{\alpha \pm \nu}$ fall on the same side of the sticking line. (For the purposes of the rule given here, the "wrapped" loci in sketches (G), (H), and (I) count as having their tip to the left of the sticking line.) In fact, the slowest COR in the slipping-slowest regime is very nearly the COR at the tip of one of the loci $\{COR\}_{\alpha \pm \nu}$. It is only because the angle of symmetry $\alpha \pm \nu$ differs from α that the tip is **not** the slowest COR. We will use the tip of one of the loci $\{COR\}_{\alpha \pm \nu}$ as an approximation to the slowest COR. The error introduced by this approximation can be bounded [15] in terms of the radius of curvature of the tip of the COR loci, but for practical purposes is negligible.

It is possible to have a transition from slipping-slowest behavior to sticking-slowest behavior within a pushing operation, as β increases. Such a transition occurs when the tip of one of the loci $\{COR\}_{\alpha \pm \nu}$ passes through the sticking line. In figure 8-3, for example, it is $\{COR\}_{\alpha + \nu}$ which passes through the sticking line. We may derive the condition for intersection:

$$a^2 + c^2 = -a^2 \tan \beta \tan (\alpha \pm \nu + \beta) \quad (45)$$

The tip of locus $\{COR\}_{\alpha \pm \nu}$ is on the same side of the sticking line as the CM when the left side of equation 45 is less than the the right side. The value of β at which the tip crosses the sticking line may be found by solving equation 45 for β :

$$\tan \beta_{transition} = \frac{c^2 \tan (\alpha \pm \nu) \pm (c^4 \tan^2 (\alpha \pm \nu) - 4a^2 (a^2 + c^2))^{1/2}}{2a^2} \quad (46)$$

The pushing distances required to advance β from its initial value to the transition, and from the transition

Figure 8-3: Transition from sticking-slowest to slipping-slowest behavior

This is the moment of "transition" from the COR responsible for slowest possible rotation of the workpiece being at the bottom of the sticking locus as in figure 8-1 to being at the tip of one of the elementary ($\mu_c = 0$) COR loci as in figure 8-2.

to the final value, must be evaluated separately. In our example, the locus $\{COR\}_{\alpha+v}$ is type same-sided split initially, but changes to type opposite-sided split. Using equation 46 we find $\beta_{transition} = 69.4$ degrees, as shown in figure 8-3.

8.1. Slipping-slowest regime

If the slowest COR is at the tip of one of the loci $\{COR\}_{\alpha \pm v}$ we have

$$\delta x = \frac{d\beta}{\sin \alpha} \alpha \cdot (\vec{c} - \vec{r}_{tip}) . \quad (47)$$

where $r_{tip} = \frac{a^2}{(\vec{a} \pm \vec{v}) \cdot \vec{c}}$

which can be integrated to yield the indefinite integral

$$x = \frac{-c \sin(\alpha \pm v + \beta)}{\sin \alpha} - \frac{a^2}{2c \sin \alpha} \log \left| \frac{1 + \sin(\alpha \pm v + \beta)}{1 - \sin(\alpha \pm v + \beta)} \right| \quad (48)$$

Since, in the example being considered, the motion from $\beta_{transition} = 69.4$ degrees until $\beta_{final} = 80$ degrees falls in the slipping-slowest behavior regime, we simply evaluate x at these two angles and subtract. Here the "-" sign in " $\alpha \pm v$ " is used. The distance Δx obtained is one component of the maximum required pushing distance to align the workpiece.

8.2. Sticking-slowest regime

In figure 8-1 the slowest COR is the lowest point of the sticking locus, labeled "B". When the COR is at point "B" $\vec{c} - \vec{r}$ may be easily approximated as

$$|\vec{c} - \vec{r}| = \frac{c^2 + a^2}{c \sin \beta} \quad (49)$$

(If the radius of curvature of the tip of the COR locus boundary were zero this approximation would be exact. As it is not zero, the bottom of the sticking locus drops slightly below the tip line. This is a negligible effect, bounded in [15]. We will neglect it here.

Note the absence of any dependence on the friction cone angle v . This is because when the pusher and

workpiece are already sticking, further increase in μ_c has no physical effect. To find the maximum required pushing distance it is only necessary to integrate equation 47 with $\vec{c} - \vec{r}$ as given here. We obtain the indefinite integral

$$x = \frac{c^2 + a^2}{2c} \log \left| \frac{1 - \cos \beta}{1 + \cos \beta} \right| \quad (50)$$

In our example, motion from $\beta_{initial} = 45$ degrees until $\beta_{transition} = 69.4$ degrees falls in the sticking-slowest behavior regime, so we simply evaluate x at these two angles and subtract. The distance Δx obtained is the second component of the maximum required pushing distance to align the workpiece. The total required pushing distance to align the workpiece is the sum of the two partial results obtained from equations 48 and 50.

9. Example: Moving point pushing aside a disk

In this example we consider a disk being pushed not by a fence, but by a point moving in a straight line. The point may be a corner of a polygonal pusher, as long as it is only a corner of the pusher that touches the disk, and not an edge.

In all cases the outcome of the collision is the same: the disk is pushed aside by the pusher, and contact is broken. The disk ceases to move at the instant the pusher loses contact with it (we assume slow motion), so the disk will be left tangent to the pusher's path when contact is broken. The initial and final configurations of the disk are shown in figure 9-1. We wish to calculate the minimum and maximum length of the encounter, $x_{encounter}$, in terms of the *collision parameter*, β , as indicated in figure 9-1. We might also wish to know the minimum and maximum angles through which the disk may rotate during the collision.

Figure 9-1: Configuration of the disk and the path of the pusher, before and after collision

A point pusher in linear motion encounters a disk. The collision is characterized by an initial value of the "collision parameter" $\beta_{initial}$. After the pusher has translated a distance $x_{encounter}$, the disk has become tangent to the path of the pusher and the two break contact, ending the collision. β_{final} is $\pi/2$. During the collision the disk rotates an angle ξ . We wish to place bounds on $x_{encounter}$ and on ξ .

9.1. Length of the encounter

In figure 9-2, the variables of interest are x , which parametrizes the advance of the pusher along its path, and β , which completely characterizes the collision. β will vary from $\beta_{initial}$, its value at first contact, to $\beta_{final}=\pi/2$ when contact is broken. $x_{encounter}$ is the corresponding change in x , as β changes from $\beta_{initial}$ to $\pi/2$.

If the instantaneous COR is known, the direction of motion of the CM of the disk is known: it makes an angle θ with the horizontal, as shown in figure 9-2. If the CM of the disk moves a distance Δl along its line of motion, we can find the resulting values of $\Delta\beta$ and Δx , and thereby relate $\Delta\beta$ and Δx to each other.

The pusher advances a distance

$$\Delta x = \Delta l \cos \theta + \Delta l \sin \theta \tan \beta \quad (51)$$

due to Δl . At all times β can be found from

$$a \sin \beta = y + \Delta l \sin \theta \quad (52)$$

where (x,y) are the coordinates of the point of contact.

Substituting Δl from equation 51, and evaluating the change in $\sin \beta$ due to Δl , we find

$$a \Delta(\sin \beta) = \frac{\Delta x \sin \theta}{\cos \theta + \sin \theta \tan \beta} \quad (53)$$

For infinitesimal motions $\Delta\beta$ and Δx become $d\beta$ and dx . Using $d(\sin \beta) = \cos \beta d\beta$, we find an equation of motion

$$dx = a d\beta \left(\sin \beta + \frac{\cos \beta}{\tan \theta} \right) \quad (54)$$

Since it will turn out that $\tan \theta > 0$, the largest and smallest values of $dx/d\beta$ will result when θ assumes its smallest and largest values, respectively.

Figure 9-2: Finding equation of motion 51

If the COR were known, we could find relations among: (a) the motion of the CM of the disk Δl , (b) the change in the collision parameter $\delta\beta$, and (c) the advance of the pusher Δx .

Figure 9-3: COR sketch for a point pushing a disk

The COR sketch for the collision between pusher and disk. The angle of the edge being pushed, α , is the tangent to the disk at the point of contact \mathcal{C} . Therefore one of the two elementary COR loci which compose the COR sketch is "wrapped" (figure 6-3). The COR sketch consists of only a down-slipping locus (left of the sticking line) and a sticking locus. This is reasonable: it would be surprising if the disk should slip up relative to the pusher.

Now we construct the COR sketch, shown in figure 9-3. Since the edge normal at \vec{r} passes through the CM, the extremes of the friction cone pass to either side of the CM, for any $\mu_c > 0$. $\{COR\}_{\alpha-v}$ is a "wrapped" locus (as described in section 6.5,), so the COR sketch must be that of figure 6-5 sketch (G), (H), or (I). In any case there must be a sticking locus, there cannot be an up-slipping locus, and there may or may not be a down-slipping locus. In figure 9-3 we have shown a down-slipping locus.

In figure 9-3, (and in general when the COR sketch is any one of distinct types (G), (H) or (I)), the smallest and largest values of θ (figure 9-2), occur when the COR is at the lower or upper endpoints, respectively, of the the sticking locus. For sketches (G) and (H) the lower endpoint of the sticking locus is well approximated by the intersection of the sticking line with the tip line, and we will use this approximation (neglecting the small effect of the curvature of the tip, though this could be included). For the lower endpoint of the sticking locus in sketch (I), and for the top of the sticking locus in all three sketches, numerical methods would have to be used. We will not find these numerical results here.

9.1.1. Greatest length of encounter

As in section 8.2, , we will neglect the slight dip of the sticking locus below the tip line, which results from the non-zero radius of curvature of the tip of the COR locus boundary.

We will also assume that the COR sketch is of type (G) or (H), not (I), so that the lower endpoint of the sticking locus can be approximated by the intersection of the sticking line with the tip line. This assumption will be addressed in section 9.1.2, below.

If the COR is at the intersection of the sticking line with the tip line, we find from figure 9-4

Figure 9-4: Finding the smallest θ (equation 55)

The length of the encounter between pusher and disk is greatest if the COR is at such a location that θ is minimal. In most cases the bottom of the sticking locus is the location of the COR which minimizes θ . Using the tip line construction we can find the minimum value of θ as shown here.

$$\tan \theta = \frac{x_{COR}}{y_{COR}} \quad (55)$$

$$x_{COR} = -a \cos \beta, \text{ and}$$

$$y_{COR} = a \frac{\sin^2 \beta - 2}{\sin \beta}$$

where y_{COR} is found from the construction of figure 9-4. Using $c = a$, equation 55 can be simplified to

$$\tan \theta = \frac{\cos \beta \sin \beta}{1 + \cos^2 \beta} \quad (56)$$

Using this value of $\tan \theta$ in the equation of motion 54 results in

$$dx = a d\beta (\sin \beta) + \frac{1 + \cos^2 \beta}{\sin \beta} \quad (57)$$

which, integrated, yields the indefinite integral

$$x_{encounter} = a \left(\ln \frac{1 - \cos \beta}{1 + \cos \beta} \right) \quad (58)$$

The maximum value of $x_{encounter}$ can be obtained by evaluating equation 58 at $\beta_{initial}$ and $\beta_{final} = \pi/2$, and subtracting. The value at $\pi/2$ is zero.

9.1.2. Condition for sketch type (I)

The above derivation of maximum $x_{encounter}$ assumed that the lower endpoint of the sticking locus is at the tip line. This is not true when the COR sketch is of type (I), in figure 6-5.

The COR sketch is of type (I) when the tip of $\{COR\}_{\alpha+\nu}$ is left of the sticking line. Simplifying equation 45

for $a = c$ and $\alpha + \beta = \pi/2$, we find the condition for sketch (I) to be:

$$\tan \beta > 2 \tan \nu = 2 \mu_c \quad (59)$$

This means that the COR sketch will always become type (I) as $\beta \rightarrow \pi/2$, unless $\mu_c = \infty$. ($\mu_c = \infty$ can occur, for example, in pushing a gear, if a tooth is engaged by the pusher.) In every case of pushing aside a disk, sketch (I) is entered eventually.

By using the tip line as the lower endpoint of the sticking locus, despite the fact that this is a poor approximation in sketch (I), we find too low a value for the minimum θ . Our calculated maximum for $x_{encounter}$ (equation 58) is unnecessarily high. We could in principle refine the upper bound by finding the lower endpoint of the sticking locus more accurately by numerical methods.

As mentioned above, we are also neglecting the slight dip of the sticking locus below the tip line (in sketches (G) and (H)), which causes us to underestimate the maximum possible value of $x_{encounter}$. Here too we could refine $x_{encounter}$ by numerical methods.

Neglect of sketch (I), and neglect of the dip due to tip curvature, cause errors of opposite sign in calculating the maximum $x_{encounter}$. The latter is a smaller error. Neither error will be addressed here.

9.1.3. Least length of encounter

The minimum possible value of $x_{encounter}$ occurs when the COR is at the top of the sticking locus. We do not have an analytical method of finding or approximating the upper endpoint of the sticking locus, as we have for the lower endpoint. The lower endpoint is similarly hard to analyze if the COR sketch is of type (I) in figure 6-5. In these cases it is necessary to find the endpoints numerically for all β in the range of interest, calculate θ for each β , and then integrate equation 54 numerically to find $x_{encounter}$.

9.2. Rotation of the Pushed Disk during Encounter

9.2.1. Maximum rotation

In section 9.1, both the largest and smallest possible values of $x_{encounter}$ resulted from CORs on the sticking line. If the COR remains on the sticking line, the pusher does not slip relative to the surface of the disk, and so evaluation of the rotation of the disk during the encounter, $\xi_{encounter}$, is trivial. We have

$$\xi_{encounter} = a(\pi/2 - \beta_{initial}) \quad (60)$$

Since only up-slipping of the pusher is possible, equation 60 is an exact upper bound for $\xi_{encounter}$; any slipping will only serve to reduce the rotation of the disk.

Maximal slipping is obtained if $\mu_c=0$. The pushing force is directed through the CM of the disk, so the disk can only translate and not rotate [10]. So if $\mu_c=0$, we have $\xi_{encounter}=0$ as both maximum and minimum rotation.

9.2.2. Minimum rotation

We found in section 9.1, that extreme values of $dx/d\beta$ occur when θ takes on extreme values. Having constructed the COR sketch, we found that the extreme values of θ for possible CORs are assumed when the COR falls at the top or bottom of the locus. In this section we will not be able to find a single geometric variable, analogous to θ , whose extremes correspond to extremes of the rate of rotation.

Rotation of the disk will be measured by the angle ξ , measured at the COR, as shown in figure 9-5. We can relate $\Delta\xi$ to advance of the pusher Δx :

$$\Delta x = l \sin \xi d\xi \quad (61)$$

Combining equation 61 with equation 54 which relates $\Delta\beta$ to Δx , we find

$$\Delta x = \frac{a d\beta (\sin \beta + \frac{\cos \beta}{\tan \theta})}{l \sin \xi} d\beta \quad (62)$$

We can eliminate θ and $l \sin \xi$ in favor of the coordinates of the COR:

$$\tan \theta = \frac{x_{COR}}{y_{COR}} \quad (63)$$

$$l \sin \xi = a \sin \beta - y$$

yielding

$$\frac{d\xi}{d\beta} = \frac{a(y_{COR} \cos \beta + x_{COR} \sin \beta)}{x_{COR}(a \sin \beta - y_{COR})} \quad (64)$$

Figure 9-5: Finding equation of motion 61

If the location of the COR is known, the rotation of the disk ξ can be related to the advance of the pusher Δx .

This has no simple geometric interpretation. Contours of constant $d\xi/d\beta$ are plotted in figure 9-6, for $\beta=45$ degrees. Minimum rotation occurs at minimum $d\xi/d\beta$. The COR sketch for $\beta=45$ degrees is superimposed on figure 9-6. The possible value of the COR which is responsible for minimum rate of rotation is the point of the COR locus which intersects the slowest valued contour line, indicated in the figure as point **A** (in this case very close to the tip). Having obtained numerically the minimum possible value of $d\xi/d\beta$, as a function of β , we can numerically find the indefinite integral:

$$\xi_{min} = \int \left(\frac{d\xi}{d\beta}\right)_{min}(\beta) d\beta \quad (65)$$

Minimum rotation in a given collision can then be evaluated by subtracting $\xi_{min}(\beta_{initial})$ from $\xi_{min}(\beta_{final}=\pi/2)$.

10. Example: Spiral localization of a disk

In this example we analyze an unusual robot motion by which the position of a disk (a washer say), free to slide on a tabletop, can be localized without sensing. If the disk is known initially to be located in some bounded area of radius b_1 , we begin by moving a point-like pusher in a circle of radius b_1 . Then we reduce the pusher's radius of turning by an amount Δb with each revolution, so that the pusher's motion describes a spiral. Eventually the spiral will intersect the disk (of radius a), bumping it. We wish the disk to be bumped toward the center of the spiral, so that it will be bumped again on the pusher's next revolution. If the spiral is shrinking too fast, however, the disk may be bumped *out* of the spiral instead of toward its center, and so the disk will be lost and not localized.

We wish to find the maximum shrinkage parameter Δb consistent with guaranteeing that the disk is bumped into the spiral, and not out. (Δb will be a function of the present spiral radius.) We also wish to find the number of revolutions that will be required to localize the disk to some radius b , with $a < b < b_1$, and

Figure 9-6: Contours of constant $d\xi/d\beta$, and the COR sketch

To find the minimum possible rotation of the disk ξ during its encounter with the pusher we seek that location of the COR which minimizes ξ for unit increase in the collision parameter β , i.e. which minimizes $\delta\xi/\delta\beta$. Plotted are contours of constant $\delta\xi/\delta\beta$. We must find numerically the point in the COR locus which intersects the least contour. For the COR locus plotted, the least contour intersected is about .46, and the COR which intersects it is, once again, very near the tip of the COR locus.

the limiting value of b , called b_∞ , below which it will not be possible to guarantee localization, regardless of number of revolutions.

10.1. Analysis

Suppose the pushing point has just made contact with the disk. Since the previous revolution had radius only Δb greater than the current revolution, the pusher must contact the disk at a distance at most Δb from the edge of the disk, as shown in figure 10-1. We will consider only the worst case, where the distance of the pusher from the edge is the full Δb .

We know that if $\Delta b < a$ the disk will move downward [10]. This is not sufficient to assure that the disk will be pushed into the spiral (rather than out of the spiral), because the pushing point will also move down, as it continues along its path (figure 10-1). To guarantee that the disk will be pushed into the spiral, we must make sure that it moves down *faster* than does the pushing point.

Note that we will continue to draw the pusher's motion as horizontal, even though the pusher must turn as it follows the spiral. This is done to maintain the convention for COR sketches used in previous sections. At every moment we simply choose to view the system from such an angle that the pusher's motion is horizontal.

One way of comparing rates of moving down is by considering the increase or decrease in the angle β , called the *collision parameter*, in figure 10-1. If, as the pusher's motion along its spiral progresses, β increases, then the disk is being pushed *into* the spiral; localization is succeeding. When β reaches $\pi/2$, the pusher grazes the disk and leaves it behind. The disk is then left tangent to the spiral. If, as the pusher's motion progresses, β decreases, the disk is being pushed *out* of the spiral; localization is failing.

Figure 10-1: Geometry at the moment of the second collision of pusher and disk

A point pusher describes a decreasing spiral about a region of radius b_1 within which a disk of radius a is known to be. As the spiral decreases in radius the disk is pushed towards the center of the spiral. We wish to find the fastest-shrinking spiral which will guarantee that the disk is always pushed in towards the center and never out of the spiral. It turns out there is a limiting radius of the spiral below which further confinement of the disk cannot be guaranteed, no matter how slowly the spiral decreases in radius.

In this figure the disk was first struck by the pusher when it was at radius b_1 , and was pushed towards the interior of the spiral. The disk was left tangent to the path of the pusher, and is about to be struck again by the pusher, which is now at radius b_2 . $\Delta b = b_1 - b_2$ is the shrinkage rate of the spiral. Notice the collision parameter β which results.

10.2. Critical case: pusher chasing the disk around a circular path

In the critical case the angle β does not change with advance of the pusher. The pusher "chases" the disk around the spiral, neither pushing it in nor out. In this section we will take the spiral to be a circle (i.e., $\Delta b = 0$), to simplify analysis. The critical case, shown in figure 10-2, is highly unstable. The pusher's motion is shown as an arc of a circle, labeled path of pusher. (Underlined names refer to elements of figure 10-2). The center of that circle is labeled PC (for pusher-center). Point PC is directly below the point of contact, in keeping with our convention of drawing the pusher's line of motion horizontal.

To maintain the critical case, the path followed by the CM of the disk (labeled critical path of CM) must be as shown in the figure: an arc of a circle, concentric with the arc path of pusher. Instantaneously, the direction of motion of the CM must be along the line labeled motion of CM, tangent to the critical path of CM. The critical line, drawn through PC and CM, is by construction perpendicular to motion of CM. The COR of the disk must fall on the critical line, in order that the instantaneous motion along the line motion of CM be tangent to the critical path of CM.

We have just seen that the COR of the disk must fall on critical line for the instantaneous motion of the CM to be consistent with the CM following the critical path of CM. If the COR falls to the left of the critical line, the CM diverges from the critical path of CM by moving *inside* the arc. Therefore β will increase with advance of the pusher, and localization is succeeding. If the COR falls to the right of the critical line, the CM diverges from the critical path of CM by moving *outside* the arc. Therefore β will decrease with advance of the pusher, and localization is failing. The critical line divides the plane into two zones: if the COR falls in the left zone, the disk is pushed into the pusher circle, while if the COR falls in the right zone, the disk is pushed out of the pusher circle.

Figure 10-2: Critical case: pusher "chasing" disk around a circular path

If the shrinkage of the spiral Δb is too great, the disk can be pushed *out* of the spiral. To find the critical value of Δb below which the disk is guaranteed to be pushed *into* the spiral, we consider the marginal case where it is possible for the pusher to "chase" the disk, with the collision parameter β neither increasing (meaning the disk is going towards the interior of the spiral) nor decreasing (meaning that the disk is going towards the exterior of the spiral.)

We wish to find a condition on the radius of the pusher circle which guarantees that the disk will always be pushed *into* the circle. We will construct the COR sketch, and then find positions for PC such that all possible CORs are to the left of the critical line.

In figure 10-3 we have constructed the COR sketch with collision parameter β . Since the edge normal at \vec{c} passes through the CM, the extremes of the friction cone pass to either side of the CM, for any $\mu_c > 0$. $\{COR\}_{\alpha-v}$ is a "wrapped" locus (section 6.5), and the COR sketch must be that of figure 6-5 (G), (H), or (I). In any case, there must be a sticking locus, there cannot be an up-slipping locus, and there may or may not be a down-slipping locus. In figure 10-3 we have shown a down-slipping locus.

To make sure that the whole COR locus falls to the left of critical line, we need only place the center of the pusher motion (PC) *below* the lower endpoint of the sticking locus. (Point PC is required to have the same x coordinate as the point of contact, in keeping with our convention of drawing the pusher's line of motion horizontal.)

10.3. Critical radius vs. collision parameter

For every value of β , (the collision parameter), we compute the distance from the pusher's line of motion to the lower endpoint of the sticking locus. This defines a critical radius $r^*(\beta)$. For each collision parameter β , $r^*(\beta)$ is the radius the tightest circle that the pusher can describe with the guarantee that the disk will be pushed into the circle, or at worst be "chased" around the circle indefinitely, but not be pushed out of the circle. In figure 10-4, $1/r^*(\beta)$ is plotted as a function of collision parameter β for each of several values of μ_c . (The discontinuity in slope results from the discontinuity in slope of the COR locus boundary at $r=a$.)

Figure 10-3: COR sketch for critical case, and solution for location of PC

We wish to find a condition on the radius of the pusher circle which guarantees that the disk will always be pushed *into* the circle. We will construct the COR sketch, and then find positions for PC such that all possible CORs are to the left of the critical line.

To make sure that the whole COR locus falls to the left of critical line, we need only place the center of the pusher motion (PC) *below* the lower endpoint of the sticking locus.

Figure 10-4: Radius $r^*(\beta)$ of the critical circle as a function of collision parameter β

For every collision parameter β (here plotted as β/π), there is a tightest radius r^\times which the pusher can describe still maintaining the guarantee that the disk can be chased or pushed inward, but never be pushed outward. For a variety of coefficients of friction μ_c we plot here the *inverse* of that tightest (critical) radius, a/r^\times .

The inverse of the function $r^*(\beta)$ will be denoted $\beta^*(r)$, representing the smallest value of β for which a pusher motion of radius r still results in guaranteed localization. In terms of the pusher's distance from the top edge of the disk, d , (figure 10-3), we can use the relationship

$$a(1 - \sin \beta) = d \quad (66)$$

to define the *critical distance from grazing* $d^*(r)$ as a function of r . $d^*(r)$ is the largest distance of the pusher from the top edge of the disk for which a pusher motion of radius r still results in guaranteed localization.

10.4. Limiting radius for localization

If there is a limiting radius b_∞ of the spiral motion below which localization cannot be guaranteed, then as the spiral approaches radius b_∞ the motion must become circular. $\Delta b \rightarrow 0$ as b_∞ is approached, so collisions become grazing collisions, and we have the distance from grazing $d \rightarrow 0$. (In terms of the collision parameter β , we have $\beta \rightarrow \pi/2$.) The COR sketch for $\beta = \pi/2$ is shown in figure 10-5. If the disk is not to be bumped out of the spiral, we must have $b_\infty = r^*(\beta = \pi/2)$. b_∞ is indicated in the figure, and can be shown analytically to be

$$\begin{aligned} b_\infty &= a(\mu_c + 1) \text{ for } \mu_c \leq 1 \\ b_\infty &= 2a \text{ for } \mu_c \geq 1 \end{aligned} \quad (67)$$

Only at $\mu_c = 0$ can a disk be localized completely, i.e. localized to within a circle the same radius as the disk. Otherwise the tightest circle within which the disk can be localized is given by equation 67.

Figure 10-5: COR sketch at the limiting radius, showing b_∞

There is a limiting radius of the spiral b_∞ , below which we cannot guarantee that the disk will be pushed inward, no matter how slowly the spiral is decreasing in radius, i.e. no matter how small Δb . As the spiral approaches this radius it must more and more accurately approximate a circle, since it cannot go below radius b_∞ . Thus the collision parameter β becomes $\pi/2$ as radius b_∞ is approached, and all collisions become grazing collisions. Drawing the COR sketch for a grazing collision we find that $b_\infty = a(\mu_c + 1)$, a general kinematic limitation on the success this herding strategy can achieve.

10.5. Computing the fastest guaranteed spiral

Let b_n be the radius of the n^{th} revolution of the pusher, so that we have initially radius b_1 , and b_∞ is the limiting radius as $n \rightarrow \infty$ (In specifying but a single radius for each revolution of the spiral, we will not truly specify the spiral completely, but this will be sufficient to characterize the number of revolutions required to achieve a desired degree of localization.)

To excellent approximation we can define the fastest spiral recursively by

$$b_n = b_{n-1} - d^*(b_n) \quad (68)$$

The difference between the radii of consecutive turns of the spiral $n-1$ and n , is therefore $\Delta b = d^*(b_n)$. Equation 68 thus enforces the condition that on the n^{th} revolution, the value of d is exactly the critical value for circular pushing motion of radius b_n . At worst, the disk is pushed neither in nor out of the spiral. A slightly slower spiral would guarantee that the disk cannot be chased in this way for long, but is pushed into the spiral. However the difference between our spiral and the "slightly slower" one is so slight that it is not worth dealing with here [15].

Figure 10-6 shows the fractional deviation of spiral radius b_n above b_∞ , vs. number of turns n , on logarithmic and on linear scales. We start (arbitrarily) with $b_1 = 100a$. The spiral radius was computed numerically for $\mu_c = .25$, using the results for $\beta^*(r)$ shown in figure 10-4, and equation 68.

Figure 10-6 shows that when the spiral radius is large compared to the disk radius a (which is taken to be 1 in the figure), we can reduce the radius of the spiral by almost a with each revolution. As the limiting radius is approached, the spiral reduces its radius more and more slowly, approaching the limiting radius b_∞ as about $n^{-1.6}$, where n is the number of revolutions.

Figure 10-6: Performance of the optimal spiral

For $\mu_c = .25$ we plot the optimal spiral. This is the fastest-decreasing spiral which still guarantees that the disk is pushed into the spiral and cannot be pushed out, i.e. localizes the disk as quickly as possible. We found that the spiral cannot decrease below a radius b_∞ while maintaining the guarantee, so that value has been subtracted from the vertical (spiral radius) axis, leaving only the difference between the spiral radius and its limiting value. In the linear plot, we can see that the radius of the optimal spiral decreases swiftly by almost the disk's radius a with each revolution until quite close to the limiting radius. It is then more instructive to look at the log-log plot to see how the spiral radius approaches the limiting radius.

Figure 10-6 demonstrates the best performance that the "herding" strategy can achieve.

11. Conclusion

We have solved for the possible instantaneous motions of a sliding workpiece as it is pushed, in the presence of unknown frictional forces between workpiece and table, and between workpiece and pusher.

We have characterized the qualitatively different kinds of sliding motion which are possible, and found the conditions under which each can occur. Using these results it is possible to find bounds for *gross* motions of a pushed workpiece as well. This is done by integrating the possible instantaneous motions.

As an example, we have found the maximum distance a polygonal sliding workpiece must be pushed by a fence in order to guarantee that a side of the workpiece has aligned itself with the fence. Using the useful *tip line construction* described here, approximate results are obtained both for the alignment problem and several others. Strict upper bounds for the maximum required pushing distance are found by using slightly more sophisticated methods, but the difference between the upper bounds and the approximate results are so slight that the effort seems hardly justified.

In a second example, we have taken the pushed workpiece to be a disk, and the pusher to be a point, or the corner of a polygon, moving in a straight line. We have found the maximum distance that the pusher and the disk may be in contact, before the disk is "pushed aside" by the moving workpiece. Bounds on the rotation of the disk during its interaction with the pusher are also found.

Finally we have analyzed an unusual robot maneuver, in which a disk known to be within a certain circular area can be "localized" to a much smaller circular area by a pusher which, perhaps under robot control, describes a decreasing spiral around the disk. Thus the disk can be located by a robot without sensors.

We found the ultimate limiting radius below which the disk cannot be localized further, no matter how slowly the spiral decreases in radius. We also found (to within tight bounds) the "optimal spiral": the spiral which localizes the disk with the fewest number of revolutions, while guaranteeing that the disk is not lost from the spiral.

12. Suggestions for Further Work

12.1. Other models of friction

An important assumption used in deriving the COR loci is that of a coefficient of sliding friction μ_s which is uniform over the sliding surface and velocity independent: simple Coulomb friction. Friction is rarely so well behaved.

Velocity dependence of μ_s will have only moderate consequences for the COR loci. The sense of rotation (CW or CCW) is not affected by velocity dependence, because pure translation of the workpiece is the marginal case dividing the senses of rotation. In pure translation all parts of the workpiece move with the same velocity, so velocity dependence of μ_s is unseen by the workpiece. If μ_s decreases with increasing velocity (the usual case), we can predict that CORs will lie closer to center of mass (i.e. rotation rates will be faster) than they would with constant μ_s . The side of the workpiece towards which it turns has a lower velocity, therefore higher μ_s , and therefore more drag, causing the workpiece to turn still faster towards that side.

Spatial non-uniformity of μ_s is more serious. In our experimental work [15] a non-uniformly worn surface caused a five degree offset in the marginal pushing direction dividing CW from CCW rotation. It would be hard to control such a major effect analytically. Instead, sliding surfaces must be kept uniform.

When it is the surface of the sliding part, rather than the surface of the table, which is non-uniform, we may hope to find simple analytic adjustments to the COR locus to compensate. The distinction between *center of friction (COF)* and *center of mass* becomes important [8] [10]. If the composition of the part surface is understood and some information about the pressure distribution is available, a COF distinct from the CM can be calculated for the part. Then the sense of rotation (at least) will be predictable. It is not known what effect a COF distinct from the CM will have on the COR locus.

12.2. Pushing above the plane

We assumed that the point of contact between pusher and pushed workpiece is not far (relative to the radius of the workpiece) above the sliding surface. In the extreme case of pushing far above the plane, the workpiece will tip over instead of sliding. For small heights, the effect creates a center of friction (COF) distinct from the center of mass (CM). The effect on the COR locus is unknown.

12.3. Non-quasistatic velocities

The results of sections 5 and 6 depend on the quasistatic assumption, discussed in section 2. We assume that dissipative effects due to friction between a workpiece and the surface it slides on overwhelm inertial effects. In the real world both effects are present, and become of comparable importance at characteristic speeds considered in section 1 here, and references [15] and [11]. The results of sections 5 and 6 may be considered to be the $v \rightarrow 0$ limit.

In the opposite extreme we may neglect sliding friction altogether, and only consider inertial effects. The motion is then independent of speed, so we may consider this case to be the $v \rightarrow \infty$ limit. The details of the contact between the sliding workpiece and the surface it slides on (the pressure distribution, section 2.5) no longer have any effect on the motion. For given initial conditions then, a *single* resulting motion

can be calculated, rather than the *locus* of possible motion calculated for slow motions.

Drawing on the work of Routh [18], Wang [19] has calculated the motion of a pushed workpiece in the $v \rightarrow \infty$ limit (the "impact" limit). The motion is a function of the coefficient of friction between the pusher and workpiece μ_c as in the quasistatic case, and of the geometry of pushing, but it also depends on the elasticity of the materials in contact. Elasticity ranges from the plastic limit $e=0$, (e.g. modeling clay,) to the elastic limit $e=1$, (e.g. spring steel.)

The instantaneous motion on impact can be described by a center of rotation (COR) somewhere in the plane. Wang finds [20] that when $e=0$ or $\mu_c=0$, the COR falls along the axis of symmetry of the quasistatic COR locus derived in section 5, and at a distance r_{impact} from the CM given by

$$r_{impact} = \frac{\rho^2}{\alpha \cdot \bar{c}} \quad (69)$$

where ρ is the radius of gyration of the workpiece. Equation 69 is the same as equation 38 (which gives the tip of the COR locus in the quasistatic case) when the workpiece pushed is a circular rim, for which $\rho=a$. For all other workpieces $\rho < a$, so we may conclude that the COR for impact lies within the COR locus for quasistatic pushing, if $e=0$ or $\mu_c=0$.

If $e > 0$ and $\mu_c > 0$, Wang finds that the sense of rotation (CW or CCW) does not necessarily agree with Mason's results for quasistatic motion [10]. This means that in realistic cases where $e > 0$, a given sliding operation which results in CW rotation of the pushed workpiece in the quasistatic limit may change over to CCW rotation as velocity is increased.

For fixed elasticity e and coefficients of friction μ_c and μ_s , as velocity is increased the locus of CORs describing the motion must change continuously from the quasistatic locus at $v=0$ to the single point

(sometimes outside the quasistatic locus) which is Wang's result at $v=\infty$. If the COR loci for intermediate velocities could be found or bounded, motion planning algorithms based on sliding friction (e.g. [14] [2] [9]) could be extended to non-quasistatic velocities.

12.4. Bounds on the COR locus for other than disks

The COR loci found in section 5 are exact if the sliding workpiece is a disk. Any COR in the locus could occur for some combination of bumps on the bottom of a disk, i.e. for some pressure distribution. The COR locus for a disk necessarily encloses the COR locus for any workpiece which could be enclosed in that disk, with the same center of mass. The COR locus for the inscribed workpiece may be considerably smaller than that for the disk, especially when the area of the inscribed workpiece is considerably less than that of the disk. The COR locus for a square, found numerically, and the outline of the COR locus for a disk circumscribing the square, are shown in figure 3-2.

For comparison, the line of CORs for a *uniform* pressure distribution on a disk is shown in figure 12-1. In the uniform case, for each α , (related to the force angle) there is of course only one COR, as the pressure distribution is completely specified. Shown in the figure is a particular α_1 for illustration, and the COR locus outline for all pressure distributions for that α_1 . The tip line for all α is shown. The point of intersection of the α_1 vector through the CM and the tip line is indicated with a dot, which is the tip of the COR locus for α_1 . The tip of the COR locus for any α lies at the intersection of the α vector through the CM and the tip line. Similarly, the COR for uniform pressure for α_1 lies at the intersection of the α_1 vector through the CM and the uniform pressure line, as indicated by a dot. The COR for uniform pressure for any α lies at the intersection of the α vector through the CM and the line of uniform pressure.

Using the COR loci of disks in planning manipulation strategies for other shapes results in unnecessarily

Figure 12-1: Tip line and line of CORs for uniform pressure distribution.

Shown is the tip line for all α . This is the curve traced out by the tip of the COR locus as α is changed. The tip is the farthest the COR can fall from the CM, no matter what pressure distribution exists beneath the disk. If we assume a *uniform* pressure distribution beneath the disk, then rather than a locus of CORs a single COR must be the result.

For comparison with the tip line, we also plot here the curve traced out by the COR for uniform pressure distribution, as α is changed. For a given α such as the one shown, the COR locus is shown, the tip of the COR locus falls at the intersection of the vector $\vec{\alpha}$ with the tip line, and the COR for uniform pressure distribution lies at the intersection of the vector $\vec{\alpha}$ with the "uniform support line".

conservative strategies. It is even possible that no strategy might be found when one exists. This problem could be alleviated if exact COR loci for arbitrarily shaped workpieces could be found. In finding the COR locus for a disk we discovered two classes of "dipods" (pressure distributions consisting of only two points of support, section 4.5,) which were responsible for the boundary of the COR locus. For workpieces other than disks, the boundary is not described by dipods, and finding the COR locus becomes considerably harder.

13. Acknowledgements

We wish to acknowledge useful discussions with Randy Brost and with Matt Mason, both of whom also contributed many helpful suggestions for improving this paper. Several equations were obtained or simplified using MACSYMA. This work was supported by a grant from the Xerox Corporation, and by the Robotics Institute, Carnegie-Mellon University.

References

1. J. Barber, R. A. Volz, R. Desai, R. Rubinfeld, B. Schipper, J. Wolter. Automatic Two-fingered Grip Selection. 1986 Int'l Conf. on Robotics and Automation, IEEE, April, 1986.
2. Randy Brost. Automatic Grasp Planning in the Presence of Uncertainty. Proceedings, IEEE Int'l Conf. on Robotics and Automation, April, 1986.
3. Michael Andreas Erdmann. On Motion Planning with Uncertainty. Master Th., Massachusetts Institute of Technology, 1984. AI-TR-810.
4. Erdmann, M. A., and Mason, M. T. An Exploration of Sensorless Manipulation. Proceedings, IEEE Int'l Conf. on Robotics and Automation, April, 1986.
5. S. Goyal, A. Ruina. The Load-Motion Relation for Rigid Bodies Sliding on Planar Surfaces with Dry Friction. draft.
6. J. H. Jellett. *A Treatise on the Theory of Friction*. MacMillan, London, 1872.
7. Tomas Lozano-Perez. "Motion Planning and the Design of Orienting Devices for Vibratory Parts Feeders". *IEEE Journal of Robotics and Automation* (1986). to be published.
8. W. D. MacMillan. *Dynamics of Rigid Bodies*. Dover, New York, 1936.
9. M. Mani and W. R. D. Wilson. A Programmable Orienting System for Flat Parts. Proceedings, NAMRII XIII, 1985.
10. Matthew T. Mason. *Manipulator Grasping and Pushing Operations*. Ph.D. Th., Mass. Inst. Tech., June 1982. AI-TR-690.
11. Matthew T. Mason. On the Scope of Quasi-static Pushing. Proceedings, 3rd Int'l Symp. on Robotics Research, October, 1985.
12. M. T. Mason and R. Brost. Automatic Grasp Planning: An Operation Space Approach. Proceedings, 6th Symposium on the Theory and Practice of Robots and Manipulators, Cracow, Poland, Sept., 1986.
13. M. A. Peshkin and A. C. Sanderson. Manipulation of a Sliding Object. 1986 Int'l Conf. on Robotics and Automation, IEEE, April, 1986, pp. 233-239.
14. M. A. Peshkin and A. C. Sanderson. Planning Robotic Manipulation Strategies for Sliding Objects. 1987 Int'l Conf. on Robotics and Automation, IEEE, April, 1987.
15. Michael A. Peshkin. *Planning Robotic Manipulation Strategies for Sliding Objects*. Ph.D. Th., Physics Department, Carnegie Mellon University, October 1986.
16. K. Pingle, R. Paul, and R. Bolles. Programmable Assembly, three short examples. Film, Stanford AI Lab, 1974.
17. J. Prescott. *Mechanics of Particles and Rigid Bodies*. Longmans, Green and Co., London, 1923.
18. E. J. Routh. *Dynamics of a System of Rigid Bodies, 7th ed.* Dover Publications, Inc., 1960.
19. Yu Wang. On Impact Dynamics of Robotic Operations. Tech. Rept. CMU-RI-TR-86-14, Robotics Institute, Carnegie-Mellon University, 1986.
20. Yu Wang. personal communication. .

Table of Contents

1. Motivation	2
1.1. Automatic Feeders	2
1.2. Grasping Strategies	3
1.3. Grasp Strength	4
1.4. Statement of "The Sliding Problem"	6
2. Range of Applicability	7
2.1. Workpiece shape	7
2.2. Point of contact between workpiece and pusher	7
2.3. Position controlled pusher	10
2.4. Center of rotation (COR)	10
2.5. Pressure distribution between workpiece and table	10
2.6. Coulomb friction	12
2.7. Quasi-static motion	12
2.8. Bounding the workpiece by a disk	13
2.9. Geometric parameters	13
3. Overview	15
3.1. Minimum power mechanics	20
3.2. Notation	23
4. Solution for the COR locus	24
4.1. Relation between motion of the pusher and rotation of the workpiece	24
4.2. Energy lost to friction with the table	26
4.3. A digression: Iterative numerical solution	27
4.4. Analytic solution	28
4.5. Extrema of the Quotient Locus	29
4.6. Numerical exploration of the Quotient Locus	32
4.7. Boundary for $ \text{COR} < a$	33
4.8. Boundary for $ \text{COR} > a$	37
4.9. Analytic form of the COR locus	39
4.10. Solution for the $ \text{COR} < a$ part of the COR locus	41
4.10.1. Extremal radius of the COR locus boundary for $ \text{COR} < a$	45
4.11. Solution for the $ \text{COR} > a$ part of the COR locus	47
4.11.1. Tip Line	49
4.12. Symmetries of the COR locus	50
4.13. Summary	51
5. Application	52
6. Solution for the COR locus including contact friction	55
6.1. Contact Friction and the Friction Cone	56
6.2. Sticking and Slipping zones	59
6.2.1. Sticking Line	59
6.2.2. Slipping Zones	61
6.3. Consistency for slipping	61
6.4. The Sticking Locus	62
6.5. Possible configurations of an elementary COR locus	63
6.6. Possible distinct COR sketches	64
7. From instantaneous motion to gross motion	69
8. Example: Aligning a workpiece by pushing with a fence	70
8.1. Slipping-slowest regime	75
8.2. Sticking-slowest regime	75
9. Example: Moving point pushing aside a disk	76
9.1. Length of the encounter	78
9.1.1. Greatest length of encounter	81
9.1.2. Condition for sketch type (I)	83
9.1.3. Least length of encounter	84
9.2. Rotation of the Pushed Disk during Encounter	84

9.2.1. Maximum rotation	84
9.2.2. Minimum rotation	85
10. Example: Spiral localization of a disk	87
10.1. Analysis	89
10.2. Critical case: pusher chasing the disk around a circular path	91
10.3. Critical radius vs. collision parameter	93
10.4. Limiting radius for localization	96
10.5. Computing the fastest guaranteed spiral	98
11. Conclusion	100
12. Suggestions for Further Work	101
12.1. Other models of friction	101
12.2. Pushing above the plane	102
12.3. Non-quasistatic velocities	102
12.4. Bounds on the COR locus for other than disks	104
13. Acknowledgements	106

List of Figures

Figure 1-1: Hinge grasp strategy (Paul [16] and Mason [10])	5
Figure 2-1: The edge of an advancing fence pushing a corner of a sliding workpiece	8
Figure 2-2: A corner of an advancing pusher pushing an edge of a sliding workpiece	9
Figure 2-3: Parameters of the pushing problem	14
Figure 3-1: COR locus for a disk found by iterative minimization (dots)	16
Figure 3-2: COR locus for a square found by iterative minimization.	17
Figure 3-3: A typical pushing problem and the boundary of the COR locus found.	19
Figure 3-4: $r_{tip}(a)$ vs. a , and construction of the tip line	21
Figure 3-5: Construction of the COR sketch	22
Figure 4-1: Relation between advance of pusher (dx) and rotation about the COR (dq)	25
Figure 4-2: Dipod responsible for the smallest value of v_y , for $r \gg a$	30
Figure 4-3: Dipod responsible for a negative value of v_y , for $r \ll a$	31
Figure 4-4: Quotient locus $\{q\}$ (dots), and empirical boundary (solid), for $r \ll a$	34
Figure 4-5: Quotient locus $\{q\}$ (dots), and empirical boundary (solid), for $r \gg a$	35
Figure 4-6: Dipods contributing to the boundary of $\{q\}$, for $r \ll a$	36
Figure 4-7: Dipods contributing to the boundary of $\{q\}$, for $r \gg a$	38
Figure 4-8: Boundaries of quotient loci $\{q\}$ for various r	40
Figure 4-9: Variables of equation 24, for a value of r in the COR locus	42
Figure 4-10: Variables of equation 24, for a value of r in the COR locus	43
Figure 4-11: Variables of equation 24, for a value of r on the boundary of the COR locus	44
Figure 4-12: COR locus boundary for $r \ll a$	46
Figure 4-13: Boundaries of COR loci for various b and a	48
Figure 5-1: Initial configuration of workpiece and fence, and resulting COR locus	53
Figure 5-2: Final configuration of workpiece and fence, and resulting COR locus	54
Figure 6-1: Construction of the friction cone	58
Figure 6-2: Construction of zones: up-slipping, down-slipping, and sticking line	60
Figure 6-3: Possible elementary configurations of the COR locus	65
Figure 6-4: Possible elementary configurations with sticking line to the right of the CM	66
Figure 6-5: Nine distinct COR sketches with respect to the sticking line	68
Figure 8-1: Initial orientation of the fence and pushed workpiece	71
Figure 8-2: Final (aligned) orientation of the fence and pushed workpiece	72
Figure 8-3: Transition from sticking-slowest to slipping-slowest behavior	74
Figure 9-1: Configuration of the disk and the path of the pusher, before and after collision	77
Figure 9-2: Finding equation of motion 51	79
Figure 9-3: COR sketch for a point pushing a disk	80
Figure 9-4: Finding the smallest q (equation 55)	82
Figure 9-5: Finding equation of motion 61	86
Figure 9-6: Contours of constant dx/db , and the COR sketch	88

Figure 10-1:	Geometry at the moment of the second collision of pusher and disk	90
Figure 10-2:	Critical case: pusher "chasing" disk around a circular path	92
Figure 10-3:	COR sketch for critical case, and solution for location of <u>PC</u>	94
Figure 10-4:	Radius $r^*(b)$ of the critical circle as a function of collision parameter b	95
Figure 10-5:	COR sketch at the limiting radius, showing b_C	97
Figure 10-6:	Performance of the optimal spiral	99
Figure 12-1:	Tip line and line of CORs for uniform pressure distribution.	105